Modelling of Landslide Susceptibilities in the Cordillera Blanca (Peru)

Master's Thesis GEO 610

31st March 2018

Emanuel Büechi
(13-739-206)

Supervised by

Dr. Holger Frey

PD Dr. Christian Huggel

Faculty Member

Prof. Dr. Andreas Vieli

Glaciology and Geomorphodynamics Group

Department of Geography

University of Zurich

I. Abstract

For this Master's Thesis several existing methods of landslide susceptibility modelling were applied to the mountainous area of the Cordillera Blanca (Peru) which is prone to landslides. The performance of a physically based approach (SINMAP) was compared to different empirical statistical models. The models were applied to three different digital elevation models (DEMs): ASTER GDEM, SRTM, and TanDEM-X. Obtained results were evaluated using the area under the receiver operating characteristics curve (AUC) amongst other techniques. The evaluation was performed using a landslide inventory which extends over the whole study area and two other ones extending over a smaller area. The first two inventories only include shallow landslides and the second inventory of the smaller area includes deep-seated movements, to evaluate how well such landslides can be detected by models for shallow landslides. A last inventory was established at two different locations by measuring the displacement of several points. The evaluation showed that the physically based approach (AUCs between 0.567 and 0.625) performed worse than the empirical statistical ones (AUCs from 0.672 to 0.759) over the large area, with the ASTER GDEM always having the lowest AUC value. This coincided with differences of the variability of the DEM-derived characteristics (e.g. elevation and curvature) from the small to the large evaluation area. A full explanation of the performance just by these characteristics is not possible. Using the smaller evaluation area of the shallow landslides all models received higher AUC values (0.743-0.799). The rather higher differences of the DEM-derived characteristics between the DEMs there resulted in a smaller variation of the model performances. Additionally, it was tried to explain the differences of the performances between the small and the large study area qualitatively. The higher variability of precipitation patterns within the large area may be decisive in this relation. A comparison from the statistical models showed that their performance is highly dependent on the slope angle. Models just considering the slope angle performed similarly to other models considering more independent parameters. The inventory of the deep-seated landslides showed that the shallow landslide models do not perform well for deep-seated landslides (all AUCs ≤ 0.69). The displacement measurements do not allow a meaningful evaluation of the models. Better results were obtained for the analysis of the susceptibility classes of the different models. It showed that mainly the same slopes are considered as most or least susceptible. The main difference is that SINMAP is classifying larger areas as unstable or stable than the statistical models. Generally, this thesis showed that regional scale landslide susceptibility modelling can lead to reasonable results, but performances of different DEMs and models need to be evaluated carefully.

II. Zusammenfassung

Für diese Masterarbeit wurden verschiedene Methoden der Erdrutsch-Anfälligkeitsmodellierung an der Cordillera Blanca (Peru) angewendet, einem Gebirge, welches anfällig auf Erdrutsche ist. Die Leistung eines physikalisch basierten Ansatzes (SINMAP) wurde mit empirisch-statistischen Modellen verglichen. Die Modelle wurden auf drei verschiedene digitale Höhenmodelle (DEMs) angewendet: ASTER GDEM, SRTM und TanDEM-X. Die erhaltenen Ergebnisse wurden unter anderem anhand der Fläche unter der "Receiver Operating Characteristics"-Kurve (AUC) evaluiert. Die Auswertung erfolgte anhand eines Erdrutschinventars, das sich über das gesamte Untersuchungsgebiet erstreckt und zwei weiteren, die sich über eine kleinere Fläche erstrecken. Die ersten beiden Inventare umfassen nur oberflächliche Erdrutsche, das zweite Inventar des kleineren Gebiets umfasst tiefere Bewegungen, um zu sehen, wie gut solche Erdrutsche durch Modelle für oberflächliche Erdrutsche erkannt werden können. Ein letztes Inventar besteht aus verschiedenen Punkten, an welchen Bewegungen gemessen wurden. Die Auswertung zeigte, dass der physikalisch basierte Ansatz (AUCs zwischen 0.567 und 0.625) über das gesamte Untersuchungsgebiet schlechter anwendbar ist als die empirisch-statistischen Modelle (AUCs von 0.672 bis 0.759), wobei das ASTER GDEM immer den niedrigsten AUC-Wert aufwies. Dies stimmte mit den Unterschieden der Variabilität der DEM-abgeleiteten Eigenschaften (z. B. Höhe und Krümmung) von dem kleinen zu dem großen Untersuchungsgebiet überein. Der Einfluss dieser Eigenschaften scheint jedoch nur beschränkt mit der Leistung der Modelle zusammenzuhängen. Unter Verwendung des kleineren Bewertungsbereichs der oberflächlichen Erdrutsche erhielten alle Modelle höhere AUC-Werte (0.743-0.799). Trotz eher grösserer Unterschiede der DEM-Charakteristika in diesem Gebiet zwischen der DEMs waren die Leistungen der Modelle näher zusammen. Zusätzlich wurde versucht, die Unterschiede der Leistungen des grossen und kleinen Untersuchungsgebiets qualitativ zu ermitteln. Eine mögliche Ursache wurde in der eher heterogeneren Niederschlagsverteilung innerhalb des grossen Gebietes entdeckt. Ein Vergleich der statistischen Modelle zeigte zudem, dass die Leistung dieser Modelle vor allem vom Neigungswinkel abhängt. Die Modelle, welche nur den Neigungswinkel betrachten, erreichen ähnliche Leistungswerte wie jenes Modell, welches noch weitere unabhängige Parameter benutzt. Das Inventare der tiefen Erdrutsche zeigte, dass die flachen Erdrutsch-Modelle für tiefe Erdrutsche nicht gut funktionieren (alle AUCs ≤ 0.69). Die Bewegungsmessungen erlauben keine aussagekräftige Bewertung der Modelle. Bessere Resultate wurden bei der Analyse der Anfälligkeitsklassen erhalten. Diese zeigte, dass hauptsächlich die gleichen Hänge von allen Modellen als am stärksten oder am wenigsten anfällig angesehen werden. Der Hauptunterschied ist, dass SINMAP größere Gebiete als instabil oder stabil klassiert als die statistischen Modelle. Im Allgemeinen zeigte diese Arbeit, dass die Modellierung der

Erdrutschanfälligkeit auf regionaler Ebene zu vernünftigen Ergebnissen führen kann, jedoch müssen die Leistungen verschiedener DEMs und Modelle sorgfältig evaluiert werden.

III. Table of Contents

IV. List of Abbreviations

AIC	Akaike Information Criteria
ANA	Autoridad Nacional del Agua (Local water authority of Peru)
ASTER GDEM	Advanced Spaceborne Thermal Emission and Reflection Radiometer Global DEM
AUC	Area Under Curve
DEM	Digital Elevation Model
DSLI	Deep-Seated Landslide Inventory
Eq.	Equation
ESA	European Space Agency
Fig.	Figure
FPR	False Positive Rate
FS	Factor of Safety
GLOF	Glacier lake outburst flood
GPS	Global Positioning Service
iid	independent and identically distributed
LRM	Logistic Regression Model
masl	Meter above sea level
MLI	Marcará Landslide Inventory
ÖAV	Österreichischer Alpenverein
RMSE	Root Mean Squared Error
ROC	Receiver Operating Characteristics
SAR	Synthetic Aperture Radar
InSAR	Synthetic Aperture Radar Interferometry
DInSAR	Differential Synthetic Aperture Radar Interferometry
SI	Stability Index
SINMAP	Stability Index Mapping
SLI	Shallow Landslide Inventory
SRTM	Shuttle Radar Topography Mission
TDX	TanDEM-X DEM
TPR	True Positive Rate
TWI	Topographic wetness index
USGS	United States Geological Service

1. Introduction

The Cordillera Blanca in Peru (Fig. 1) has always been prone to disastrous landslides or related events. Several events like the landslides at Nevado Huascarán (1962/1970) (Vilímek et al. 2000; Evans et al. 2009) or the glacial lake outburst flood of Palcacocha (1941) (Carey 2010) with thousands of victims caused intense hazard and risk related research in this area (Lliboutry 1975; Lliboutry et al. 1977; Vilímek et al. 2005, 2000; Hubbard et al. 2005; Klimeš and Vilímek 2011; Somos-Valenzuela and Mckinney 2011; Huggel et al. 2012b; Klimeš 2012; Schneider et al. 2014; Klimeš et al. 2016). This research usually concentrated on specific slopes or regions. An exception is the work done by Villacorta et al. (2012) who established a landslide susceptibility map covering the whole country of Peru. Due to the spatial resolution of their work of 100m most of the Cordillera Blanca is just considered having high or very high susceptibilities of landslides. Such spatially coarse information is hardly applicable for the local population and administration, thus more detailed studies possibly distinguishing different landslide types are needed. The presented work investigates the susceptibility to shallow landslides of the Cordillera Blanca using different methods of landslide susceptibility models.

Physically based models like SINMAP, SHALSTAB, or TRIGRS (Crosta and Frattini 2003; Meisina and Scarabelli 2007; Terhorst and Kreja 2009; Zizioli et al. 2013; Michel et al. 2014; Pradhan and Kim 2015; Sarkar et al. 2016; Thiebes et al. 2016) or empirical statistical models (Van Den Eeckhaut et al. 2006; Bai et al. 2011; Felicísimo et al. 2012; He et al. 2012; Park et al. 2013b) have been applied in many different regions around the world. All the mentioned studies used different additional information like geological, land-use, or soil maps to better describe occurrence conditions of the studied landslides. Data availability largely constrains the extent of the application of the models, which would otherwise require extensive field work. Applications in mountainous regions are often even more challenging, as the landslide preparatory factors change abruptly in space (e.g. slope dip or soil characteristics due to the different altitudinal belts (Portes et al. 2016)), and available maps may lack important details of their spatial distribution pattern. Therefore, the model parametrisation on a regional scale always introduces uncertainties which are very difficult to assess or even quantify limiting the applicability of the final susceptibility maps (Guzzetti et al. 2006; Levermore et al. 2012).

To contribute to overcome this problem, this Master's Thesis aims at elaborating how landslide susceptibility models perform in areas without any additional information to the ones given by a digital elevation model (DEM), as the elevation information is increasingly more reliable and available even in high mountains due to variety of remotely sensed data (Lacroix et al. 2015). To assess the influence of the DEMs and possibly improve the models, three different DEMs are used for each model. Two of

them have a spatial resolution of 30m (ASTER GDEM and SRTM) and the third one, TanDEM-X, has a spatial resolution of 12m.

Furthermore, the mentioned problems related to data scarcity are not only an issue of the Peruvian Andes (Suárez et al. 1983; Neukom et al. 2015). There are many regions with a lack of information (Frich et al. 2002), especially authors who study high mountain areas such as the Himalaya (Remesan and Holman 2015), Tien Shan (Pieczonka and Bolch 2015), or even the Rocky Mountains (Kunkel et al. 2009; Pugin et al. 2014) need to deal with limited data. Therefore, the results of this thesis concerning the Cordillera Blanca could act representatively for many data-scarce high mountain regions.

The main part of this thesis is the comparison of the physically based model SINMAP to a statistically based model using logistic regression. As a third and a fourth model, two different slope models have been established. One of these uses the logistic regression considering only the slope angle as independent parameter, and another one using failure rates per slope class, to evaluate the added value of the parameters considered additionally by SINMAP and the logistic regression model (LRM). These four models have been applied to the three DEMs. The evaluation of these model runs is done using three different landslide inventories. One of the inventories includes shallow landslides distributed over the whole study area, and another one is restricted to a much smaller region (see Fig. 1). These two inventories are used to avoid model uncertainties caused by the highly variable conditions of the large study area. A final inventory is used which constrains to a smaller area too. It includes no shallow landslides but more deep-seated movements. This last inventory is used to evaluate if even different kinds of landslides can be detected by such models.

These efforts should answer the following questions:

-How do regional-scale landslide susceptibility models perform in areas with highly variable morphology and soil characteristics that are typical for high mountain regions?

-How much of the performance of a model can be explained by considering only the slope angle?

-What is the influence of the used DEMs on the performance of the models?

-How do these models perform for landslide inventories with different kinds of landslides?

This thesis first describes the study area, before a general introduction into the science of landslides is given. The next part then presents the used data and methods and special attention is given to the related uncertainties. The obtained results and their evaluation and validation are presented in the subsequent chapter. Finally, these results are discussed, and the conclusions are drawn.

2. Study Area

The Cordillera Blanca is situated in Áncash, Peru. Large parts of it are considered in this thesis (Fig. 1). The mountain range is margined by the Río Santa in the west. This river flows through Huaraz on around 3000 m above sea level (masl) and flows down to 1400 masl in the north of the study area. There are several peaks on altitudes above 6000 masl, including Nevado Huascarán, the highest mountain of Peru with 6768 masl (ÖAV, 2006). Therefore, big parts of the study area are glacierised or of its surface consist of bare rocks (1381 km^2). The remaining area (2861 km^2) consists of many steep slopes (for example Fig. 2A) which are on average around 23° steep. The large interval of the elevations leads to the above-mentioned variability of the soils. Some soils reach thicknesses of more than 2 meters, whereas in the higher elevations there are no soils anymore (Portes et al. 2016)

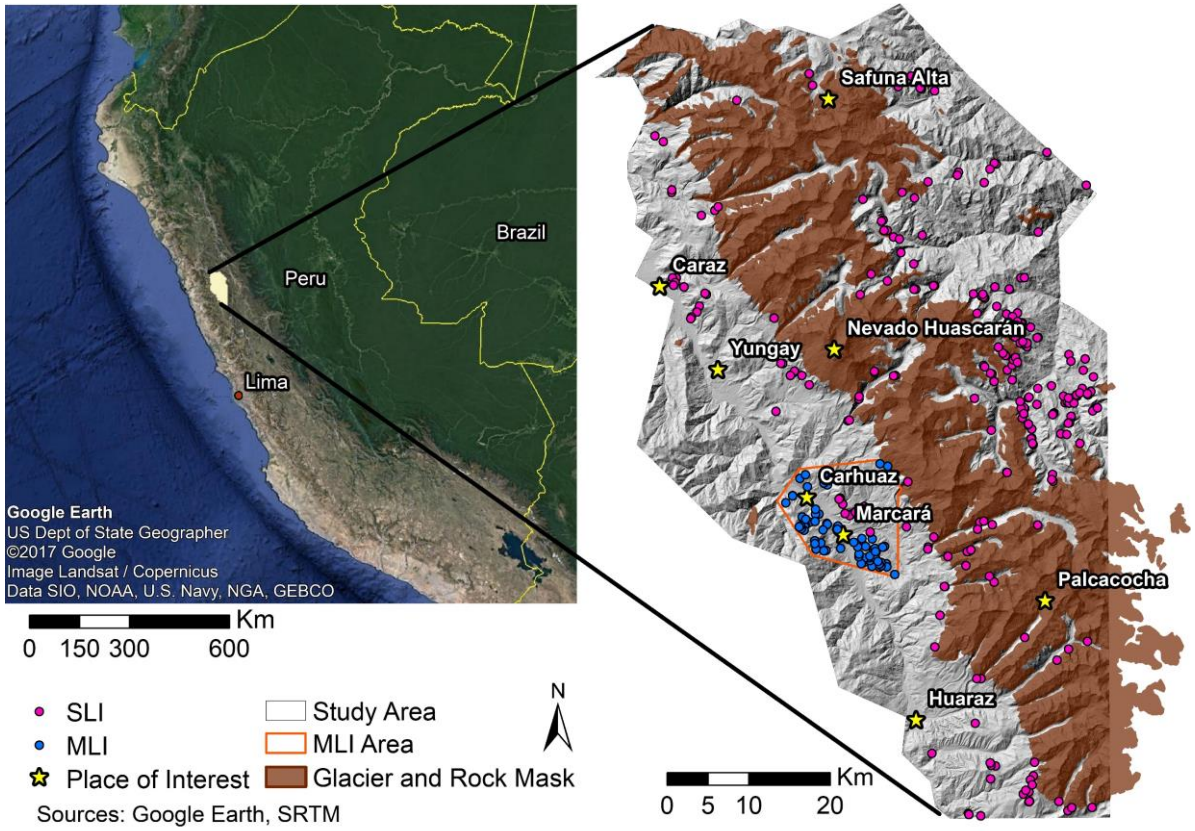

Fig. 1 Study area and landslide inventories. Overview map from Google Earth (2017). The term SLI refers to shallow landslide inventory, MLI to Marcará landslide inventory. More detailed view of the area around Safuna Alta and Marcará on Fig. 3

The climate is dominated by a dry and a wet season. During the wet season from October to March, about 400 to 800 mm of precipitation is recorded, generally increasing with elevation while during the dry season from April to September only 100 to 200 mm of precipitation is observed. This combination of steep topography, extreme precipitation, and other factors, such as earthquakes, led to several landslides in the past (see Fig. 1 and 2). Furthermore, this region is highly inhabited. Only the major towns of Huaraz, Yungay, Caraz, and Carhuaz together, all located in the Santa valley at the western foot of the Cordillera Blanca, have around 300'000 inhabitants (Instituto Nacional de Estadística e

Informática 2015). These conditions make it imperative to address landslide susceptibility zoning to make a first step towards increasing landslide resilience of the local population.

After having considered the whole study area as one, further research is done by just considering two smaller regions of the study area. The first is the region around the Safuna lakes (Safuna Alta and Safuna Baja) (see Fig. 3). It is in the northern part of the study area. The two lakes lay at the end of the Pucajirca Glacier and are on altitudes of 4330 masl (Safuna Alta) and 4244 masl (Safuna Baja) (ÖAV 2006). The two lakes are separated by a moraine which reaches elevations of around 4400 masl in its frontal part (Veliz et al. 1973). The water level of Safuna Alta is controlled by two tunnels (Portilla et al. 2000) of which the lower one is situated in the frontal moraine on 4330 masl (Veliz et al. 1973). In recent years, the water table did not reach the altitude of the tunnel. It stayed around 1 meter below the tunnel (Checa 2016). The two lakes belong to the accumulation area of the Río Quitaracsa which flows into the Río Santa (Portilla et al. 2000), passing a hydroelectric power station, close to the town of Huallanca (Hubbard et al. 2005). In 2002, a landslide of several millions m^3 of rock occurred close to Safuna Alta and big parts of it fell into the lake, causing a glacier lake outburst flood (GLOF). The terminal moraine was overtopped by a large wave. The bursting water masses led to a measurable increase of the water level in the hydroelectric power station in Huallanca which is about 40 km downstream (Hubbard et al. 2005).

The second region which is considered separately is the region around the town of Marcará (2748 masl) (see Fig. 3). The considered slopes are mainly the ones which are situated in the west of Marcará. This is not part of the Cordillera Blanca anymore, but of the Cordillera Negra (ÖAV 2006). This region is of specific interest because of two reasons. Generally, the whole region there is highly prone to landslides, because of its lithology, sparse vegetation, and other factors. Besides, several smaller landslides, in the northwest of the town already happened a deep-seated landslide which caused casualties and damaged properties in 2009 (Klimeš and Vilímek 2011). The other reason is the vulnerability. More than 47’000 people live in the region of Carhuaz, which includes Marcará (Instituto Nacional de Estadística e Informática 2015), and the airport of the Santa Valley to reach Huaraz is situated below these slopes. This airport was already blocked once by a debris flow which originated in the Cordillera Negra (Vilímek et al. 2000). Besides the risk at this location, a recent study by Strozzi et al. (submitted), who measured slope movements with Synthetic Aperture Radar Interferometry (InSAR) data in this region, made it reasonable to consider these slopes separately, as different datasets about this region they produced can be used for this thesis.

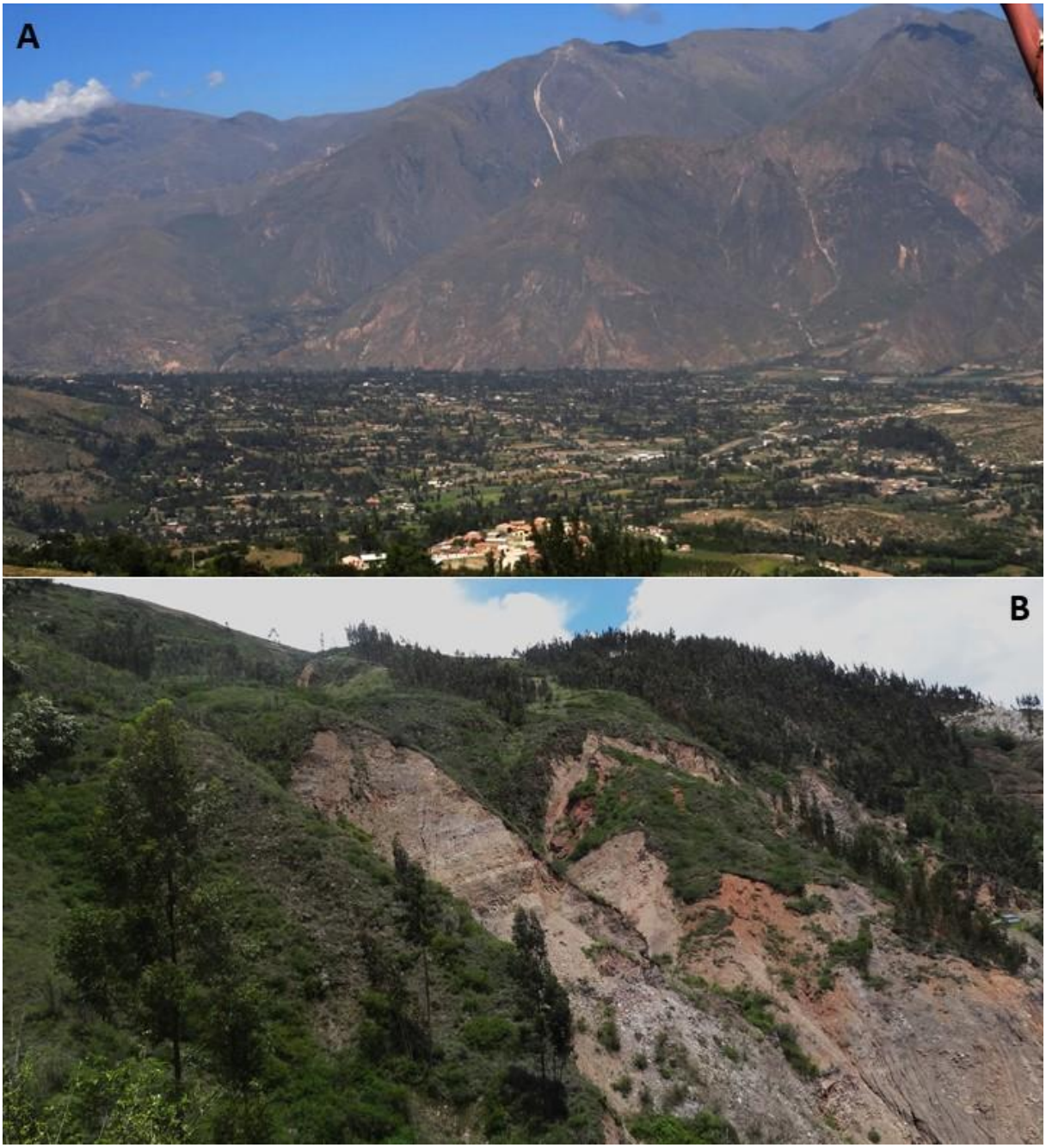

Fig. 2 A shows the steep and by landslide scarred landscape above Caraz and Yungay. B shows shallow landslides in the region of Yungay (Photos by E. Bueechi)

Fig. 3 Study area with a focus on the two smaller areas which are considered additionally (sources: Overview map by Google Earth, map of Marcará and Safuna by ÖAV (2006), Photos by E. Bueechi

3. Gravitational Mass Movements

This part of the thesis aims to understand the phenomenon landslides. This includes the morphology and terminology of landslides, two classifications systems, some basic laws of friction, and landslide causing factors. This chapter is, on the one hand, relevant for getting to know possibly meaningful factors for establishing models. On the other hand, it is crucial to understand landslides for the evaluation of the models (Guzzetti et al. 2012). For example, which parts of the mass movement are responsible for the movement and should therefore be modelled as insecure?

3.1. General Characteristics

The term landslide is a subcategory of gravitational mass movements. An exact distinction of what still belongs to landslides and what are other kinds of gravitational mass movements is not that clear, though. De Blasio (2011) defines landslides as movement of rock, debris, or soil due to gravity. The density of the moving mass needs to be higher than 1100 kg/m^3, thus, 10% higher than the one of water. The argument of the water content is used by other authors as well, but not with a that strict limit (Davies and Shroder 2014; Zepp 2014). This definition mainly excludes snow and ice avalanches, flood water waves, and suspension flows. Even though this exact limit seems a bit artificial, this definition is used for this thesis. Besides this restriction, the two terms gravitational mass movement and landslides are used as synonyms. Still, landslides, as showed in this chapter, are a diverse phenomenon. However, there are some characteristics and forms which they have all in common. Fig. 4 shows a rotational landslide. Some of the labelled landforms, like the crown and the main body occur in most landslides (Highland and Bobrowsky 2008). The terms of Fig. 4 are used as a basic for any description of landslides in the following.

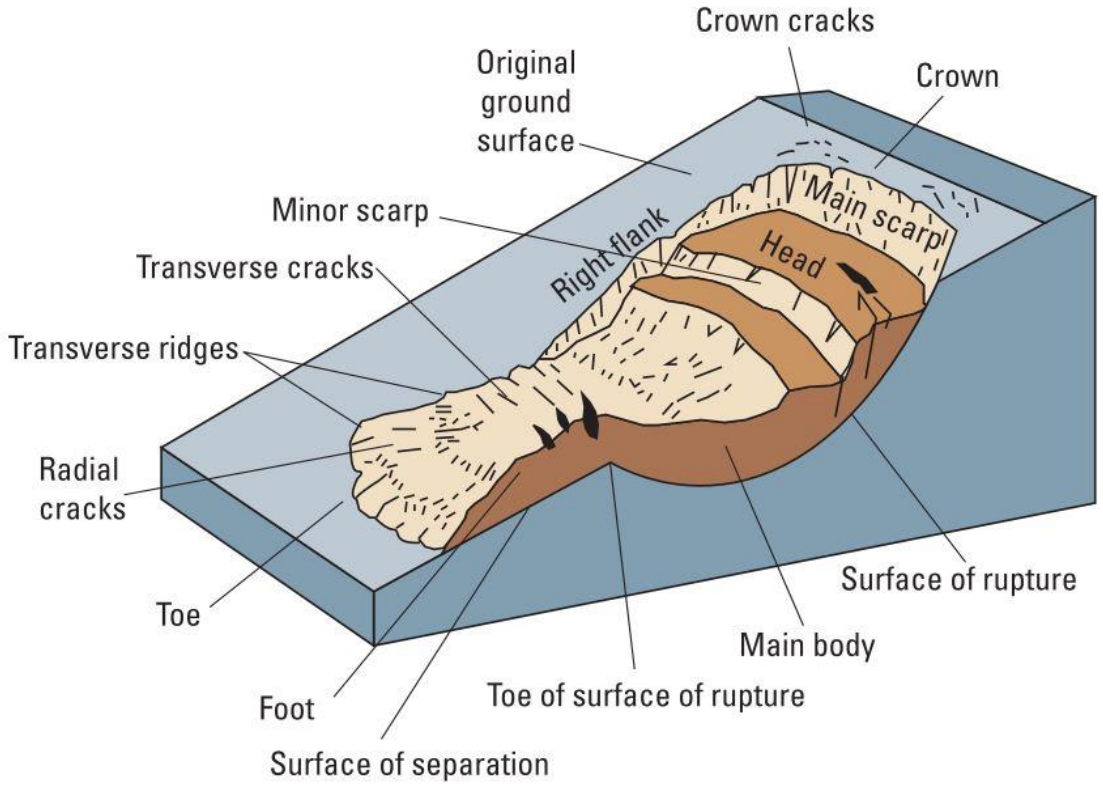

Fig. 4 Sketch of a rotational landslide with label of most important forms (Highland and Bobrowsky 2008)

3.2. Landslide Classification

The earlier mentioned collapse of the Nevado Huascarán was triggered by an earthquake. The falling mass consisted of snow, ice, and rocks (Evans et al. 2009). More than 30 years after this, in 2002, a big rock fall occurred close to Safuna Alta and triggered a GLOF (Hubbard et al. 2005). Within the same decade a deep-seated earth flow occurred in Rampac and destroyed several houses (Klimeš and Vilímek 2011). These are just three examples of bigger events. However, there are as well rapid, shallow landslides in the study area which occur much more frequently (See Fig. 1 and 2). Just by looking at all these different events it gets obvious that the term landslide is wide, and so are their causes and consequences. Triggering factors like earthquakes, intense rainfall, and anthropogenic activities and preconditioning factors like topography, geology, and soils are just some examples of causes (Corominas et al. 2014). This diversity makes it almost impossible to model landslide susceptibilities generally. Therefore, models like SINMAP and SHALSTAB among others just concentrate on shallow landslides (Wu and Sidle 1995; Dietrich et al. 1998; Pack et al. 1998; Baum et al. 2002; Haneberg 2004). Shallow landslides are as well the focus of this thesis. A description of what these shallow landslides are, and a categorisation of mass movements are the aims of this chapter.

Classification systems exist several ones and are as diverse as the mass movements themselves. An early one was developed by Sharpe (1938). He distinguished between slow- and rapid-flowage types, landslides, and subsidence (Sidle and Ochiai 2006). A slightly more complex one was then established by Carson and Kirkby (1972). The movements are there classified by their velocities and water content. They range from heave to slide and flow (Zepp 2014). There are other examples of different complexities (Hutchinson 1988; WP/WLI 1993; Cruden and Varnes 1996; Cruden and Couture 2011; Cruden and VanDine 2013). All of these classification systems are frequently quoted, but they are probably not as much used as the one of Varnes (Kienholz et al. 1984; Jäger and Wieczorek 1994; Deschamps and Lange 1999; Hungr et al. 2001; Popescu 2002; Malamud et al. 2004; D'Amato Avanzi et al. 2004; Galang et al. 2004; Witt and Kimberley 2005; Godt et al. 2006; Christanto 2008; Huggel et al. 2010; Bai et al. 2011; Cruden and Couture 2011; Kavzoglu et al. 2014; Pourghasemi et al. 2014; Scaioni et al. 2014). Varnes (1978) created a detailed classification scheme with around 20 different classes of mass movements (see Table 1). Especially his description of landforms, causes, and processes are useful for the classification of the landslides considered in this thesis. The first part of this chapter describes his work, as it is used as well as a basis for the second part. There, some of the classes of Varnes are summarised into more general, trigger-based classes, as done by Sidle and Ochiai (2006). They established a less differentiated scheme with only five categories. However, as these categories focus less on geomorphologic factors, but more on the required triggers it is frequently used as well (Turner et al. 2010; Safaei et al. 2011; Tsai et al. 2012; Lee and Park 2016). One of their classes, (rapid,) shallow landslides have been used a lot before their classification was published by many authors who modelled slope stabilities (Caine 1980; Wu and Sidle 1995; Dietrich and Montgomery 1998; Pack et al. 1998; Wang et al. 2005; Tsai and Yang 2006; Baum et al. 2008). Hence, such a trigger-based approach seems to be a reasonable classification for modelling landslide susceptibilities and is, therefore, mainly used in this thesis.

3.2.1. Varnes Landslide Classification Scheme

Already in the 1950s, when Varnes developed his first classification scheme, there were plenty of other ones (Heim 1932; Ladd 1935; Sharpe 1938). In fact, there were many concerns if there was still a need of a new scheme by then (Varnes 1958). Varnes (1978) himself justified his work with the words of Ward (1945): "*A classification of the types of failure is necessary to the engineer to enable him to distinguish and recognise the different phenomena for purposes of design and also to enable him to take the appropriate remedial or safety measures where necessary. The geographer, and geologist need a classification so that they may interpret the past and predict the present trends of topography as revealed by their observations.*" According to Varnes, these conditions were not met by the recent schemes. Hence, he developed his own scheme and updated it in 1978 and 1996 (Varnes, 1978; Cruden and Varnes, 1996).

The mass movements are classified mainly according to the type and rate of movement, its material, and the geometry of the failure plane (see Table 1). Especially the types of movements are analysed in the following. The focus here is laid on slides and flows, as these are the main concern of this thesis. The presented categories are the ones presented and described by Varnes (1978).

Falls

Falls occur mainly at steep slopes or cliffs. A mass is detached and usually falls through the air. Such movements are characterised by their high velocities and the separation of the mass from its source.

Topples

If there is enough pressure on the up-front part of a cliff or a steep slope, topples can happen. This means that an entire unit of the cliff starts rotating forward around a point below or low in the unit. In the end the whole mass just tilts over. The pressure required for this is usually exerted by freeze and thaw processes of water in cracks.

Slides

This category is still very heterogeneous. The term slide includes every movement which includes shear strain and a displacement of a mass along one or more surfaces. The development of the shear failure at the crown can be simultaneous or progressive. The latter means that local failure occurs, and the rupture area propagates. The proposed subdivisions of this class by Varnes (1978) consists, on the one hand, of a movement of few units or many units. The one of ‘few units’ slides predominantly homogeneous and constant over the whole area. ‘Many units’ means that the material is deformed and there are within the slide some almost independent units. On the other hand, slides can be subclassified into translational and rotational slides.

The main characteristic of rotational slides is their sliding surface which is curved concavely upwards. It looks like a rotation around an axis parallel to the surface. The so-called slumps have in most cases a sliding surface formed like a spoon (spoon-shaped landslides). Just when the crown gets wider the slide can have a cylindrical form. In the field, though, this uniform curvature happens rarely. The sliding surface is strongly influenced by faults, joints, bedding, and other discontinuities of the soil. Despite these differences, characteristic for rotational slides are their steep surface of rupture below the crown and sometimes an upwards thrusting area at the foot. This topography leads to ponding. Any further water which reaches the slump leads to high water content within the soil, as it is hindered of flowing further. The concerned regions keep being unstable until they attain a low slope angle.

The length of a rotational slide is limited by geologic factors or soil characteristics. Depending on where the slope angle of the sliding surface starts being faced upwards to the sliding direction the mass starts to decelerate.

Translational slides, on the other hand, are characterised by a quite planar surface of rupture. Therefore, there is no upwards thrusting area. The mass continues sliding until the shear resistance gets big enough again. The sliding mass is often much deformed and splits into many units. Like this, slides can then transform into flows, especially if there is much water included and velocities increase.

Table 1 Varnes landslide classification scheme. The term engineering soils describes aggregates of solid particles of natural mineral, rock, and inorganic matter. They can be loose, unconsolidated, or poorly cemented (Varnes 1978)

<table>
<tr><td colspan="3" rowspan="2">Type of movement</td><td colspan="3">Type of material</td></tr>
<tr><td rowspan="2">Bedrock</td><td colspan="2">Engineering soils</td></tr>
<tr><td>Predominantly coarse</td><td>Predominantly fine</td></tr>
<tr><td colspan="3">Falls</td><td>Rock fall</td><td>Debris fall</td><td>Earth fall</td></tr>
<tr><td colspan="3">Topples</td><td>Rock topple</td><td>Debris topple</td><td>Earth topple</td></tr>
<tr><td rowspan="3">Slides</td><td rowspan="2">Rotational</td><td rowspan="2">Few units</td><td>Rock slump</td><td>Debris slump</td><td>Earth slump</td></tr>
<tr><td>Rock block slide</td><td>Debris block slide</td><td>Earth block slide</td></tr>
<tr><td rowspan="2">Translational</td><td>Many units</td><td>Rock slide</td><td>Debris slide</td><td>Earth slide</td></tr>
<tr><td colspan="3">Lateral spreads</td><td>Rock spread</td><td>Debris spread</td><td>Earth spread</td></tr>
<tr><td colspan="3" rowspan="2">Flows</td><td rowspan="2">Rock flow
(deep creep)</td><td>Debris flow</td><td>Earth flow</td></tr>
<tr><td colspan="2">Soil creep</td></tr>
<tr><td colspan="3">Complex</td><td colspan="3">Combination of two or more principle types of movement</td></tr>
</table>

Lateral Spreads

Extension is the main process which leads to lateral spreads. This can either be an overall extension due to distributed movements without a well-defined basal shear surface, or more complex mechanisms of failure leading to different kind of movements of the coherent material. This second type of lateral spreads can as well be classified as complex movement, as they include many different mechanisms.

Flows

The velocities within flows are uniformly distributed. Between different flows, however, they can be divergent. There is a big variety of flows from slow to fast and from dry to wet. For a better differentiation Varnes (1978) splits it up into flows in bedrock and flows in debris and earth. The flows in bedrock requires many fractures of all sizes in order that the deformations can be distributed over a larger area and not concentrate on one single fracture. This usually results in very slow but steady flows.

Flows in debris and earth are easier to recognise as flows. The only difference there is to tell for example debris flows from debris slides. This is mainly done by the water content and the resulting cohesion, as well as the velocity and their composition. Hence, the higher water content of flows leads to higher velocities and lower cohesion. Additionally, it is possible in a debris flow, that there can be

some slump blocks at the head. This is usually not the case in debris slides. Flows typically have a bigger power and reach further than slides. Characteristic is the V-shaped channel they form.

As earth and debris flows are still very heterogeneous according to their grain sizes and velocities, they can be subdivided into categories like: subaerial flows, subaqueous flows, mudflows, and solifluction. The ones which shall be pointed out here are generally the rapid earth flows. They can happen in fine grained soils like clay and silt. Usually they occur in soils with a relatively low shear strength. The shear strength is then decreased to a small fraction by liquefaction of the whole mass. Earth flows can develop in a drier form too. Then, they are usually caused by earthquakes.

Complex

Landslides which cannot be assigned to one single of the precedent types belongs to this category of complex movements. This can be due to the variety of included materials or the combination of different movement types.

3.2.2. Sidle and Ochiai's Landslide Classification Scheme

Sidle and Ochiai (2006) base their classification mainly on the triggering factors, the velocity and depth of the movement, and the involved processes. The resulting categories are "shallow, rapid landslides", "rapid, deep slides and flows", "slower, deep-seated landslides", "slow flows and deformations", and "surficial mass wasting". These classes are introduced in the following, based on the descriptions by Sidle and Ochiai (2006).

Shallow, Rapid Landslides

As proposed by their name, shallow, rapid landslides occur mainly in shallow soils (<2m depth) (see Fig. 2B and 5). They require soils with low cohesion and usually occur on slopes with a inclination higher than 25°. Additionally, the surface of rupture is often a layer with low permeability, and is approximately parallel to the surface of the soil. Therefore, the processes of rotational slides defined by Varnes (1978) are excluded of this class. It includes debris and earth slides and flows (thus, it is congruent with the kind of mass movements Pack et al. (1998) wants to model). Shallow, rapid landslides are influenced by land management. Especially close to roads such failures are frequent (see Fig. 5).

The described mass movements share similar geomorphologic evidences. They are recognisable by the crown, the main scarp, and usually the foot. Characterisitically, they are longer than wide and are at least ten times longer than their depth.

Fig. 5 Shallow, rapid landslides on the eastern slopes of the Cordillera Blanca close to Piscobamba, Peru (Photo by E. Bueechi)

Rapid, Deep Slides and Flows

This category is similar to shallow, rapid landslides. They occur as well on steep slopes within materials of low cohesion. However, as they are deep seated (>5m) they have a bigger potential of damage, have different triggers, and require other management activities. The decisive factor is a liquefaction along the surface of rupture. For sites which do not have any tension cracks extending from the soil surface to the regolith large amounts of antecedent rainfall is needed. For those which have such cracks or fractured bedrock single events of rainstorms can trigger a failure. More frequent, though, are earthquakes, after or during the rainfalls, the triggering factor. Unlike shallow, rapid landslides, rapid, deep slides and flows are not much influenced by human land management. In terms of the Varnes classification debris slides and flows, (bed-)rock slides, block slides, and earth flows can be part of this category.

Slower, Deep-Seated Landslides

Slow means that the movement rates are within a range from millimetres per year to a maximum of some meters per day. They do not need as steep slopes as the precedent categories. Undeveloped drainage system can cause these landslides as well on moderately steep slopes. The movement can stop during the dry season and is then reactivated as soon as the critical level of groundwater is reached again. Further water input afterwards can dramatically increase the velocity.

Slow Flows and Deformations

The required soil characteristics are similar to the ones of slower, deep-seated landslides. Slow flows and deformations can happen in many different depths of soils and are not much dependent on the cohesion neither. Generally, the movement rates are very low, and they are dependent on cumulative rainfalls. The velocity characteristically decreases within the flow with increasing distance from the surface. Therefore, there is no real surface of rupture. The most common type of landslides defined by Varnes belonging to this category is soil creep. The risk soil creep pose mainly concerns properties. Just if they transform into deep-seated or rapid shallow landslides they can endanger humans as well. Other subcategories like gelifluction are not only gravity-driven, but also dependent on freeze-thaw mechanisms.

Surficial Mass Wasting

Surficial mass wasting mainly describes individual grains, aggregates, and fragments which move downslope by rolling, sliding, or bounding. This can be caused by the loss of interlocking frictional resistance due to freeze-thaw and wetting-drying cycles. This is a frequent phenomenon on steeper slopes with right conditions concerning moisture, temperature, wind, and exposition. It is not considered having a high potential to endanger properties nor humans.

3.2.3. Implications for This Thesis

The more diverse classification of landslides by Varnes provides a detailed description of mass movements. The three main materials and the six processes combined, sum up to 23 different kinds of slope movements. Additionally, there is some information about possible triggers as well. This combination of diverse classification and information about triggers are probably a reason, why it has been frequently cited by many authors.

From a modelling point of view, though, it seems to be a rather too fine classification. Pack and Goodwin (2001), the developer of SINMAP, for example point out that their model is for all kind of shallow translational landslide phenomena. Similarly state Dietrich et al. (1998), one of the developer of SHALSTAB, that their model is a tool for mapping the potential of shallow landslides in general. This implies that both have used a different and more coarse classification scheme. Therefore, the other landslide classification scheme of Sidle and Ochiai was introduced. They just use five classes to categorise the phenomena of landslides. Hence, it is much less differentiated than the one of Varnes. Its main advantage is that it is more trigger-based. Landslides which have similar causes are put together. Therefore, in this thesis the second classification scheme is mainly used.

3.3. Mechanics of Landslides

The analysis of slope stabilities has existed for more than 100 years now. In 1916, a first method of splitting the sliding body into several slices was established (Petterson 1955). Since then many other strategies of how to deal with landslides from a physical perspective developed (Morgenstern and Price 1965; Fredlund and Krahn 1977; Krahn 2003). The most commonly used nowadays is the method of limit equilibrium analysis with the factor of safety (Baum et al. 2002; De Blasio 2011; GEO-SLOPE International Ltd. 2012; Hartge et al. 2014; Griffiths 2015; McColl 2015). The factor of safety is defined as the ratio of the resisting forces (shear strength) and the driving forces (shear stress). As soon as the shear stress exceeds the shear strength the slope is unstable and is expected to fail. The involved forces can be assessed on many different levels of complexities. There are nonlinear solutions (Cheng and Zhu 2004), solutions which are split into different summands (Krahn 2003), 3D solutions (Xie et al. 2006) or comparatively simple solutions (Pack et al. 2005; Sidle and Ochiai 2006; Zepp 2014). For this thesis one of these simpler solutions has been chosen, as the included parameters are similar for all. Eq. 1-5 show the factor of safety used by Sidle and Ochiai (2006).

For the use of this model several simplifications have to be assumed. First, the bedding plane is smooth and parallel to the groundwater table and the ground surface. Second, a potential slip surface is sufficiently longer than the depth of the moving body. Third, an infinite slope with a constant angle is considered (Sidle and Ochiai 2006). Fig. 6 shows some of these simplifications and the forces acting on the soils. The relevant formulas for the involved forces are as followed:

$$S = c + (W * \cos[\beta] - u) * \tan(\phi) \quad (1)$$

where S = shear strength, c = cohesion of the soil, W = weight acting on slice, β = slope angle, u see Eq. 2, and ϕ = internal friction angle

$$u = \gamma_w * h * \cos^2(\beta) \quad (2)$$

where γ_w = unit weight of water (9.81 kN/m^3) and h = vertical depth of water table

$$W = (\gamma_t * [D - h] + \gamma_{sat} * h) * \cos(\beta) \quad (3)$$

where W = weight acting on slice, γ_t = moist unit weight of soil (above groundwater), D = vertical soil depth, and γ_{sat} = saturated unit weight of soil

$$T = W * \sin(\beta) \quad (4)$$

where T = shear stress

The factor of safety (FS) can be defined out of this equations as the ratio of the shear strength and the shear stress. This then results in:

$$FS = \frac{c}{W*\sin(\beta)} + \frac{\tan(\phi)}{\tan(\beta)} - \frac{u*\tan(\phi)}{W*\sin(\beta)} \quad (5)$$

Out of a physical point of view a landslide occurs as soon as the denominators exceed the numerators. The denominators are dependent on the cohesion, the internal friction angle, the height of the groundwater table, and the slope angle. The unit weight of water is as well part of u, but as it is a constant it is not further considered. The destabilising factors are the slope angle (twice as sinus, once as tangent, and once as cosine), the unit weights of moist and saturated soils, and the vertical depths of the soil and the water table (Sidle and Ochiai 2006). These factors and their impact on the formulas are presented here (see Fig. 7).

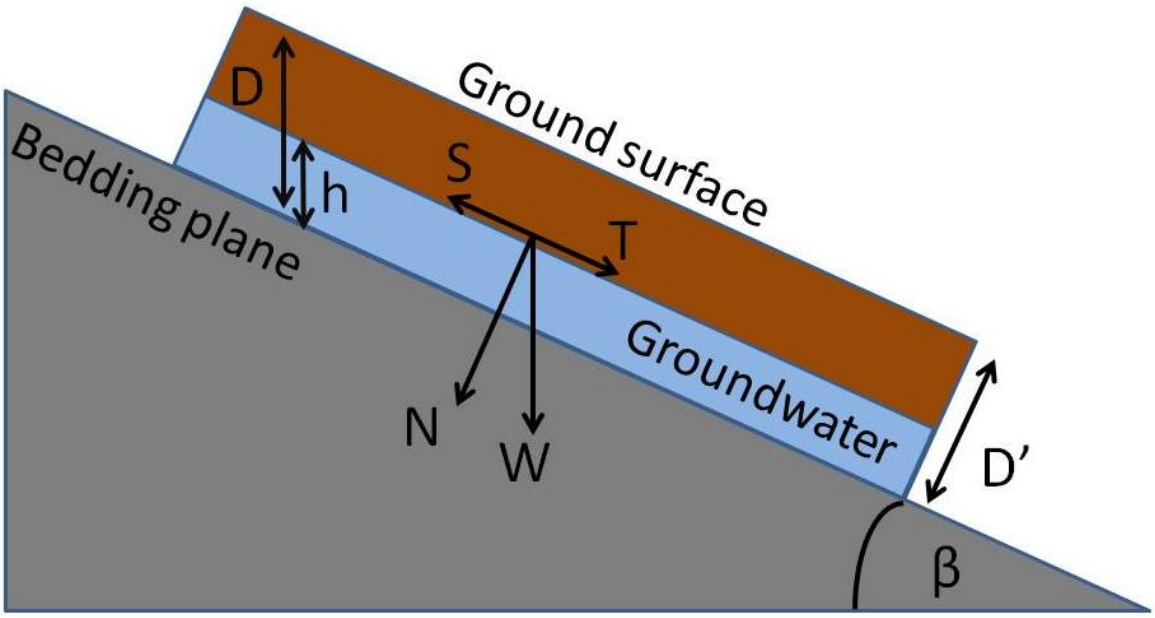

Fig. 6 Basic Laws of Friction. β=slope angle; D=soil depth (vertical); D'=soil depth (orthographic); h=vertical depth of water table N=normal force along sliding surface (=W*cos(β)); S=shear strength; T=shear stress; W=weight acting on slice (modified after De Blasio, 2011; Sidle and Ochiai, 2006)

3.3.1. Cohesion

Cohesion is the resistance force which accompanies shear deformation resulting of an applied shear force. It is measured in Pa and is in soils usually in the range of some kPa and for rocks even some MPa (De Blasio 2011). The force of cohesion consists of different other forces: electrostatic bonds between clay and silt particles, organic matter which causes cementation, and van der Waals forces. It is impacted by the water content (Sidle and Ochiai 2006). Wet sands, for example, have little water bridges between the particles which results in negative pore pressure, thus, higher cohesion (De Blasio 2011). As soon as there is too much water between the grains, they lose contact. The soil is then even more unstable than in a dry state (Grotzinger and Jordan 2017). This effect of water on the stability of soils was already examined by Thorne and Tovey (1981). They compared the erosion of two similar slopes, but one with wet and the other with dry material. According to them, the stability of the dry

and therefore cohesionless material is just dependent on the slope angle and the internal friction angle. This makes this soil vulnerable to erosion due to water. This is not the case for the wet, thus, cohesive material. There, they did not observe much movement. Besides this dependency on the water content another factor influencing the cohesion needs to be pointed out: roots. Schmidt et al. (2001) split the total cohesion into the two factors effective cohesion of soils and the apparent cohesion provided by roots. They conclude that root cohesion varies significantly between the vegetation types and is in the range of some kPa to more than 90 kPa for some trees. These different types of cohesion together have a linear influence on the factor of safety (see Eq. 5). It increases with increasing cohesion (see Fig. 7).

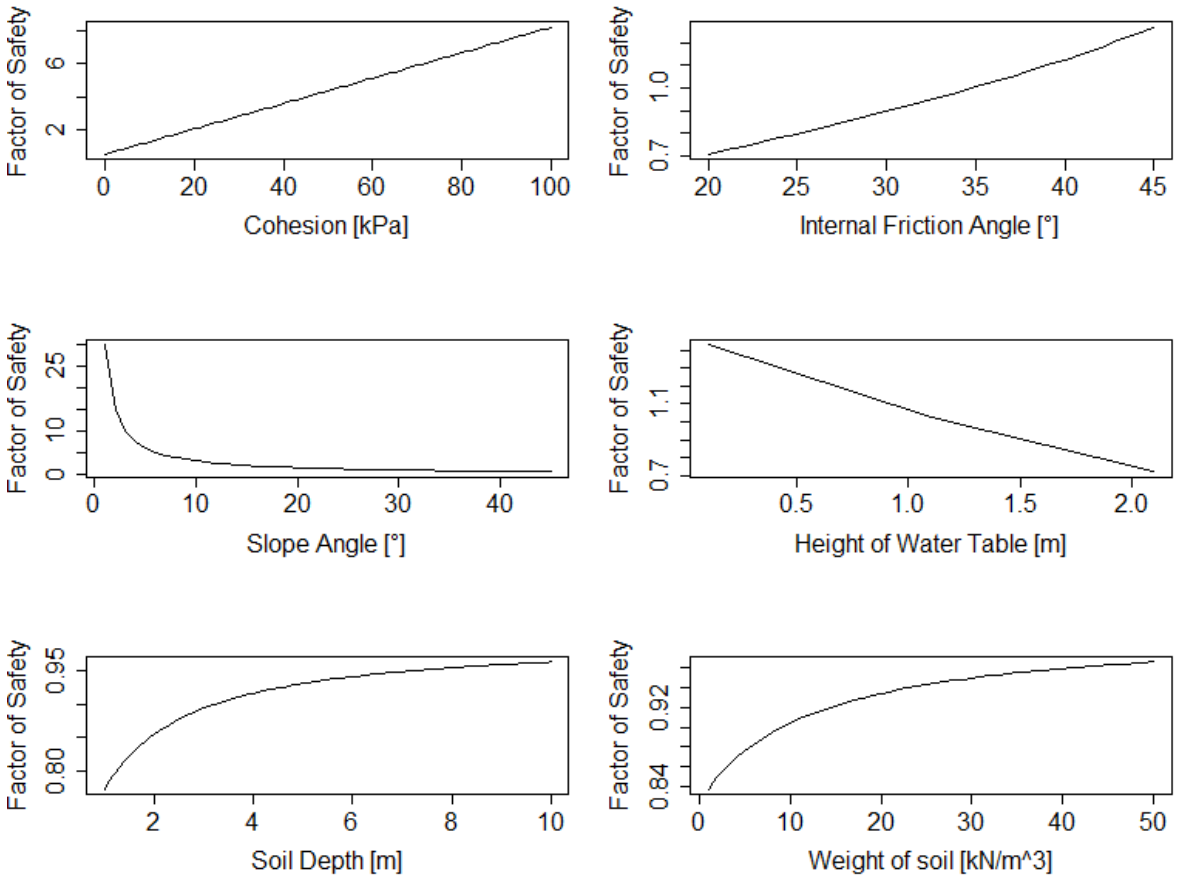

Fig. 7 The different parameters influencing the factor of safety. The different lines represent a variation of the considered parameter within reasonable ranges. The not considered parameters are put as a constant. For example, the graph on the top left represents the factor of safety for constant values of all parameters, except the cohesion which varies from 1 to 100 kPa. The constant values are set as followed: cohesion=5 kPa (De Blasio 2011), internal friction angle=30° (Schellart 2000), slope angle=30°, height of water table=1.5 m (except for variations of soil depths, there 0.1 m is used), soil depth=3 m (Crosta and Frattini 2003), unit weight of moist soil=8 kN/m³, unit weight of saturated soil=13 kN/m³ (Capparelli and Versace 2014), unit weight of water=9.81 kN/m³ (Thorne and Tovey 1981). The influence of some of the parameters changes when the constants are set differently. The internal friction angle, for example can correlate negatively with the FoS for high values of u

3.3.2. Internal Friction Angle

If the considered material is dried and bulked on a plane, the internal friction angle is the slope angle the developed accumulation takes (Zepp 2014). This angle is dependent on different factors like size and shape of the grains. Bigger and flat particles can withstand steeper slope angles (Grotzinger and Jordan 2017). The range of possible values starts approximately at 26° for some sandstones and can reach around 45° for Blair dolomite (Schellart 2000).

Its influence on the slope stability is positive: the higher the internal friction angle, the higher is the slope stability (Zepp 2014) (Fig. 7). Looking at Eq. 5 this is not that clearly visible. It is twice in the formula as a tangent on the numerator. As it is within a tangent function the value increases fast with a higher internal friction angle. However, the term appears twice in the formula, and the second time it is negative (-u*tan[ϕ]). Thus, its influence on the factor of safety is not as big and more dependent on the particular ratios of the second summand and the subtrahend.

3.3.3. Slope Angle

Many slope stability modellers consider the slope angle as one of the most important preconditioning factor of landslides (Swanston 1973; Lee et al. 2002; van Beek et al. 2002; Sidle and Ochiai 2006; Yilmaz 2009; Felicísimo et al. 2012; Kavzoglu et al. 2014; Pourghasemi et al. 2014; Posner and Georgakakos 2015). Fig. 7 supports this assumption. In the graph of the slope angle the variations of the factor of safety is biggest. The factor of safety decreases from over 30 in flat regions to less than 1 for slope angles bigger than 15°. This gets clear as well from Eq. 4. There the shear stress is defined as X*cos(β)*sin(β) (X is always positive and independent of β). This means that the shear stress increases rapidly with the slope angle, especially in the first 10-20 degrees.

3.3.4. Water Table

The height of the water table has an influence on two parameters of the factor of safety. u increases linearly with the water table and is subtracted of the shear strength. Additionally, it is included in W, and therefore twice in the denominator. Therefore, a higher water table leads the a lower factor of safety. Cohen et al. (2009) explains this mainly with the positive pore water pressure which develops. Two other processes are pointed out by them. First, there is additional loading as saturated soil is heavier than moist soil. This is expressed as well in Eq. 3. The weight acting on the slice increases with a higher water table. The second process Cohen et al. (2009) point out, is that the cohesion is reduced as soon as a certain wetness of the soil is exceeded. Another important characteristic of the water table is its high variability. It can change rapidly with severe consequences for the slope stability. Heavy rainfall or snowmelt events can cause sudden increase of the water table and raise the shear stress (Sidle and Ochiai 2006; McColl 2015), and with its effect on the cohesion reduce the shear strength at the same time (Hartge et al. 2014; Zepp 2014).

3.3.5. Soil Depth

The soil depth is here defined as the vertical soil height of the ground from the surface to the bedding plane (Sidle and Ochiai 2006). For the considered shallow landslides this corresponds to the actual soil depth (Pack et al. 2005). The factor of safety just increases slightly with increasing soil depth (see Fig. 7). Its influence is restricted to the difference of the soil depth and the height of the water table (see Eq. 3 and 4). Hence an increasing soil depth does not change anything when the water table raises simultaneously. In practice, though, higher soil depths are considered to rather reduce the stability of soils, when considered independently from the water table (Sidle and Ochiai 2006; McColl 2015).

3.3.6. Weight of Soil

The weight of the soil influencing the factor of safety needs to be differentiated. The first one is γ_t, the unit weight of the soil (Sidle and Ochiai 2006). This may vary between the horizons, but does not change rapidly over time (Capparelli and Versace 2014). The second definition of the weight of soil is the whole weight acting on the bedding plane, defined as W in Eq. 3 (which includes γ_t). They both correlate positively with the factor of safety. What is not considered here, though, is an additional external load. External loads can act contrarious as preparatory and triggering factors (McColl 2015) (see as well the following chapter 3.4).

3.4. Preconditioning, Preparatory, and Triggering Factors

The occurrence of landslides is dependent on three different factors: preconditioning factors, preparatory factors, and triggers (Zimmermann et al. 1997; McColl 2015). Preconditioning factors describe slope characteristics which influence slope stability and are constant on timescales of decades to centuries. Preparatory factors are more variable over time. They reduce the stability of slopes but do not initiate failures (t0-t3 on Fig. 9). The factor which then causes the landslide is the trigger (see Fig. 8, Fig. 9 at t4). The border between preparatory factors and triggers can be fluent (McColl 2015). All these factors concerning shallow, rapid landslides are described in the following subchapters.

3.4.1. Preconditioning Factors

Preconditioning factors are mainly related to the relief and the included material. Landslides are favoured by a high relief energy (Zimmermann et al. 1997), hence high differences of altitudes in small areas (Burak et al. 2006). This is due to the fact, that this leads to steeper slopes, what is considered by many authors as a crucial preconditioning factor, as mentioned before. Increasing slope angles enhance the landslide susceptibility until slope angles around 45°. Afterwards, the susceptibility decreases again, due to a lack of soil, as they constantly erode (Sidle and Ochiai 2006). Sidle and Ochiai (2006) complement that it is still just one of many factors, as shallow landslides generally occur on slope angles between 20° and 67.5°. This wide range which includes many stable slopes too shows that there need to be as well other factors. One of which is the curvature. Divergent and convex landforms

are less susceptible to landslides. This is due to the distribution of the subsurface water flow, which can be more easily distributed over larger areas for these two forms. Convergent or concave landforms, on the other hand, enhance the accumulation of subsurface water, leading to higher pore-water pressures. This increases the susceptibility (Sidle and Ochiai 2006). Furthermore, there are two other relief-related factors which have an indirect impact on the landslide susceptibility: elevation and aspect. They have an influence on the weathering of soils and their development (Zimmermann et al. 1997) and further developed soils, are more susceptible to landslides (Sidle and Ochiai 2006). Elevation and aspect affect hydrologic processes, mainly via evapotranspiration, as well. North-facing slopes in the northern hemisphere are usually wetter (Sidle and Ochiai 2006). These two factors of the soil development and wetness lead to the assumption, that north-facing slopes in the northern hemisphere, south-facing slopes in the southern hemisphere respectively, are more prone to landslides. Empiric studies, however, have found as well contradicting or insignificant results (Lineback Gritzner et al. 2001; Dai and Lee 2002; Ayalew and Yamagishi 2005; Gokceoglu et al. 2005; Yilmaz 2009). Therefore, Sidle and Ochiai (2006) conclude that the aspect does have an influence on the mentioned factors, but other factors can relativise its impact.

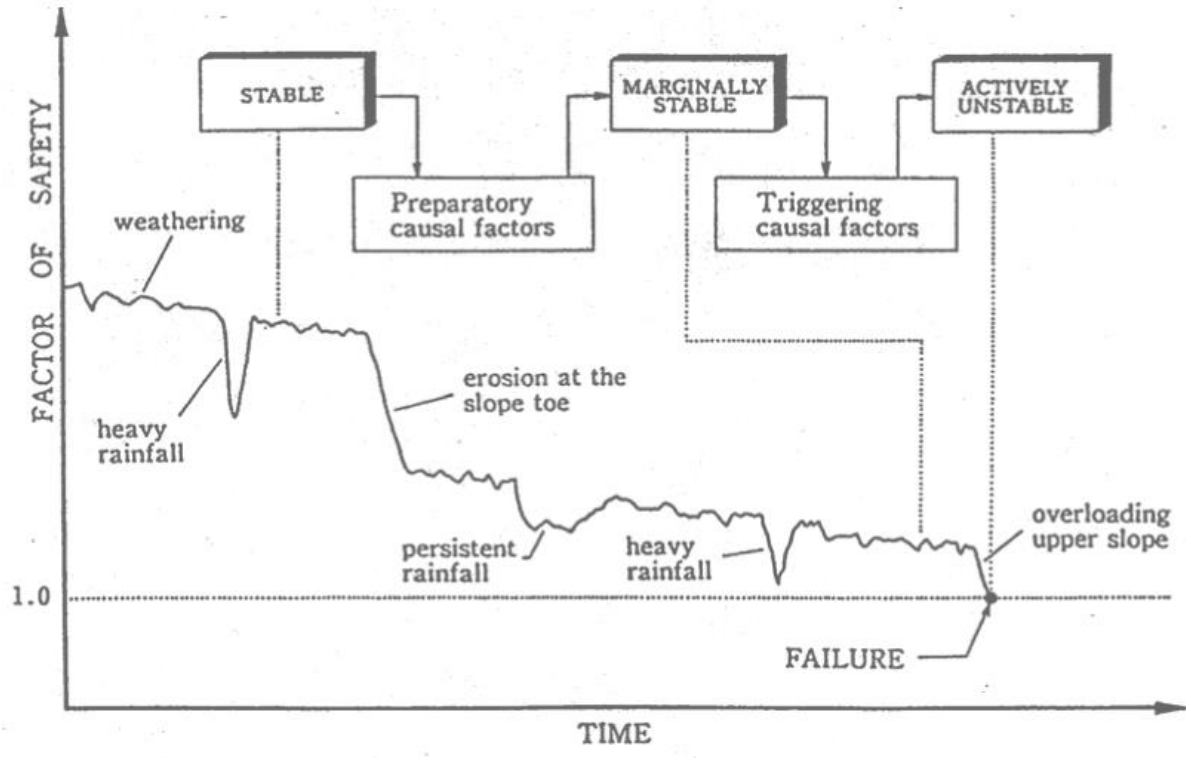

Fig. 8 Explanation of different stability states of a slope, and factors which can change these states (Popescu 2002)

The included materials concern the soils, and the geology (bedrock and parent material) (McColl 2015). For defining the susceptibility of soils, looking at their shear strength is crucial (Sidle and Ochiai 2006). This is mainly composed by the cohesion, internal friction angle, and the depth of the soils (Eq. 1-3). Their influence is explained in the previous chapter. Additionally, it is of importance how the soil

horizons are composited. Stiff horizons overlaying weak plastic horizons enhance susceptibilities (McColl 2015) just like changes of the permeability. A permeable horizon above an impermeable horizon leads to fast saturation during rainfall what can cause failure (Cruden and Lan 2015). Due to this reason clay-rich horizons can act as a good sliding plane (Sidle and Ochiai 2006). Soils which change their characteristics fast when water enters the system are critical too (Glade and Crozier 2005a).

Geological factors which can enhance the slopes susceptibility to shallow, rapid landslides are diverse (Cruden and Varnes 1996). The weatherability of the parent material plays an important role. Even though, this is not only dependent on the geology, but as well on the predominant kind of weathering. Sidle and Ochiai (2006) state that for example granite rocks weather slow compared to other rocks in regions of predominantly physical weathering. In regions with high chemical weathering, though, granite rocks weather fast. This is probably a reason why Glade and Crozier (2005a) consider as well vegetative and climatic conditions as preconditioning. Further influences of the geology are mainly related to the vulnerability of the bedrock to different preparatory factors which are described in the following subchapter.

3.4.2. Preparatory Factors

Preparatory factors are variable over time. Depending on the factor the considered time-scale where it varies can be days to centuries. One of the main factor here is water related. Periods of intense rainfall or snowmelt can increase the groundwater table and the pore-water pressure and, therefore, reduce the stability of the soil (Popescu 2002). Human reasons for changing groundwater levels can be irrigation and broken pipes. Over a time period of some decades, climate change can have an impact on the groundwater level too (McColl 2015). One of the rather long-term changing factors is the increase of the slope steepness caused by tectonic uplift (Glade and Crozier 2005a). The slope angle can increase in shorter time as well due to fluvial, marine, and glacial erosion (McColl 2015). Humans can change it even faster with construction work or mining (Cruden and Lan 2015). Another rather slow process is weathering (Glade and Crozier 2005a). The cohesion is reduced when the bare rock surface is turned into soils (Sidle and Ochiai 2006). The already developed soils or as well the bedrock can be undercut by fluvial or marine erosion (Zimmermann et al. 1997). Similar impacts can have the construction of roads (McColl 2015). This leads to a lower stability of the slope as the stabilising effects of the slope toe are removed (Zimmermann et al. 1997). In glacierised regions debuttressing is a common preparatory factor. The retreat of the glaciers or the permafrost can destabilise slopes and expose them (Huggel et al. 2013). Further important factors are deforestation (Glade and Crozier 2005a; Cruden and Lan 2015) what removes the root cohesion (Schmidt et al. 2001), or the loading of the slopes. This final factor mentioned here can be produced by humans or naturally by landslides or other loads (Cruden and Lan 2015; McColl 2015).

3.4.3. Triggering Factors

One of the most frequent trigger for shallow, rapid landslides is water. Soils which receive too much moisture get oversaturated and may start sliding. This water can come from different sources. Long or convective precipitation, rapid snow and ice melt, and GLOFs are the most frequent ones (Zimmermann et al. 1997; Van Asch et al. 1999; Glade and Crozier 2005a; De Blasio 2011; McColl 2015). McColl (2015) mentions as well the other extreme: the absence of water. The drawdown of groundwater can decrease cohesion what can cause a failure of the slope as well. Other strength reducing factors which can lead to active instabilities are decreasing permafrost area, weathering, and stress-induced fatigue (McColl 2015). A typical stress increasing factor is seismic shaking caused by earthquakes (Glade and Crozier 2005a; Lin et al. 2008; Chen et al. 2011; de Blasio 2011) or by explosions (Crozier and Glade 2005). Additionally, volcanic eruptions, slope undercutting or slope overloading can act as triggering factors too (Crozier and Glade 2005).

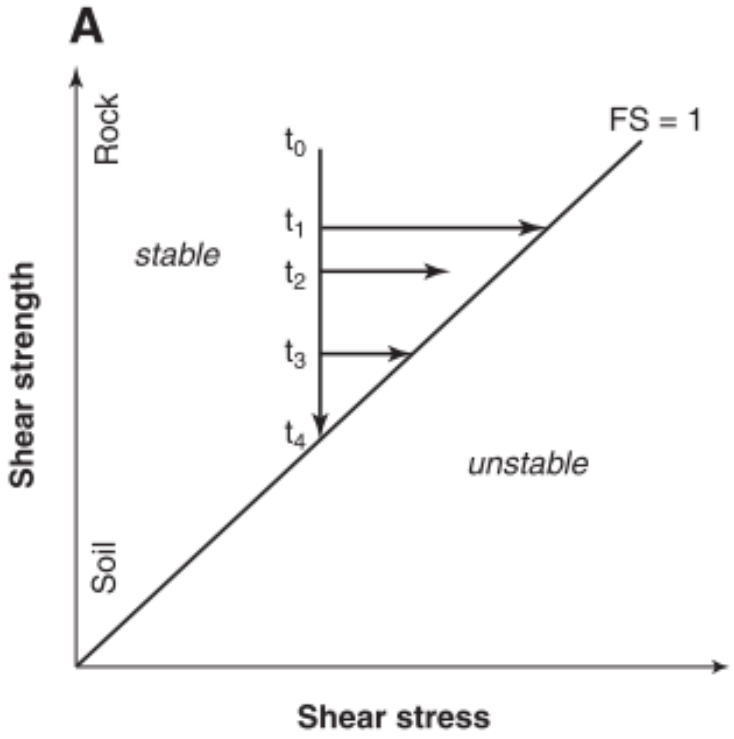

Fig. 9 t0-t3 show different states of stabilities during the process of destabilisation due to preparatory factors. T4 changes the slope into the state of active instability, thus shows a triggering event (Huggel et al. 2012a)

3.4.4. Implications for the Study Area

Concerning the preconditioning factors, it can be stated, that the study area extends over elevations from 1400 masl to 6768 masl. These elevations often change over small distances (see chapter 2 and Fig. 18 where the slope regression model indicates the steepness of the slopes). This leads to a high relief energy. Other preconditioning factors like curvature, elevation, and aspect are mainly too variable over the study area (ÖAV 2006), to make any generalisations. The predominant geologic

settings in the study area consist of granodiorite and glaciofluvial deposits (INGEMMET 1999). The weathering is dependent on the region (vegetation cover, altitude, etc.) and can be chemical and physical (Portes et al. 2016). Hence, general implications for the study area from a geologic point of view, is imprecise too.

The precipitation and the related pore water pressure can act as preparatory and as triggering factor for landslides. In the Cordillera Blanca rainfall mostly occurs in the months between October and March. Depending on the location and altitude within the study area, between 400mm and 800mm of precipitation occur in these months on average. In the southeast of Huaraz extreme events of 100 mm within 5 days are expected to happen with a return period of around 40 years (Schauwecker et al. 2017).

The worldwide trend of retreating glaciers and permafrost degradation is observed in the Cordillera Blanca as well (Kaser et al. 1990; Mark and Mckenzie 2007; Vuille et al. 2008; Baraer et al. 2012; Schneider et al. 2014). This leads to the debuttressing effect which can act as preparatory and triggering effect.

Earthquakes are frequent in Peru. Even earthquakes with magnitudes of Mw 6 or larger have been observed a lot in the past (Suárez et al. 1983; Bellier et al. 1991; Lemoine et al. 2002; Daniels et al. 2009; Grant et al. 2015; Lacroix et al. 2015; IGP 2017; Ruiz et al. 2017). The distribution within the country shows, that Áncash is one of the most affected regions of Peru (Bernal et al. 2002). The already mentioned devastating landslide of Nevado Huascarán in 1970 was triggered by an earthquake (Lliboutry 1975; Carey 2010). Hence, earthquakes can be expected to have an impact on landslides in the study area. Less likely are influences by volcanic eruptions, as the closest active volcano is around 700 km north of the study area in Sangay, Ecuador (Siebert et al. 2010).

4. Methods and Data

4.1. Landslide Susceptibility Models

4.1.1. SINMAP

Stability Index Mapping (SINMAP) is a physically based slope stability model developed by Pack et al. (1998). As an extension of the program ArcGIS it calculates for each grid cell of a given DEM the stability index (SI) (Pack et al. 2005). The SI is based on a dimensionless form of the infinite slope stability model's factor of safety (FS) (see Eq. 6). This is a slight adaption of the FS presented in Eq. 5. The FS used by SINMAP includes a term for the relative wetness index (w) additionally (Eq. 8). The height of the water table is not included here, unlike the FS by Sidle and Ochiai (2006) presented before. For the final calculation of the SI (Eq. 9), though, it is used again.

$$FS = \frac{C+\cos(\beta)[1-w\frac{\rho_w}{\rho_s}]\tan(\phi)}{\sin(\beta)} \quad (6)$$

where C = cohesion which is used in a dimensionless form (see Eq. 7), β = slope angle, w = relative wetness index, ρ_w = density of water, ρ_s = density of the soil, and ϕ = internal friction angle.

$$C = \frac{C_r+C_s}{h*\rho_s*g} \quad (7)$$

where C_r = root cohesion, C_s = soil cohesion, h = perpendicular soil depth, and g = gravitational constant. The water destabilising effects on the FS is represented by the topographic wetness index (TWI) which provides the value of w. This value is used to include the upslope area which drains into given grid cells.

$$w = \mathrm{Min}(\frac{R*a}{T*\sin(\beta)}, 1) \quad (8)$$

where R = steady state recharge (m/hr), a = contributing upslope area per unit contour length [m^2/m], and T = soil transmissivity [m^2/hr] (ex. hydraulic conductivity [m/hr] times soil thickness[m]). The combination of these two generalised assumptions (FS and TWI, see Eq. 6-8) results in the SI.

$$SI = \frac{C_r+C_s+\cos^2(\beta)[\rho_s g(D-D_w)+(\rho_s g-\rho_w g)D_w]\tan(\phi)}{D\rho_s g\sin(\beta)\cos(\beta)} \quad (9)$$

where D = vertical soil depth and D_w = vertical height of the water table. The required parameters can either be used as proposed by the authors (see Table 2) or they can be updated manually if further information about the soils are available. For this thesis the default values are used, as the study area has a big extent and highly variable soil characteristics. The other parameters can be derived from the DEM (Pack et al. 1999). At first a pit fill is applied on the DEM, to raise all points which do not drain, up to a point where they drain again. Then, the remaining required parameters like the slope angle, flow direction and flow accumulation are calculated. Afterwards, w and the SI can be calculated. This is done using different values of the soil characteristics within the defined interval. Points which are still stable under the worst case scenario, what means lowest cohesion and internal friction angle, and highest transmissivity / effective recharge, obtain an FS larger than 1 (Pack et al. 2005). In doing so, SINMAP tries to handle not only the spatial variability of the soil characteristics, but the temporal variability too (Meisina and Scarabelli 2007). For these calculations several simplifications with respect to landslide occurrence need to be assumed. (I) The water table is parallel to the soil surface and the layer below. (II) The layer below the soil is relatively impermeable. (III) The shallow lateral flow can be derived from the surface topography and therefore follows the topographic gradient. (IV) There is an equilibrium of the lateral discharge at each point and the steady state recharge. (V) T*sin(β) defines the capacity for lateral flux at each point (Pack et al. 1998).

Table 2 Default values for the required soil characteristics (Pack et al. 1999)

Transmissivity / effective recharge	2000-3000m
Dimensionless cohesion	0-0.25
Internal friction angle	30-45°
Soil density	2000 kg/m^3

The obtained SI values for each grid cell are then classified into six different classes. The most stable class includes all cells with SI values higher than 1.5 and is called “Stable slope zone”. With increasing susceptibility of landslides, the other classes are: “Moderately stable zone” (1.25<SI<1.5), “Quasi-stable slope zone” (1<SI<1.25), “Lower threshold slope zone” (0.5<SI<1), “Upper threshold slope zone“ (0<SI<0.5), and "Defended slope zone" (SI<0). This last class characterises pixels which are unstable for any values within the considered parameter range (Table 2). Stability in such regions cannot be explained by the model (Pack et al. 1998).

4.1.2. Multiple Logistic Regression

Regressions are used to model a dependent variable with one or more independent (explanatory) variables. The frequently used linear regression model assumes a straight-line relationship between the independent and the dependent variable, except an error term (Ross 2010). For many problems in Earth sciences this is a reasonable model (Yilmaz 2009).

For binary response data, though, where just the presence or absence of a phenomenon is of interest, logistic regressions are more often used (Lee and Sambath 2006). Especially in the case of landslide susceptibility modelling this is a frequent approach (Lee 2004; Ayalew and Yamagishi 2005; Lee and Sambath 2006; Van Den Eeckhaut et al. 2006; Yilmaz 2009; Bai et al. 2011; Felicísimo et al. 2012; Devkota et al. 2013; Park et al. 2013b; Kavzoglu et al. 2014). The aim of a logistic regression is to model the probability of the occurrence of an event based on some independent variables (Hilbe 2011). In the case of landslide modelling popular independent variables are listed in Table 3.

For this thesis, only information which can be gained from a DEM is used: elevation, slope, aspect, curvature, flow accumulation, and distance to rivers (derived from flow accumulation).

Table 3 Common independent parameters for logistic regression modelling of landslide susceptibilities

Authors	Independent variables
(Devkota et al. 2013)	Slope, aspect, curvature, elevation, stream power index (SPI), TWI, sediment transport index, land use map, lithology, distance from faults, rivers, and roads
(Yilmaz 2009)	Geology, elevation, slope, aspect, SPI, TWI, distance from faults, and drainage
(Kavzoglu et al. 2014)	Slope, drainage density, elevation, TWI, slope length, land cover, distance to road, lithology, and aspect
(He et al. 2012)	Lithology, elevation, slope, aspect, plan and profile curvature, and distance to rivers

To perform a logistic regression with these variables a calibration dataset is required. This dataset consists of several event points (1) as well as several non-event points (0). 196 landslide points were taken from the shallow landslide inventory (see subchapter 5.2.1) and compared to 798 non-landslide points. For data, where non-events are much more frequent than events as it is the case for landslide occurrence, it is recommended to reflect this as well in the calibration set, with up to five times more non-event points (King and Zeng 2001; Van Den Eeckhaut et al. 2006; Bai et al. 2011). The non-landslide points are randomly distributed over the area of the inventory. The observed landslides were at first subtracted from the study area, using a 5 meter buffer zone. The calibration set was then analysed using the *glm* function of the *stats* package in *R*. The considered independent parameters were combined in different ways to find the lowest AIC (Akaike Information Criteria), and hence the best model (Hilbe 2011). The first regression model included all parameters and was then compared to different regression models with less explanatory parameters. Parameters which had no significant influence on the model for any combination were not used. From the remaining parameters the ones were chosen which resulted in the lowest AIC. The best parameter combination was then used for the model using Eq. 10 and 11.

$$P(Y = 1) = \mu_i = \frac{1}{1+e^{-z}} \tag{10}$$

$$z = x_i\beta = \beta_0 + x_1\beta_1 + \cdots + x_n\beta_n \quad (11)$$

where μ_i = probability that a landslide occurs, β = calculated weights for the explanatory variables, x_i = explanatory variables, n = number of explanatory parameters (Hilbe 2011).

The final map of resulting landslide susceptibilities was classified into 5 classes using the natural breaks method (Slocum et al. 2009).

4.1.3. Slope Models

As the slope angle is a crucial preconditioning factor, within many slope stability models it plays a main role for determining the stability of slopes (Baum et al., 2002; Dietrich and Montgomery, 1998; GEO-SLOPE International Ltd., 2012; Haneberg, 2004; Kavzoglu et al., 2014; Lee et al., 2002; van Beek et al., 2002; Wu and Sidle, 1995). Also the two models used in this thesis include, and also largely depend (Pack et al. 1998) on the slope angle. Hence, as it is one of the main factors used, two models more were established which are just based on the slope angle. The first one is another logistic regression model, using the slope angle as the only explanatory variable. It was trained using the same calibration set as the LRM model. This model was compared to SINMAP and LRM, to see how much the increasing number of explanatory parameters improved the model performance. The classification process was done identically to the one of the LRM. Since this logistic regression slope model is very similar to the LRM, further simplification was done using bi-variate statistics to define slope angle/landslide occurrence relationship. This second slope model is based on the failure rate method described in Jäger and Wieczorek (1994). The slope maps were classified into classes of 5° (0-5°,5-10°,…) up to the final class which includes all areas with slope angles >50°. The landslide density was calculated by dividing the number of landslides in the calibration set of the shallow landslide inventory, divided by the total area of the slope class. The landslide densities can then be transformed into failure rates by subtracting the landslide density of the whole area. Like this the classes show if the considered slope angles lead to increased or decreased susceptibility of landslides compared to the general susceptibility of the area (Jäger and Wieczorek 1994). The resulting map is classified using natural breaks too (Slocum et al. 2009).

4.2. Landslide Inventories

The established models were evaluated using three different landslide inventories. Two of these just include shallow landslides, as these are the ones which are modelled by SINMAP (Pack et al. 1998) and the LRM. The first shallow landslide inventory was established over the whole study area (Shallow landslide inventory (SLI)). The second one is restricted to a smaller area around the town of Marcará (Marcará landslide inventory (MLI)). The third inventory extends over a similar area as the MLI but considers slower, deep-seated landslides (Deep-seated landslide inventory (DSLI)). This third inventory

is used to detect possible differences of the performance. Is it possible to detect even other kinds of landslides than the ones which are modelled, or how big is the difference of the performances for shallow and deep-seated landslides?

4.2.1. Shallow Landslide Inventory

High resolution optical data like aerial photography or satellite images have proven to be a useful tool for establishing landslide inventories, in particular because such data is increasingly becoming freely available in a georeferenced format (He et al. 2012; van Westen et al. 2012; Zizioli et al. 2013; Kritikos and Davies 2014; Raia et al. 2014; Steger et al. 2015a; Alejandrino et al. 2016; Rossi and Reichenbach 2016; Pradhan and Mezaal 2017). Google Earth, for example, has been used a lot for this purpose (England 2011; Guzzetti et al. 2012; Corominas et al. 2014; Fuchs et al. 2014; Posner and Georgakakos 2015; Sarkar et al. 2016). Therefore, the SLI was based on Google Earth images dated between August 2013 and July 2017.

This landslide inventory is restricted to shallow landslides as defined by Sidle and Ochiai (2006). This corresponds to the kind of landslides which are modelled by SINMAP (Pack et al. 1998). The inventory covers the entire study area. A landslide point was set at locations where one or several of the following recognition features proposed by Rowbotham and Dudycha (1998) were detected: (I) disrupted vegetation patterns, (II) scars, or (III) obviously displaced blocks of unconsolidated material. For each landslide, a point was set in its uppermost part (Fig. 12). The landslides considered in the Marcará landslide inventory are not considered in this inventory for having two exclusively distinct inventories. The resulting inventory was then split into a calibration set for the statistical models (about 75% of the landslides) and a validation set (25% of landslides) for all models. This is a slightly more equilibrated ratio than the 80/20% used by Bai et al. (2011) and Van Den Eeckhaut et al. (2006). By doing so it was ensured to still have enough points for the validation.

4.2.2. Marcará Landslide Inventory

This is an already existing landslide inventory for the region around Carhuaz and Marcará. It was prepared using the high resolution optical data available on Google Earth as well and then it was validated with extensive fieldwork (Strozzi et al. submitted). It includes all landslide types which could be identified in the field from which just the shallow ones were selected for this work. Due to the field check of this inventory, I consider it to be more complete. The purpose of this second inventory is having a smaller, but more homogenous evaluation area. None of the landslides of the MLI were used for the calibration of the models, but they were used for their evaluation.

4.2.3. Deep-Seated Landslide Inventory

InSAR is a remote sensing technique using microwaves. It can be used to measure the topography of surfaces and, if datasets of different times are available, the changes of the topography over time as well (Rosen et al. 2000). Like this, surface displacements can be measured with an accuracy of some millimetres (Guzzetti et al. 2012; Herrera et al. 2013). The considered landslides are mainly slower, deep-seated landslides, slow flows, and deformations (Riedel and Walther 2008; Guzzetti et al. 2009; Delgado et al. 2011; Cascini et al. 2013; Herrera et al. 2013). This technique was used by Strozzi et al. (submitted). They established a landslide inventory of deep-seated landslides which could be used for this thesis. It was established using Differential Synthetic Aperture Radar Interferometry (DInSAR) and Permanent Scatterer Interferometry (PSI) (Strozzi et al. submitted; Frey et al. 2017). These techniques are considered as powerful and cost-effective techniques to detect even small movements on the surface (Guzzetti et al. 2012; Herrera et al. 2013; Scaioni et al. 2014; Ciampalini et al. 2016). Therefore, they have been used by many authors to monitor or inventory landslides in different regions (Guzzetti et al. 2009; Cascini et al. 2010, 2013; Delgado et al. 2011; Auflic and Komac 2012; Greif and Vlcko 2013; Herrera et al. 2013; Cigna et al. 2013; Jebur et al. 2015; Bianchini and Pratesi 2016; Rosi et al. 2018).

4.2.4. Total Station

Additional to the inventories, displacement rates were measured on site. The displacement of different points close to Marcará and around the Safuna Alta (Fig. 15) were measured using the total station Leica TS-06 PLUS. Therefore, several points were chosen in these two regions at stable and unstable places (indicated by the DInSAR and PSI measurements). The chosen points were marked with iron sticks which were installed with concrete into the ground. One of the points which was considered as stable and, furthermore, had a good visibility to all other points was used as base. All other points are measured from there as rovers. The idea was similar to what Tsai et al. (2012) did. Two measurements should be undertaken which include the rainy season. For this thesis the first measurement was planned for January or beginning of February 2017, hence within the rainy season and a second measurement after the rainy season in July / August. This inventory should be used complementary to the DSLI as it focuses on the slower landslides too.

4.3. DEMs

The four landslide susceptibility models were applied to large parts of the Cordillera Blanca using three different DEMs: the Advanced Spaceborne Thermal Emission and Reflection Radiometer Global DEM (ASTER GDEM) (version 2), the Shuttle Radar Topography Mission (SRTM) DEM (version 4) (herein just called SRTM), and TanDEM-X DEM (TDX). All of these DEMs were co-registered using the co-registration tool developed by Nuth and Kääb (2011). This was applied with the SRTM DEM as master, as the used SRTM and TDX were already co-registered. The study area was extracted from these DEMs for the modelling. An additional co-registration of the DEMs to Google Earth data (SLI) was not performed. Its fitting was just analysed qualitatively by comparing the flow accumulation of the SRTM to Google Earth images (see Fig. 10).

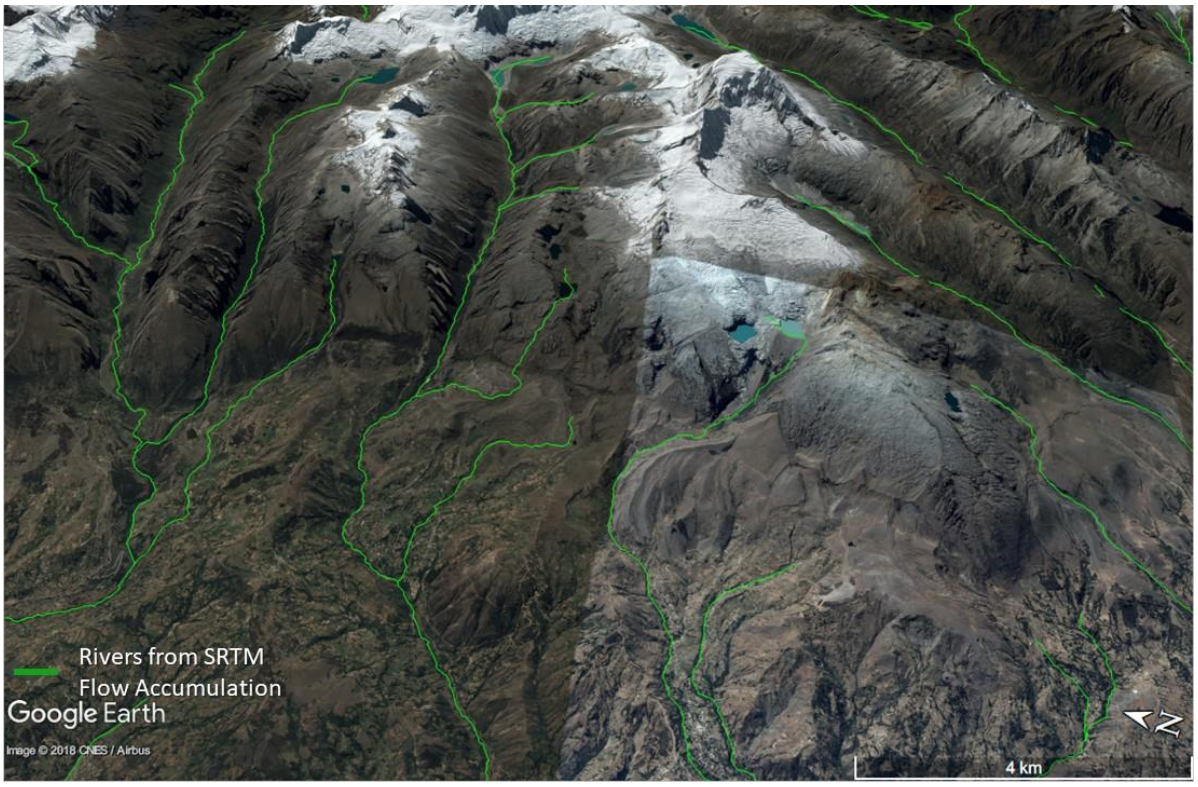

Fig. 10 Visual control of the co-registration of the Google Earth images and the SRTM DEM using the flow accumulation map of the SRTM DEM

4.3.1. ASTER GDEM

The first used DEM was the ASTER GDEM version 2. It was retrieved online from the Global Data Explorer Tool (in October 2016), maintained by the NASA Land Processes Distributed Active Archive Center, USGS/Earth Resources Observation and Science Center, Sioux Falls, South Dakota (NASA LP DAAC 2011). The DEM is based on photogrammetric processing of optical satellite images acquired between 18th December 1999 and 28th February 2011 (ASTER Science Team 2014). It has postings of one arc-second (ca. 30m). The validation study performed by Tachikawa et al. (2011) in Japan showed an elevation error of +7.4m in mountainous areas with standard deviations of 12.7m. External

validations by means of Global Positioning System (GPS) and comparisons to other DEMs showed elevation errors of 0.99m to 8.1m with standard deviations of 7.45m to 11.3m (Athmania and Achour 2014; Rexer and Hirt 2014; Satgé et al. 2015; Elkhrachy 2017). Hence, the results are in a similar range. According to the co-registration tool the final co-registered ASTER GDEM had a root mean squared error (RMSE) of 36.78 to the SRTM.

4.3.2. SRTM DEM

The SRTM DEM version 4 from the 24th September 2014 was retrieved online from the EarthExplorer tool, maintained by the NASA Land Processes Distributed Active Archive Center too (USGS 2015). It is based on the datasets of two SARs, one C-band and one X-band system. These two SARs were on board of a space shuttle, from where the measurement took place (Farr et al. 2007). The void filled version was used, which has for the considered area a spatial resolution of one arc-second. The validation of the SRTM DEM was performed by Farr et al. (2007). It showed an absolute geolocation error of 9 m in South America and an absolute vertical error of 6.2 m. External validations of the SRTM DEM v4 have been performed in different places of the world. They showed better results of around 3m or less of vertical error with standard deviations of 3.2-8.4 m (Mouratidis et al. 2010; Athmania and Achour 2014; Rexer and Hirt 2014). Higher elevation errors were detected in the Altiplano of southern Peru, Bolivia, and northern Chile, with a mean error of 10.6 m and standard deviation of 11.3 m (Satgé et al. 2015).

4.3.3. TanDEM-X DEM

This DEM was produced in-house by Gamma Remote Sensing from TanDEM-X acquisitions performed along ascending (24th January 2013) and descending (1st October 2013) orbits with a posting of 0.0001 decimal degrees, corresponding to about 10 m (Strozzi et al. submitted). Voids that occurred due to radar specific issues such as layover, radar shadow, etc. were filled with data from the SRTM DEM. For TanDEM-X DEMs produced with the same methodology in the past over Mount Etna in Italy (Wegmüller et al. 2014) and the Chomolhari region in Bhutan (Ambrosi et al. in Press), mean differences of the elevations were found between the DEMs and ground control points measured by means of GPS of 0.6 m and 3.6 m, respectively, and standard deviations of 4.3 m and 2.8 m, respectively. Its accuracy with respect to the SRTM is a RMSE of 61.02m according to the co-registration tool.

4.3.4. Glacier and Rock Mask

Since the SINMAP model works only on slope stabilities of soils and weathered slope material, areas without any sediment cover like glaciers and rocks were excluded from the analysis (see Fig. 1). This was done by establishing a glacier and rock mask. At first areas were selected for slope angles steeper than 50° and elevations higher than 5200 masl. The resulting polygons, were manually completed and

adjusted using Google Earth imagery. This mask was applied on all DEMs after the model runs, for not excluding any parts of the flow accumulation area.

4.4. Evaluation and Validation

All four models were applied to each of the three DEMs. Hence, possible differences of the performances of the DEMs could relate to the DEM derived morphologic characteristics. In a first step, such differences between the DEMs were analysed. Afterwards, the twelve realisations were evaluated with the three landslide inventories: the validation set of the SLI extending over the whole area, the MLI extending over the smaller area around Marcará only, and the DSLI. The evaluation was done using the receiver operating characteristics (ROC) and the related area under curve (AUC) method as done by many authors which established landslide susceptibility maps (He et al. 2012; Günther et al. 2013; Kavzoglu et al. 2014; Ghazvinei et al. 2015; Kim et al. 2015; Posner and Georgakakos 2015; Steger et al. 2015a; Lee and Park 2016; Rossi and Reichenbach 2016; Samia et al. 2017). Furthermore, a confusion matrix was established for further evaluation (Legorreta Paulin et al. 2010; van Den Eeckhaut et al. 2012; Park et al. 2013a; Petschko et al. 2014). A final evaluation technique is to just look at the cumulative distribution function of the landslides according to their susceptibility (Lee 2004; Guzzetti et al. 2006; England 2011; Chen et al. 2013). The validation was performed by comparing the areas which are considered as most and least susceptible by the different models (Haneberg 2004; Michel et al. 2014). These methods are described in the following subchapters.

4.4.1. Comparison of the DEMs and the Study Areas

All the model runs are based on the DEMs and their derivatives like slope angle, flow accumulation, curvature, and elevation. Potential differences of the performance of the model runs could, therefore, relate to the variability of these characteristics. Hence, these variabilities were compared between the DEMs and the different study areas of the MLI and SLI using a t-test for random point clouds within the two areas, MLI and SLI. For all the points the deviation from the mean was tested to check the variabilities of the considered parameters. It was worked using a 1% significance level.

4.4.2. Evaluation

Receiver Operating Characteristics

The process of the evaluation was done using the ROC and the related AUC. These methods are useful and frequently used tools for comparing landslide susceptibility models. A point dataset with a similar amount of non-landslide cells and landslide cells which are distributed within the same area is required. The additional points of the non-landslide cells were again calculated randomly within the area of the inventory, except the 5m buffer around the observed landslides. The calculated values of the model at the given points are then evaluated. This is done calculating the true positive rate (TPR,

Eq. 12 and Table 4) and the false positive rate (FPR, Eq. 13) for different thresholds dividing the model into stable and unstable (e.g. for thresholds which define large parts of the map as unstable the TPR is close to one, as a large unstable area increases the probability that the observed landslides are in this unstable area. Simultaneously the FPR increases too, as the likelihood of non-landslide points being in an unstable region increases as well). The received rates are then plotted against each other. The true positive rate is the y-axis and the false positive rate the x-axis. The points on the plot resemble a curve and the bigger the area below this curve, the better the model performance (Fawcett 2006). For this concern the AUC value was developed. It expresses the amount of the area which lays below the ROC curve (Lee and Park 2016). Hence, the closer it is to one, the better the model performance. An AUC of 0.5 denotes a random prediction of landslides (Posner and Georgakakos 2015).

$$TPR = \frac{\text{True Positives}}{\text{True Positives+False Negatives}} \tag{12}$$

$$FPR = \frac{\text{False Positives}}{\text{False Positives+True Negatives}} \tag{13}$$

Table 4 Definition of true positives etc.

True positives	landslide occurred where model is unstable
True negatives	landslide did not occur where model is stable
False positives	landslide did not occur where model is unstable
False negatives	landslide occurred where model is stable

Confusion Matrix

The ROC curve is basically a visual representation of the confusion matrix for many different threshold values (Beguería 2006). The definition of single threshold values, though, is crucial for the final susceptibility map and has a big influence on the quality of the map (Petschko et al. 2014). Hence for this thesis two different approaches were tested to classify the resulting maps into stable and unstable regions. The first one is the method natural breaks and the second one is quartiles (Slocum et al. 2009; Kritikos and Davies 2014; Foery and Sturm 2015; Constantin 2016). For SINMAP instead of the method natural breaks the classes proposed by the authors (Pack et al. 1998) were used. The comparison of the susceptibility classes was performed by comparing the percentage of landslides which occurred in the least susceptible classes to the percentage of landslides occurring in the most susceptible classes. The percentage of the area which corresponds to each class is considered as well (Dietrich et al. 1998; Beguería 2006; van Den Eeckhaut et al. 2012; Michel et al. 2014).

Cumulative Distribution of Landslides

Plots were established which show how much of the study area needs to be modelled as unstable for detecting how many landslides. This means that the percentage of the study area ranked from most

to least susceptible is plotted as the x-axis, and the cumulative occurrence of landslides for these susceptibilities on the y-axis (Guzzetti et al. 2006). To ensure a better comparability of this method the area under these curves was calculated too.

Velocity Modelling

The measurements which were done using the total station cannot really be considered as a landslide inventory. It just depicts distances how far certain points travelled within some months. Therefore, the evaluation process needs to be different from the other inventories. Such movement rates can mainly be used for the validation of some numerical models on single slope scale for deeper landslides (Corsini et al. 2005). Bertolini and Pizziolo (2008) complement that such measurements are mainly useful in regions where limit equilibrium models cannot be applied due to the depth of the movement. This means that the usefulness of such an evaluation for shallow landslide models can be questioned. However, with this inventory it shall be controlled if there still are correlations between the velocities of the measured points and the landslide susceptibilities.

4.4.3. Comparison of the Models (Validation)

The consistency of different models concerning which slopes are most or least stable is of high relevance for mapping landslide susceptibilities and its plausibility (Sterlacchini et al. 2011). Hence, the different models were compared, to see if the same regions were modelled as most / least susceptible (Michel et al. 2014). As the confusion matrix, this is established twice, once using the originally used classification (natural breaks and the classes by SINMAP) and once using quartiles (Slocum et al. 2009) for all model runs. The comparison was performed for the three models LRM, SINMAP, and slope regression model. The failure rate model was not considered due to its similarity to the slope regression model.

4.5. Uncertainties, Errors, and Limitations

Models are always simplifications of the reality and cannot represent its whole complexity (Stachowiak 1973; Jeffers 1988). Landslide susceptibility models are no exception and are, therefore, *"inherently riddled with uncertainties"* (Petschko et al. 2014). Guzzetti et al. (2006) distinguishes four sources of uncertainties for the modelling process itself. (I) Landslide and thematic information for the analysis is incomplete or defective; (II) the understanding of landslides is limited, just like (III) the techniques to determine the susceptibility; (IV) the phenomenon landslide inheres natural variability. Further uncertainties can be added by the used material like DEMs (Fisher and Tate 2006), landslide inventory, the assignment of the hazard class to the stability values, and others (Carrara et al. 1992). A list of these uncertainties and errors which concern this thesis are presented in the following subchapters.

4.5.1. Digital Elevation Model

The models used in this thesis are either physically based or empirical-statistical ones. They require different information as inputs. Some of them are just used for one of these models, others are used by all models. One of the used input they have all in common are the DEMs on which they are based (Jäger and Wieczorek 1994; Pack et al. 1998; Bai et al. 2011). Therefore, the uncertainties which relate to the DEMs are presented first.

The quality of DEMs has increased over the years but is still subject to uncertainties. Possible errors occurring on DEMs are diverse. They can be systematic, spatially autocorrelated, biased, or just random (Fisher and Tate 2006) (see Fig. 11). They are to some degree quantifiable (Wechsler and Kroll 2006). The deviation of the model elevation from the real elevation (measured by GPS or more precise DEMs) can be calculated by the RMSE. Such calculations are, though, not valid over the whole region and can deviate locally (Carlisle 2002). Global datasets like the ASTER GDEM, SRTM, and TanDEM-X are usually validated just in some specific regions (see chapter 4.3.1-4.3.3). Hence, it needs to be considered, that RMSEs calculated in some regions are not necessarily the same as within the considered area. Mountainous areas, or generally areas of steep slopes, are associated with higher errors (Carlisle 2002). Thus, even quantifiable errors can be uncertain. Other factors which influence the quality of DEMs which are less tangible contribute to the uncertainty too. This concerns for example the interpolation of the DEMs. The used DEMs in this thesis have a spatial resolution of 10 m or 30 m. The area in between needs to be interpolated for assessing characteristics like the slope angle (Carlisle 2002; Fisher and Tate 2006). Another uncertainty arises from temporal variabilities of the surface. Surface changing processes like erosion, landslides, and glacier retreat, among others (McColl 2015) create deviations from the DEM to the actual state of the reality. This phenomenon can be used to derive landslide inventories, when there are two DEMs acquired at two different moments (Weirich and Blesius 2007; Guzzetti et al. 2012). However, it means as well, the DEM does not represent the actual state of the earth's surface (Raia et al. 2014).

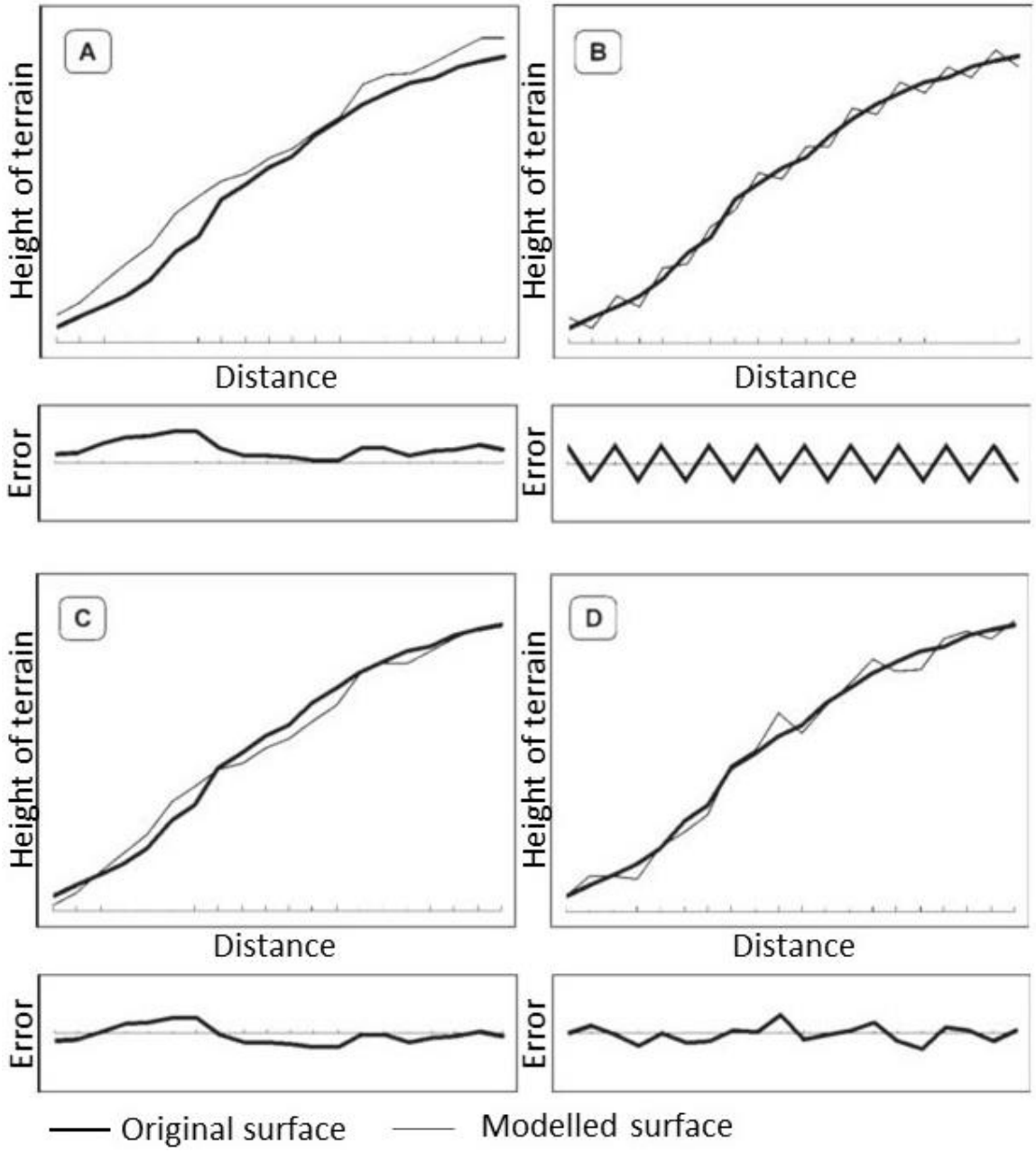

Fig. 11 Illustration of the different errors which can occur on DEMs (modified after Fisher and Tate 2006). (A) Biased error; (B) systematic error; (C) spatially autocorrelated error; (D) random error

4.5.2. Susceptibility Models

A second source of uncertainties are the susceptibility models. There are considered being three main sources of uncertainties in the process of modelling: (I) the structure of the model which includes uncertainties of input-output relationship and its degree of complexity, as for example if there are important factors neglected; (II) measurement of the required input data; (III) temporal and spatial variations of the parameters (Rowe 1994; Loucks et al. 2005; Chatfield 2006; Coppi 2008; Levermore et al. 2012). The used models are analysed based on these main uncertainties. Some other sources were added, but the following lists of possible sources of uncertainties presented do not claim completeness. It was tried to pick the most relevant ones concerning this thesis.

SINMAP and Limit Equilibrium Analysis

SINMAP models slope stabilities using the limit equilibrium analysis by considering several factors like cohesion, soil depth, and more (see chapter 4.1.1). It is in the nature of modelling, though, that not all factors can be represented by the model and many simplifications are assumed (Chatfield 2006). Rowe (1994) even state that there are more factors we do not know than the ones we know in such models. In the case of SINMAP this means that there are many factors missing. Some of these missing factors include the precipitation patterns, distribution of shear layers or how they are composed (Iverson 1997; Al-Hurban et al. 2006), the underlaying geology in general (Pack et al. 2005), or the process of failure (Cohen et al. 2009). The process of failure can have a significant impact on the location of the landslide-crown. Deformation, debuttressing and related stresses and strengths can cause larger failures upslope from the original landslides (Krahn 2003; Cohen et al. 2009). Other examples of an incomplete representation of the reality are presented by Krahn (2003). The factor of safety does not consider possible existences of anchors which stabilize slopes from below. Generally, special attention needs to be paid when there are concentrations of stresses within the slope.

During the process of the measurement of the considered input data further uncertainties arise. The developers of SINMAP handled measurement errors and data handling problems by the design of the model. The required soil properties can be defined within an interval. SINMAP then defines the stability of the slopes by considering the most stable and most unstable combination (Pack et al. 2005). By doing so, the uncertainties can be attacked but not reduced (Meisina and Scarabelli 2007). Besides the effect of reducing measurement errors, this procedure helps to deal with uncertainties caused by spatial and temporal variations of the input parameters. These variabilities are, though, not represented in the result of the modelling. The SI is set deterministically (Pack et al. 2005).

The limitations of the model's applicability mainly relate to the fact, that SINMAP just models shallow translational landsliding phenomena which are controlled by shallow groundwater flow convergence (Pack et al. 2005). Hence, soils are required (no bare rock or glaciers), and the layer below should not have a considerable permeability (Kim et al. 2015). Else, shallow groundwater flow drains and cannot accumulate in the way predicted by the model. Additionally, the authors recommend performing a thorough calibration using meaningful calibration regions. Even when having considered these requirements, the resulting SI should not be expected being numerically precise and just used to compare the susceptibility of the regions within the modelled area (Pack et al. 2005).

Besides all these limitations and uncertainties of the limit equilibrium method, the FS, and the related SI of SINMAP, remains a useful tool for getting first impressions of the stability of slopes. Especially, when its limitations and areas of application are fully understood (Malkawi et al. 2000; Krahn 2003; Al-Hurban et al. 2006; Meisina and Scarabelli 2007; McColl 2015).

Logistic Regression Models

Linear statistical models are usually expressed like Eq. 14. The first part shows the dependency of the dependent and independent variables and the last summand describes the statistical error of the model. In doing so, the deviation from the model to the training set is considered. Uncertainties arising from the input-output relationship are tackled and quantified like this (Ross 2010).

$$y = a + b_i * x_i + \varepsilon \tag{14}$$

Where y is the dependent variable, a the intercept, b_i the weights of the independent variables (x_i), and ε the error term which is usually gaussian distributed with values which are independent and identically distributed (iid) with 0 mean and σ^2 as variance ($\varepsilon \overset{iid}{\sim} \mathcal{N}(0, \sigma^2)$) (Ross 2010). In the case of logistic regression models, it is harder to reasonably assess such an error term. A basic assumption of the error term of the linear model is violated in case of logistic regression models, as the error term cannot be normally distributed. Additionally, it cannot be spoken of an error, as the model just calculates probabilities of an event. Therefore, it is usually not used for logistic regression models (Faraway 2006) (see Eq. 10 and 11). Still, the uncertainties are quantified, but not used in the model. The *glm* function of the *stats* package of the program *R* calculates for all weights an uncertainty term using the standard deviation. The uncertainties arising from the input parameter selection in the model is not quantified (Faraway 2006). Neither are the ones deriving from the model selection (Faraway 2006; Levermore et al. 2012). The uncertainties from parameter measurement are for the used logistic regression models a combination of the accuracy of the training set of the landslide inventory (explained below) and the uncertainties of the DEMs. The spatial variabilities of the used parameters are considered by the spatially distributed information from the DEM. The temporal variabilities, though, concern the DEMs and, therefore, the input parameters too.

The presented errors and uncertainties described above show to some degree how well the model is suited for determining landslide susceptibilities from a statistical point of view. Decreasing uncertainties and higher correlations of the dependent and independent variable should lead to a better model (Hilbe 2011). This does not need to result in higher model performances, though. In some cases, the statistical correctness of the model did not correlate with the predictive power of the model. Lower correlations of the input parameters and the landslides, leading to higher uncertainties, improved the performance of the model (Brenning 2005). Hence, such uncertainty analysis need to be handled with care.

Failure Rate Model

The failure rate model is one of the simplest models which was used. Lower complexities of the model, on the one hand, may reduce its capability to represent the complexity of the real system, thus increasing uncertainties. On the other hand, a smaller amount of input parameters reduces the

uncertainties and errors which are related to the not used input parameters (Loucks et al. 2005). Also, they are suitable for applications to mountain areas, where data and information typically is sparse. The main uncertainties which still exist are related to the ones mentioned before, as this is a statistical model too. Additional uncertainties can arise from the chosen interval which is used to classify the slope map (Jäger and Wieczorek 1994; Guzzetti et al. 2006).

4.5.3. Classification Process

All used models calculate for each grid cell a value representing its susceptibility to landslides, either in form of a Stability Index (SINMAP) (Pack et al. 1998), as a probability of failure (logistic regression models) (Hilbe 2011), or as a failure rate (Jäger and Wieczorek 1994). The resulting values are then classified into different susceptibility classes. Depending on the method used to define the limits of the classes certain points can belong to different susceptibility classes (Jebur et al. 2014). This has an impact especially on the amounts of landslides which lay within certain classes (Ayalew and Yamagishi 2005; Kritikos and Davies 2014). Hence, uncertainties arise of which area is considered as being most or least susceptible (Carrara et al. 1992).

4.5.4. Landslide Inventory

The quality of landslide inventories is crucial in landslide susceptibility modelling. It is not only responsible for the quality of the statistical models (van Westen et al. 2006), but as well the evaluation of all models is heavily dependent on the quality of the inventory (Pack et al. 2005; Steger et al. 2015a). It is not trivial to define the accuracy of such maps (Galli et al. 2008; Guzzetti et al. 2012). Easier to asses are the uncertainties and errors which impact the outcome. The completeness of the inventory is one such factor (Carrara et al. 1992). It refers to the percentage of mapped landslides to the total amount of landslides (of certain sizes) within the area (mostly unknown) (Guzzetti et al. 2012). Two other factors influence the cartographic mismatch. The scale of the interpreted optical data and the experience of the investigator correlate negatively with the cartographic mismatch of the inventory (Carrara et al. 1992; Guzzetti et al. 2012). The first one is certainly a factor which has improved due to the technologic improvements. Not only are nowadays high-resolution optical data available for large parts of the world, it is even in a georeferenced format (Scaioni et al. 2014). Some years ago it was one of the main sources of uncertainties to correctly map the landslides found in the field or on non-georeferenced aerial images (Carrara et al. 1992; Malamud et al. 2004). Further, still actual, sources of uncertainties are the timing (van Westen et al. 2006) and the specific trigger of the landslide within the inventory (Guzzetti et al. 2006). The used landslide inventories of this thesis do not have information about the exact moment when the landslides occurred, nor about their triggers. The only restriction of the timing when the landslides of the SLI happened is that they happened before the used Google Earth images were taken but are still visible. Landslides which occurred some time ago

and are already covered by vegetation again are hard to detect (Carrara et al. 1992). Another factor which arises uncertainties is the accuracy of Google Earth and how well it correlates with the used DEMs. The accuracy of Google Earth has been tested worldwide and showed low accuracies. It showed a RMSE of 39.7m (Potere 2008; Yu and Gong 2012; Visser et al. 2014). Even though, there are regions where Google Earth has much lower RMSEs (Benker et al. 2011; Mohammed et al. 2013), it needs to be assumed, that its accuracy in the study area is lower than the ones of the used DEMs (see chapter 4.3.1-4.3.3). The correlations from Google Earth and the DEMs are generally dependent on the considered area and range from quite high correlations (Rusli et al. 2014) to high average location errors of 107.9m (Sato and Harp 2009).

Additionally, Google Earth has as well some internal uncertainties of correct georeferencing. On some scales it is visible, that for example roads can be interrupted and being continued slightly displaced. Similar things occur when images of different years are considered. Specific objects can have varying locations between the years (Potere 2008) (see Fig. 12). Since the SLI is based on Google Earth images between 2013 and 2017, errors can be caused by these deviations.

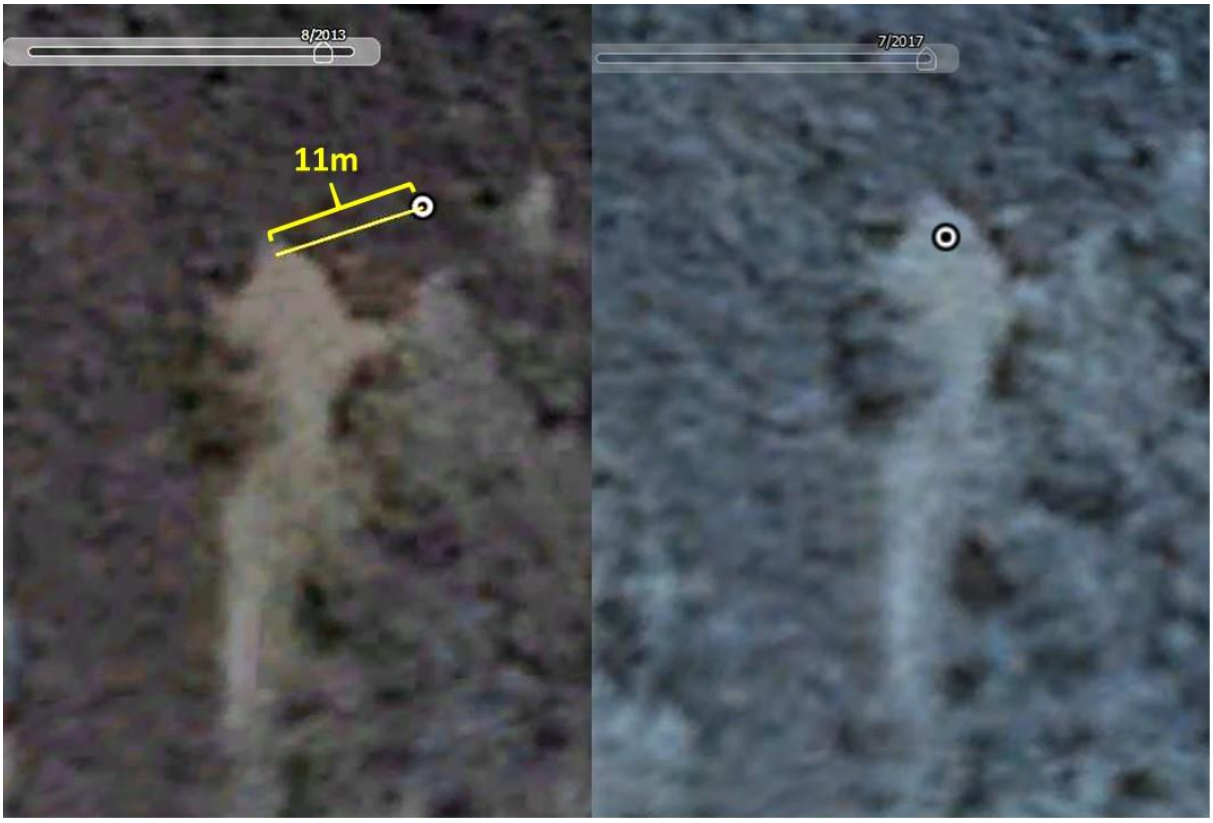

Fig. 12 A shallow landslide in the Cordillera Blanca as seen in Google Earth. On the left-hand side from a dataset of August 2013, and on the right-hand side from July 2017. The yellow line shows the distance from the landslide point set on the image of 2017 to where it would have been set on the image of 2013

The landslide inventory which was used for the evaluation of this thesis is a point dataset. Each landslide is represented by one single point (see Fig. 12). Therefore, one of the main error can be avoided, namely, the correct selection of the boundary of the landslide (Van Den Eeckhaut et al. 2006).

Still, this point needs to be set accurately for ensuring the quality of the inventory (Pack et al. 2005). If this point then really is the one which origins the movement is another question and cannot be assured (Michel et al. 2014).

4.5.5. Evaluation

A meaningful evaluation of landslide susceptibility models is dependent on the quality of the landslide inventory (Guzzetti et al. 2012), which was analysed before, and the selection of an evaluation method (Guzzetti et al. 2006; Petschko et al. 2014). It was tried to minimize the impact of the chosen evaluation method by using different ones. However, Steger et al. (2015b) state that statistical performances generally do not represent the plausibility of maps. They base this assumption on 16 susceptibility models for a certain area which all performed similarly well according to the ROC analysis. The spatial patterns of the model, though, revealed considerable differences.

5. Results

5.1. Morphologic Comparison of the Study Areas and DEMs

First, the different DEMs and the considered study areas were compared. 385 points distributed within the small area (MLI) were compared to the same amount of points distributed over the large area (SLI). A t-test revealed that the differences between the DEMs are mainly restricted to the curvature (see Table 5, last four columns). Its variability is different for all DEMs. The only additional significance was obtained within the small study area of the MLI, where the slope angle variability of the ASTER GDEM is not equal to the one of the TDX.

The comparison of the variabilities between the study areas, from the MLI to the SLI, showed statistically significant results for the elevation within all DEMs (see Table 5, first 5 columns). Furthermore, the ASTER GDEM had statistically significant results for the variability of the slope angle and the curvature between the two study areas. The one-sided t-test shows that the assumption that the variabilities within the MLI is bigger, can be rejected for all mentioned statistically significant results.

Table 5 p-values of the t-tests comparing the morphologic variability of the areas of the MLI and the SLI in the first five columns and the ones between the DEMs in the last four columns. Both-sided just indicates differences of the means, whereas MLI less and larger tests the assumption, that the mean of the MLI is lower or higher. For the variabilities between the DEMs it was just tested if there are differences and not in which DEM they are bigger, hence just a two-sided t test was performed. The significant results (<1%) are highlighted in grey

DEM	Characteristic	Two sided	MLI less	MLI larger	Characteristic	DEM	SLI	MLI
GDEM	Slope	0.0007	0.9996	0.00035	Slope	GDEM/SRTM	0.7893	0.2267
	Flow accum.	0.0225	0.01127	0.9887		GDEM/TDX	0.9792	0.0009
	Curvature	0.00089	0.9996	0.00045		SRTM/TDX	0.8120	0.0380
	Elevation	2.2E-16	1	2.2E-16	Flow accum.	GDEM/SRTM	0.0769	0.4225
SRTM	Slope	0.0578	0.9711	0.0289		GDEM/TDX	0.0524	0.0109
	Flow accum.	0.407	0.2035	0.7965		SRTM/TDX	0.0477	0.0453
	Curvature	0.03682	0.9816	0.01841	Curvature	GDEM/SRTM	2.2E-16	2.2E-16
	Elevation	2.2E-16	1	2.2E-16		GDEM/TDX	2.2E-16	2.2E-16
TDX	Slope	0.8691	0.5655	0.4345		SRTM/TDX	2.2E-16	2.2E-16
	Flow accum.	0.8959	0.5521	0.4479	Elevation	GDEM/SRTM	0.9506	0.9056
	Curvature	0.2738	0.1369	0.8631		GDEM/TDX	0.2554	0.9038
	Elevation	2.5E-04	0.9999	1.2E-04		SRTM/TDX	0.2679	0.9984

5.2. Landslide Inventory

5.2.1. Shallow Landslide Inventory

The first landslide inventory is presented in Fig. 1. It contains exclusively shallow landslides which are distributed over the whole study area. The landslides were marked at places where clearly visible scars of the landscape were found (see Fig. 12). The final inventory included a total of 254 landslides, whereof 196 were used to calibrate the logistic regression models and 58 for the evaluation.

5.2.2. Marcará Landslide Inventory

The received datasets from Strozzi et al. (submitted) were checked again with Google Earth images. Therefore, it could be ensured, that just the shallow landslides are used for this inventory. This resulted in a point dataset including 77 landslides (blue points in Fig. 13). The evaluation area, within which the non-landslide points were defined, was obtained by drawing a boarder around the mapped landslides approximately.

5.2.3. Deep-Seated Landslide Inventory

The DSLI is as well an inventory established by Strozzi et al. (submitted). As movement rates in the range of some cm/year were looked for, this inventory focusses on slower, deep-seated landslides shallow landslides are not likely being included in this inventory. The landslides of this inventory are barely visible in the field (Fig. 14) and on Google Earth usually not recognisable. Hence, for the inventory the polygons obtained by Strozzi et al. (submitted) were taken and points were set in the uppermost part of each of those. The resulting inventory included 78 landslides (green points in Fig. 13). As for the MLI, all of them were just used for the evaluation and the evaluation area was defined approximately around the landslide points.

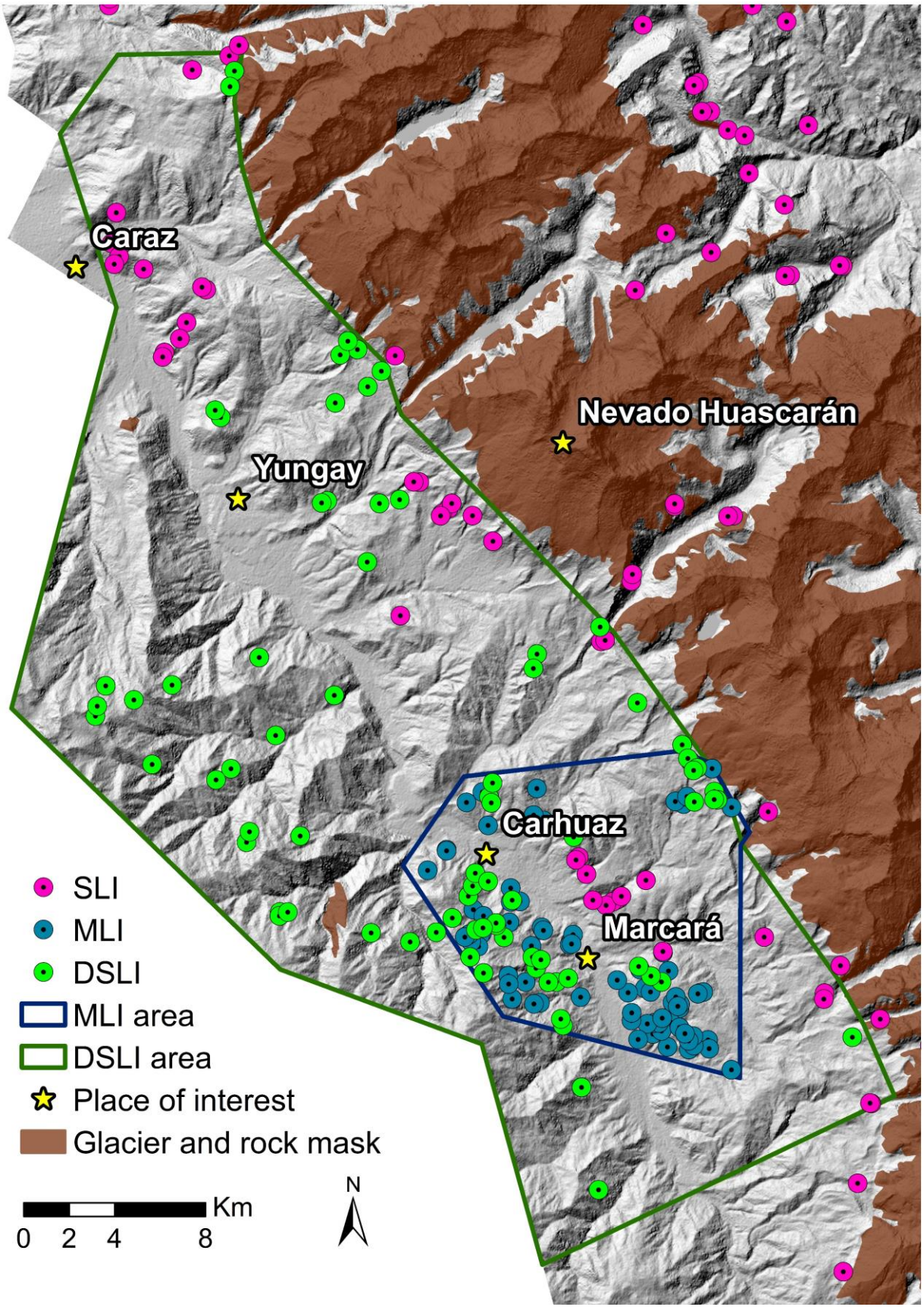

Fig. 13 The used landslide inventories for the evaluation. The SLI is not complete on this figure. For its whole extent see Fig. 1

5.2.4. Total Station

Additionally to the landslide inventories, several points in the west of Marcará and around Safuna Alta (see Fig. 15) were measured with a total station. The points were installed on the 2nd February 2017 in Marcará and on the 11th February 2017 around Safuna Alta, respectively. Due to technical constraints it was not possible to measure them by then. The first time they were measured on 19th May 2017 and the second measurement took place on 8th August 2017 (Marcará). The points around Safuna Alta were measured three times: 15th May 2017, 11th August 2017, and on the 8th December 2017. The measured movements are summarised in Table 6 and Fig. 16. Due to the extremely large movements, which for two points are even more than 70 cm higher than before these values are not considered for the evaluation. The second control seems more likely being useful results.

Fig. 14 A deep-seated landslide in the east of Yungay which is part of the DSLI. The main scar is highlighted by the red ellipsoid

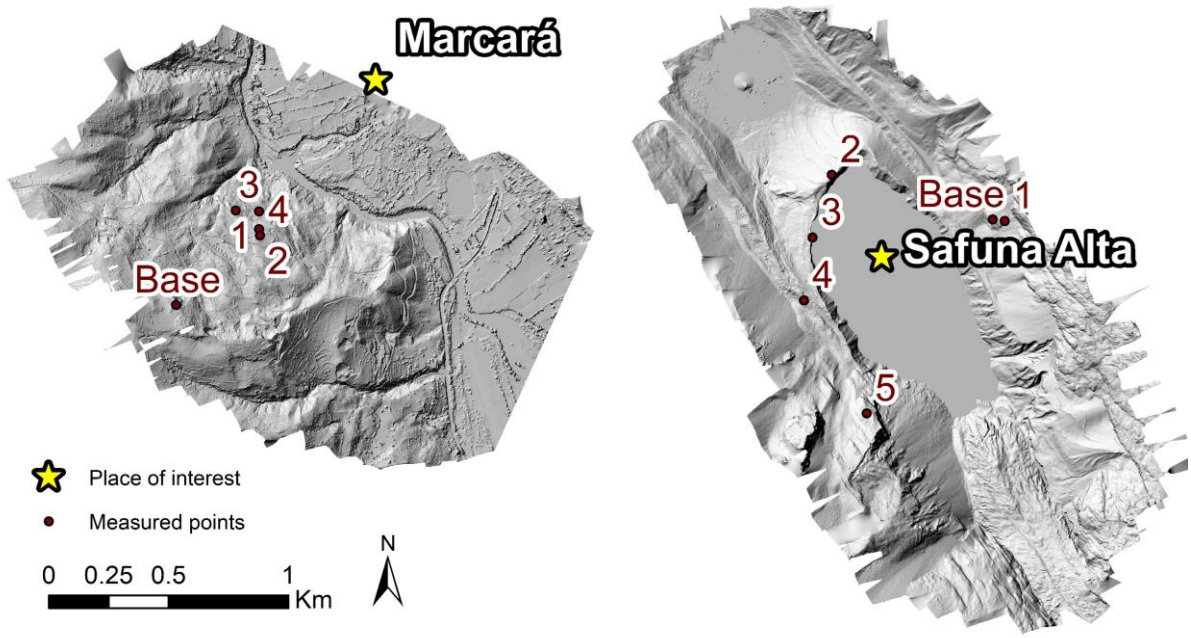

Fig. 15 Location of the points measured next to Marcará and the Safuna Alta

Table 6 Movement rates measured at the two locations. The values of the second control depict the difference of the second and the first control, the first control is the difference of the original measurement and the first control

		1st Control		2nd Control	
		Elevation change	Total movement	Elevation change	Total movement
Safuna	Base	-4.47	4.47	3.36	3.39
	1	4.43	4.45	-4.39	4.51
	2	-69.37	69.71	-3.21	10.36
	3	1.09	20.93	-10.11	16.77
	4	75.25	76.13	-27.28	27.49
	5	73.21	75.08	-15.07	24.61
Marcará	Base	5.84	6.33	-	-
	1	1.14	6.10	-	-
	2	-1.35	5.03	-	-
	3	1.27	3.18	-	-
	4	0.29	1.54	-	-

5.3. Model Runs

5.3.1. SINMAP

The SINMAP model was applied on the three DEMs over the study area (see Fig. 18). It was used as one single calibration area and no further calibration of the soil characteristics parameter was performed. Thus, two recommendations of the authors of SINMAP were violated, as meaningful calibration areas with a thorough calibration are highly recommended (Pack et al. 1998). The resulting maps using the different DEMs had no SI values below 0. Hence, the SINMAP class 'defended slope zone' was not used. The remaining classes were all used and classified by the proposed threshold values from Pack et al. (1998) (see Table 8).

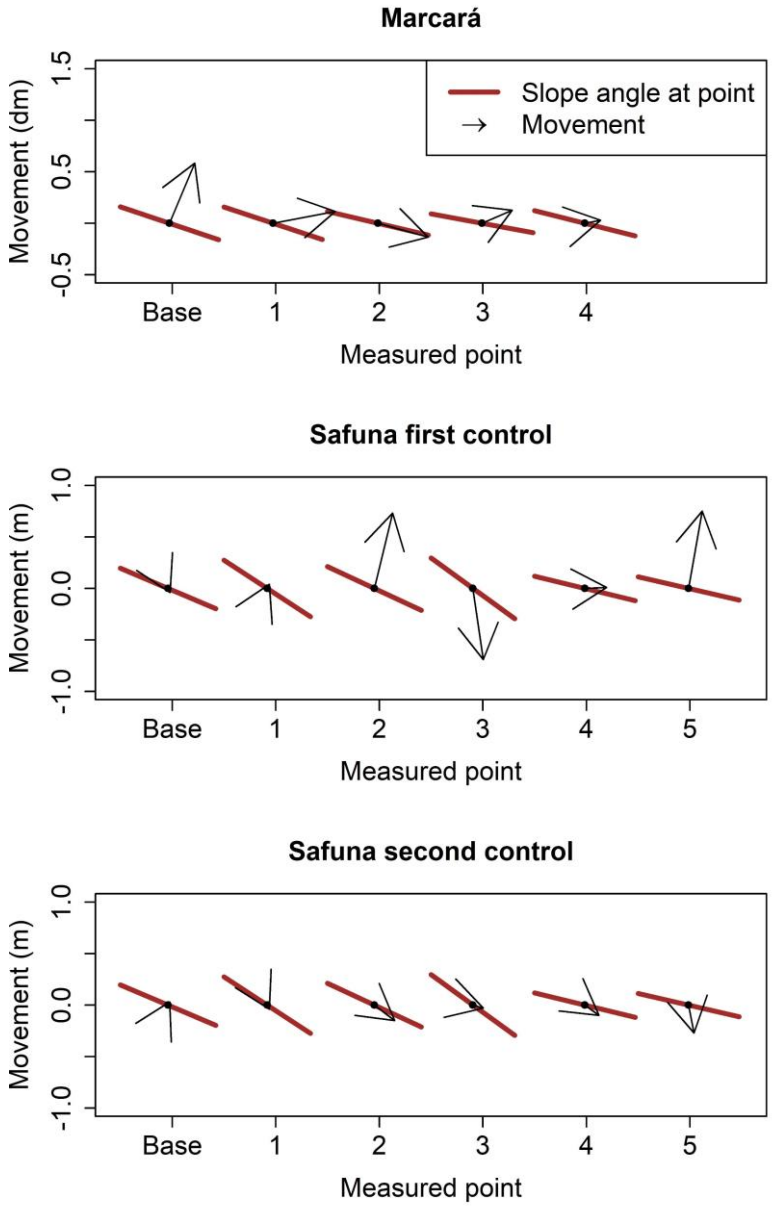

Fig. 16 Graphical illustration of the movement rates. The red line represents the slope angle at the measured point. The length of the vector shows the total movement of the point and its direction shows if it increased or decreased in height. Hence, an upwards directed arrow illustrates increasing elevation from the first to the second measurement

5.3.2. Logistic Regression Model

The logistic regression was calculated for all three DEMs (result of the SRTM see Fig. 18). The obtained weights for the explanatory variables elevation and slope angle, just like the intercept values are all similar for the DEMs (see Table 7). However, the lowest AIC was obtained for all DEMs with different additional parameters. The SRTM DEM just used the already mentioned explanatory variables, whereas for the ASTER GDEM and the TDX the models were improved by considering additionally the curvature and the distance to rivers, respectively. The parameters aspect and flow accumulation had no significant impact on the models for no DEM and were, therefore, not used. The classification using the natural breaks resulted in the threshold values presented in Table 8.

Table 7 Summary of the used weights for the logistic regression models. The first columns are the parameters of the LRM, the last two are the ones of the slope model. '-' means that this parameter was not used for the considered DEM

	Intercept	Elevation	Slope angle	Curvature	Distance to river	Intercept	Slope angle
GDEM	-0.283	7.15E-05	9.14E-03	3.41E-02	-	-0.036	9.59E-03
SRTM	-0.308	7.26E-05	9.66E-03	-	-	-0.058	10.27E-03
TDX	-0.311	7.58E-05	10E-03	-	-4.1179	-0.077	10.8E-03

5.3.3. Slope Model

The first slope model was established using the logistic regression too. The weights of the independent parameters were calculated in the same way as for the LRM. The obtained results are summarized in Table 7. The weights are more variable between the DEMs than for the LRM, but still they are close to each other. The classification threshold values are displayed in Table 8. Using this information, the maps were calculated and classified (Fig. 18 shows the example of the SRTM DEM).

5.3.4. Failure Rate

The second slope model was applied on a more basic approach. For each of the slope angle classes the landslide density was calculated and compared to the total mean over the study area (see Fig. 17). The classification process into susceptibility classes was performed manually based on natural breaks (Table 8). The adjustments which were done were to make sure, that failure rates higher than 0 are within the two most susceptible classes.

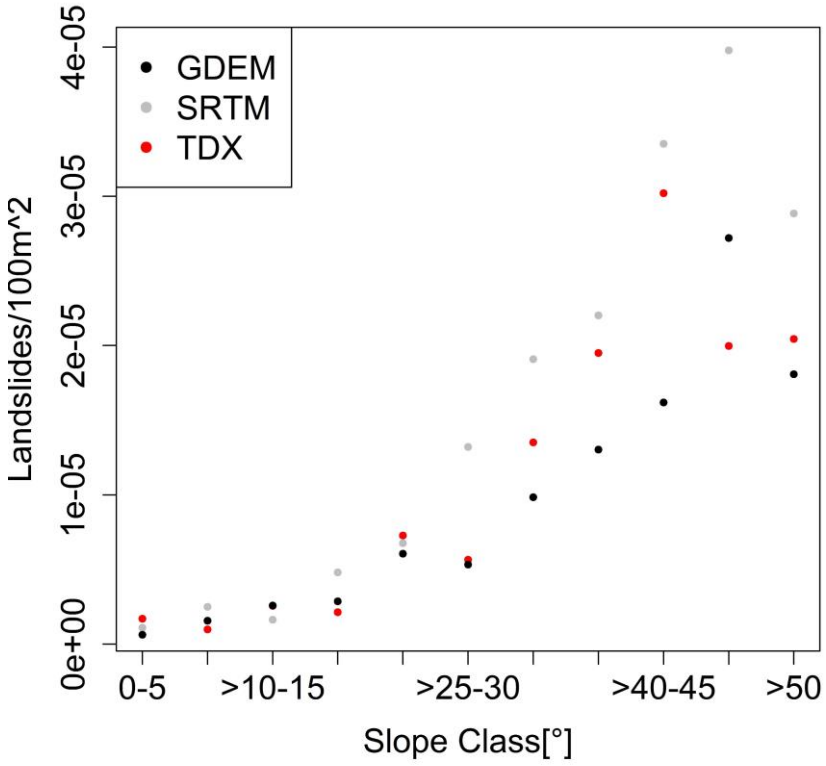

Fig. 17 Used values for the classes of the failure rate model

Table 8 List of the used threshold values for the classification. The class names are the ones proposed for the SINMAP model (Pack et al. 1998), starting with the least susceptible class

	Stable slope zone	Moderately stable slope zone	Quasi-stable slope zone	Lower threshold slope zone	Upper threshold slope zone
SINMAP	>1.5	1.25	1	0.5	0
LRM					
GDEM	<0.517	0.545	0.571	0.599	1
SRTM	<0.512	0.539	0.564	0.593	1
TDX	<0.510	0.537	0.563	0.593	1
Slope model					
GDEM	<0.520	0.542	0.563	0.587	1
SRTM	<0.517	0.540	0.564	0.593	1
TDX	<0.514	0.539	0.563	0.591	1
Failure rate					
GDEM	<-6e-5	-3.7e-5	0	8e-5	1.8e-4
SRTM	<-1.25e-5	-7.78e-6	0	8.17e-6	2.5e-5
TDX	<-9.3e-6	-7e-6	0	8.5e-6	1.9e-5

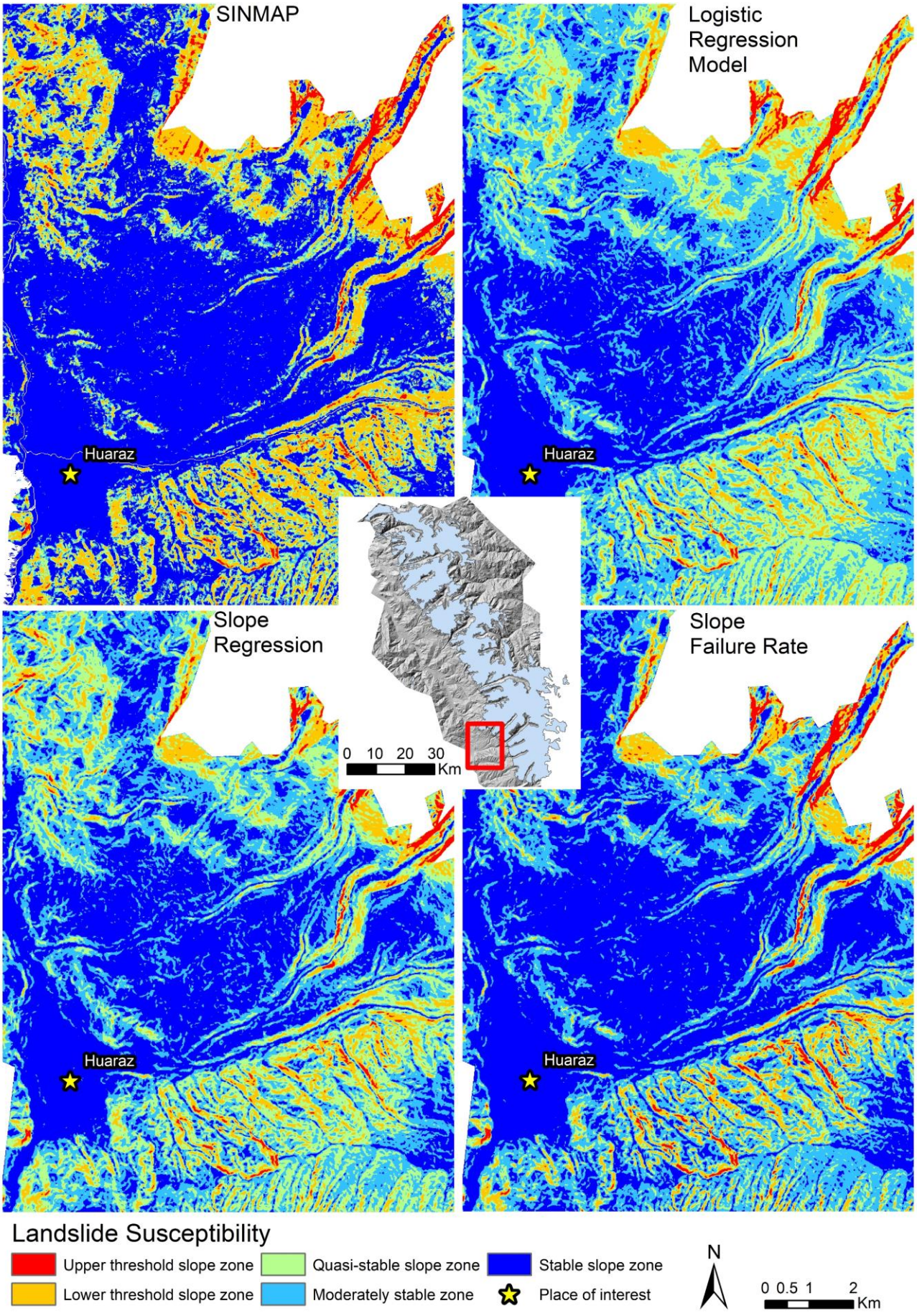

Fig. 18 Results for the four different landslide susceptibility models using SRTM data

5.4. Evaluation

5.4.1. Receiver Operating Characteristics

In a next step, the evaluation using the AUC / ROC method was performed for all realisations (see Table 9, Fig. 19 A). The physically based SINMAP approach seems to be problematic for modelling slope stabilities over the entire study area. SINMAP does not perform well with the SLI which extends over the whole study area (see Table 9). Especially the result obtained with the ASTER GDEM is close to a random prediction of landslides. Within the smaller area (MLI), on the other hand, it performs much better. A similar pattern is visible for the other models. The statistical models (LRM, slope model, and failure rate model) receive as well higher AUC values for the smaller area and have the lowest AUC values over the entire study area using the ASTER GDEM. However, all statistical models obtained better results than the ones of SINMAP considering the entire study area. The results using the LRM has generally the best performances. It receives AUC values between 0.684 and 0.759 over the large study area. Within the smaller study area, it even received AUC values from 0.768 to 0.799. Similar values were received for the slope model, which obtained AUC values between 0.672 and 0.742 for SLI and 0.767 to 0.783 for MLI. The two slope models (the logistic regression and density model) performed very similar, except for the TDX, where the failure rate model performed worse over the SLI area, but better over the whole area. The failure rate model also reached the highest AUC from all applied models for the MLI area (TDX). For the further analysis the focus is laid on the first slope model, as it can be easier compared to the other models, since it is established similar to the LRM. For all models it is noticeable that the AUC values of the different DEMs are much closer to each other for the evaluation with the MLI.

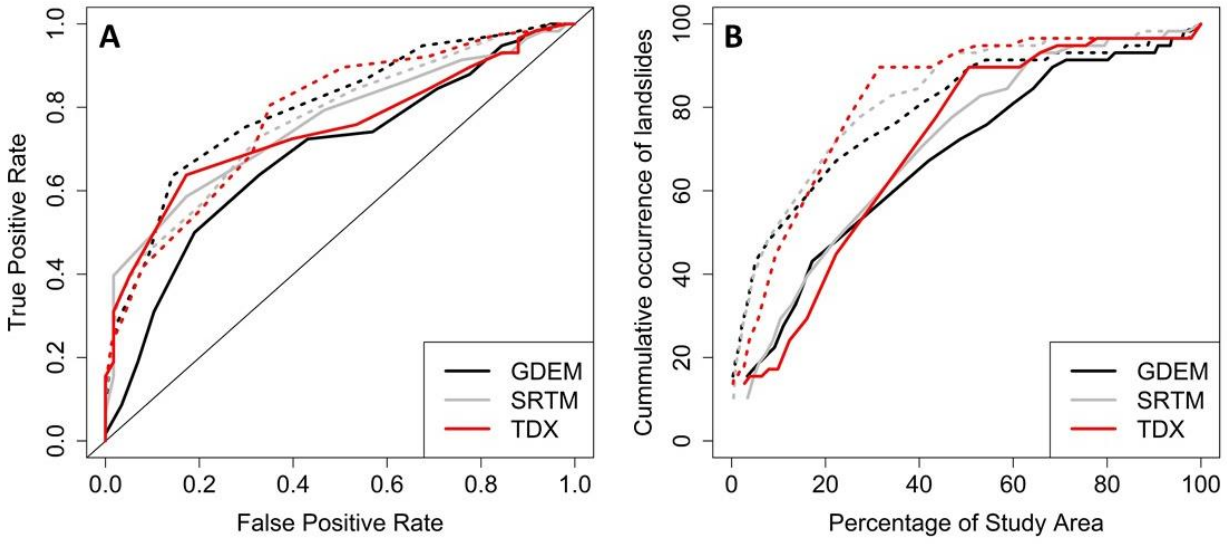

Fig. 19 A: ROC plot for the results of the LRM, B: Cumulative distribution of landslides for the results of SINMAP. The evaluation using the shallow landslide inventory (SLI) are displayed as a solid line, the one of the Marcará landslide inventory (MLI) as dotted line. Cf. Table 9

Table 9 Results of the AUC calculations for all the model runs. In the first columns the results of the ROC evaluation are displayed and in the last ones the ones of the cumulative distribution function. The cells highlighted in green are very close to the values of the ROC (+/-0.03)

ROC	SLI	MLI	DSLI	Cumulative distribution	SLI	MLI	DSLI
	SINMAP				**SINMAP**		
GDEM	0.567	0.749	0.551	GDEM	0.674	0.754	0.591
SRTM	0.605	0.743	0.626	SRTM	0.701	0.755	0.624
TDX	0.625	0.744	0.583	TDX	0.704	0.789	0.604
	LRM				**LRM**		
GDEM	0.684	0.799	0.69	GDEM	0.684	0.783	0.654
SRTM	0.759	0.768	0.683	SRTM	0.755	0.777	0.659
TDX	0.746	0.78	0.659	TDX	0.745	0.798	0.647
	Slope model				**Slope Model**		
GDEM	0.672	0.767	0.657	GDEM	0.692	0.759	0.575
SRTM	0.742	0.764	0.653	SRTM	0.75	0.774	0.616
TDX	0.719	0.783	0.655	TDX	0.739	0.813	0.626
	Slope model II (failure rate)				**Slope model II (failure rate)**		
GDEM	0.687	0.757	0.647	GDEM	0.702	0.759	0.614
SRTM	0.74	0.751	0.642	SRTM	0.739	0.759	0.621
TDX	0.674	0.804	0.632	TDX	0.677	0.813	0.616

5.4.2. Confusion Matrix

The portion of the landslides used for the model validation (58 and 77 cases for the SLI and MLI, respectively) within each susceptibility class can be considered as a measure of the success of the model to predict the distribution of landslides unknown during its preparation. The portion of landslides captured by the most susceptible classes shows correct spatial prediction, while landslides which fall into the least susceptible class may be considered as an error of the models. The most susceptible class of all models has a rather small extent (e.g. up to 7 percent of the pixels from the entire study area). The landslides occurring in this class are less than a quarter for all the model runs. A much higher ratio of correctly modelled landslides can be obtained by considering the two most susceptible classes together. Then, 43.1-77.6% of the landslides of the SLI fall within these two classes which extent over 18.29-42.76% of the whole area (Table 10).

5.4.3. Cumulative Distribution of Landslides

This evaluation technique looks similar to the ROC method. The difference is that it does not focus on the threshold values, nor on the true or false positive rates, it just shows how much of the area needs to be considered as unstable for detecting which number of landslides of the validation set. The idea of the area under curve value is the same as before, that the faster the y values increase, the higher is the AUC and the better the model. The received values are close to the ones of the ROC. Most of them are in the same range (highlighted in green on Table 9) and depict similar patterns of which model /

DEM combinations lead to better results. Only the evaluation of SINMAP looks significantly better than with ROC. The DSLI for all other models performs even worse than with the ROC. Fig. 19 B shows that for the MLI area it is possible to classify around 90% of the landslides in unstable regions when 30% of the region are considered as unstable using the TDX. For the whole area already 45% of the area need to be considered as unstable for correctly model 90% of the landslides.

Table 10 Summary of the comparison of the different susceptibility classes. The classes were obtained using natural breaks for the LRM and the slope model. The SINMAP classes are the ones proposed by the authors (Pack et al. 1998). The two most susceptible classes refer to upper and lower threshold unstable, the least susceptible to stable slope zone

	Percentage of occurred landslides			Percentage of class area to total area		
	Two most susceptible	most susceptible	least susceptible	Two most susceptible	most susceptible	least susceptible
	SINMAP for SLI					
GDEM	67.2	22.4	10.3	41.0	7.0	31.0
SRTM	70.7	24.1	6.9	39.7	6.3	33.2
TDX	77.6	17.2	5.2	42.8	6.1	29.3
	Logistic regression for SLI					
GDEM	43.1	15.5	6.9	18.3	3.9	21.0
SRTM	63.8	17.2	1.7	26.1	6.4	16.4
TDX	56.9	20.7	0.0	28.6	6.8	15.3
	Slope model for SLI					
GDEM	55.2	15.5	5.2	25.6	6.8	20.4
SRTM	58.6	19.0	1.7	24.2	5.7	19.4
TDX	51.7	19.0	1.7	28.0	6.4	18.8
	SINMAP for MLI					
GDEM	52.0	7.8	9.1	24.4	1.6	47.5
SRTM	54.6	11.7	16.9	23.9	1.6	49.7
TDX	66.2	13.0	10.4	27.1	1.6	45.5
	Logistic regression for MLI					
GDEM	13.0	1.3	5.2	3.6	0.2	38.8
SRTM	22.1	3.9	3.9	6.2	0.5	34.9
TDX	44.2	5.2	3.9	8.7	0.5	32.9
	Slope model for MLI					
GDEM	36.4	6.5	5.2	11.2	1.2	32.3
SRTM	39.0	6.5	2.6	10.9	1.1	31.3
TDX	59.7	16.9	2.6	15.7	1.8	30.3

5.4.4. Velocity modelling

Fig. 20 shows the correlation of the velocities measured with the total station to the values calculated by the landslide susceptibility models. The points around Marcará show the correlations which would be expected if the models explained the velocities. There are negative correlations to the SI of SINMAP. This means that the velocity is higher at places where the stability is low (higher susceptibility). For the other three models there are positive correlations (except for the Failure Rate ASTER GDEM combination). This means that velocities are higher, at places where the probability of landslides is higher (higher susceptibility). The points measured around Safuna, though, do not follow such a pattern. Additionally, it needs to be considered, that these two datasets just include five or six

measurements each. Correlations can happen by coincidence and do not have statistical significances (Ross 2010).

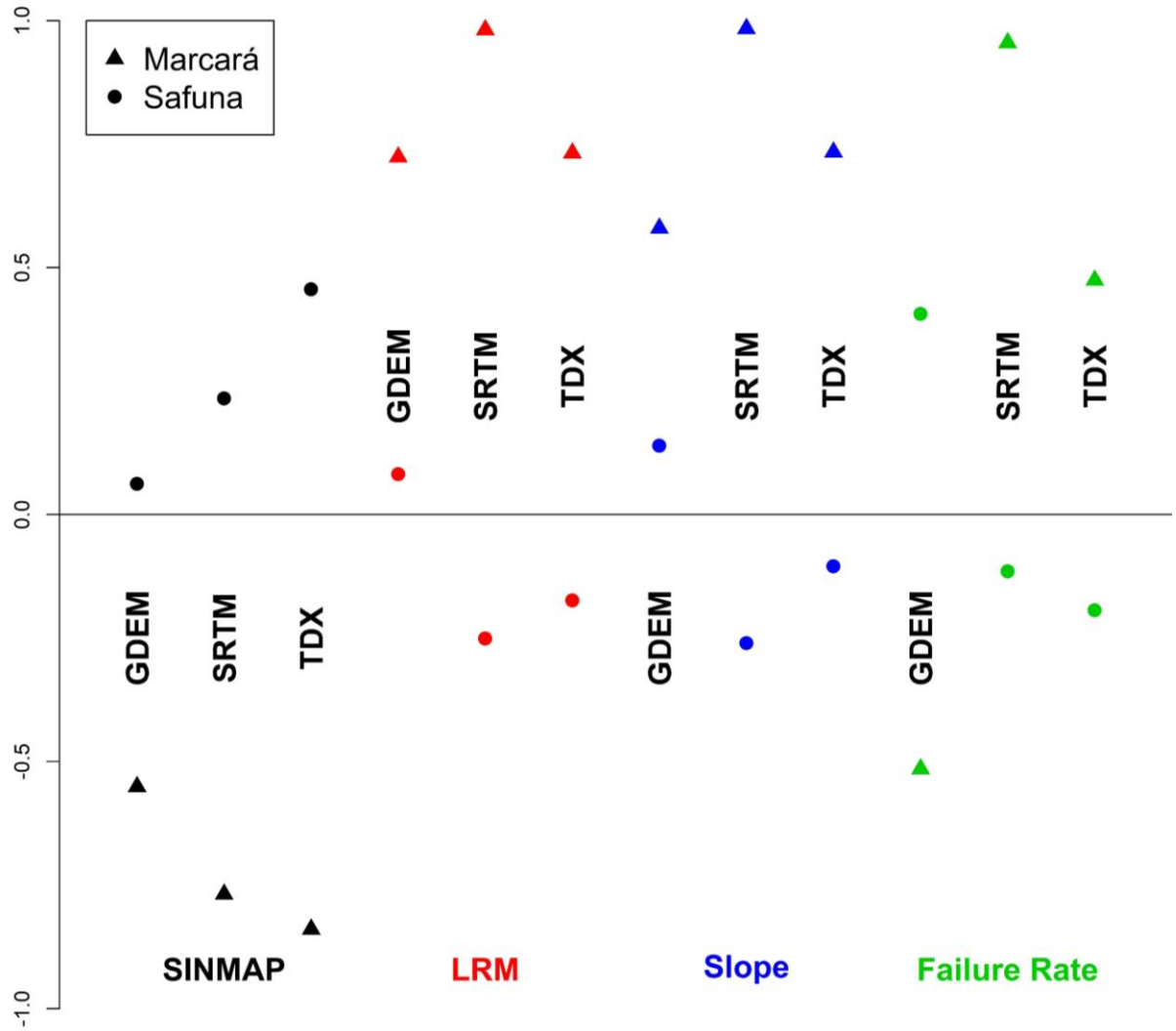

Fig. 20 Correlation of the measured velocities around Marcará and Safuna and the modelled landslide susceptibilities

5.5. Comparison of the Spatial Extent of the Model Classes

This final control of the quality of the models aims to describe the accordance of the models. In doing so, the failure rate was neglected, thus, the slope model is just represented by the slope regression model. Of the remaining three models the areas which are considered as most or least susceptible are considered. Fig. 21 shows the percentages of the areas which are considered by one, two, or all models as most or least susceptible. Contradictions occur if one or two of the models consider a region as most and another one considers it as least susceptible. 100% depicts the total area of all regions which are modelled as most or least susceptible by at least one of the models. The spatial distribution of these results is presented in Fig. 22

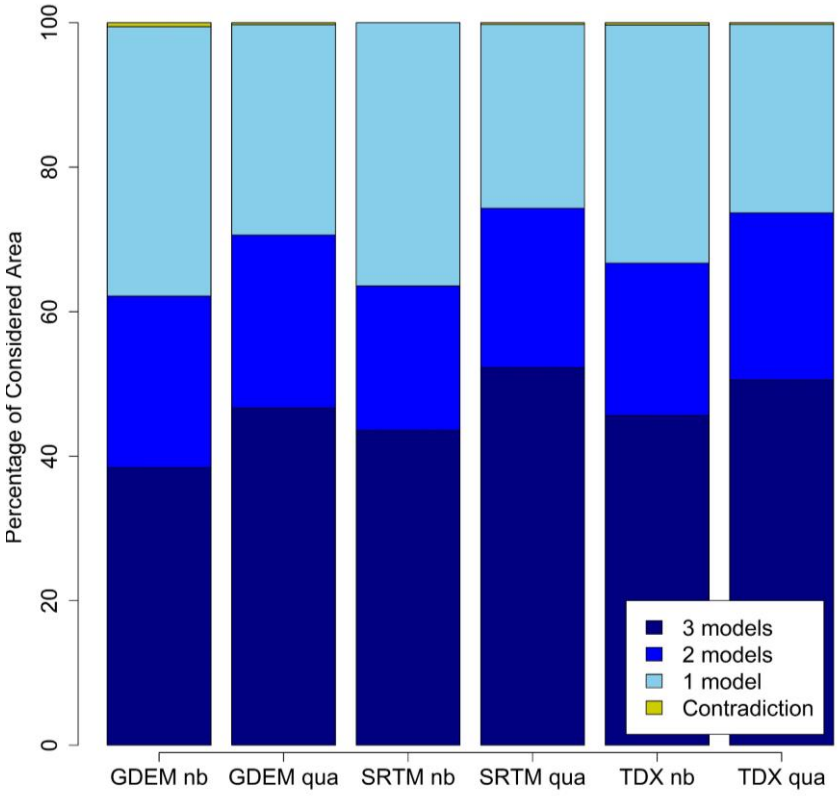

Fig. 21 Spatial agreement of the different models. The percentage which is displayed in dark blue shows the area, where all three models predict the same stability, either all very stable or all very unstable (e.g. for quantiles the most and least susceptible 25% are considered). Blue depicts the area where two of the models agree (and the third model does not consider this area neither as very unstable nor as very stable), and sky blue is the area which is considered as stable or unstable just by one model. The last class, contradiction in yellow describes areas which are considered as most susceptible by one and least susceptible by another model. The acronyms nb and qua stand for the classification processes natural breaks, and quantiles, respectively, on which the classification of the susceptibilities was based on

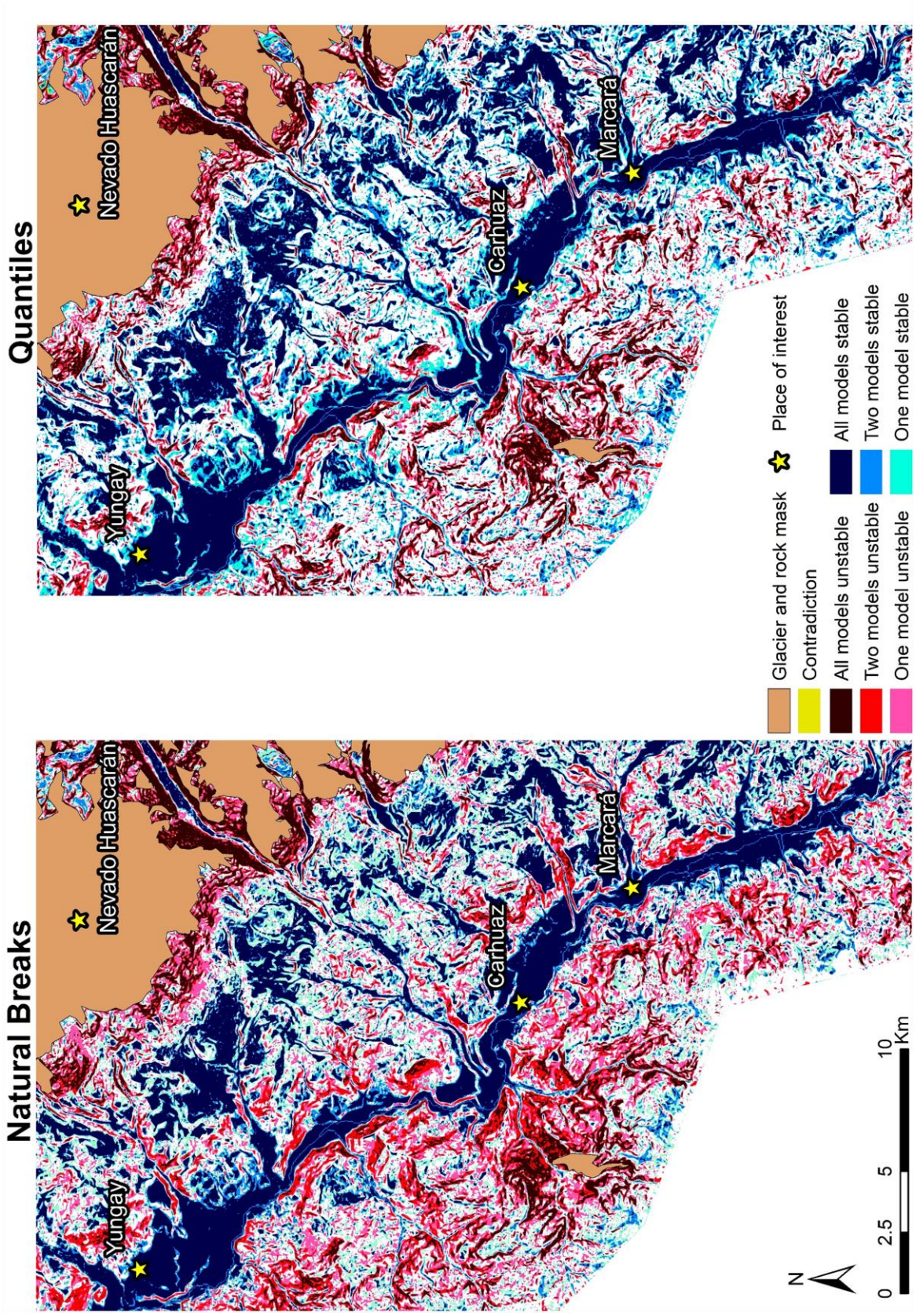

Fig. 22 The study area showing the spatial agreement between the most and the least susceptible classes calculated by the different models using the ASTER GDEM. On the left the results using natural breaks classifier is displayed and on the right quantiles was used. The class 'Contradiction' refers to areas which are considered as stable by one and unstable by another model

6. Discussion

6.1. Comparison Evaluation Techniques

This first subchapter of the discussion part shall compare the used evaluation techniques – the ROC, confusion matrix, cumulative distribution of landslides, and the velocity modelling. Except the latter, all these methods are similar, as they all show in a way, how large areas of the study area include which amounts of landslides. For the comparison, the ROC / AUC is used as basis and all other ones are compared to it.

The confusion matrix is generally in agreement with the ROC. The high AUC values using the SLI for the combinations LRM/SRTM, LRM/TDX, and slope model/SRTM have high percentages of landslides in the most susceptible (56.9-63.8%) and low percentages in the least susceptible class (0-1.7%). The LRM/ASTER GDEM combination, though, seems to have a contradiction of the evaluation techniques within the small study area (MLI). It received a high AUC value (0.799) but just classifies 12.99% of the landslides correctly (in the most susceptible classes). Already 5.2% of the landslides occurred in regions considered as least susceptible. An adjustment of the classes could possibly improve its performance there, as just a small area is considered as most susceptible (3.6%) and a big area is considered as least susceptible (38.8%).

The distribution of landslides within the susceptibility classes shows slightly better results for SINMAP considering the SLI (see Table 10). It includes by far the highest percentage of landslides occurring in the least stable classes for the whole region. It also has, though, the highest number of landslides occurring in the most stable class. Looking at the extents of these classes this is not surprising. SINMAP considers around 40% of the area as most susceptible and 30% as least susceptible. The LRM and the slope model consider no more than 28.6% as most susceptible, no more than 21% as least susceptible, respectively. A similar pattern is visible within the MLI. SINMAP classifies regions where up to 66.2% of the landslides occurred as unstable. On the other hand, depending on the DEM, 9.1-16.9% of the landslides occurred in the most stable class. Both these values are higher than the ones of the LRM and the slope model. Thus, it can be concluded, that the confusion matrix performance is highly dependent on the size of the considered area. Still, the general trends are for both techniques similar.

Easier to compare is the ROC with the cumulative distribution of the landslides. Both evaluation techniques can be displayed as curves and the higher the area below it, the better the model. Hence, for both the AUC was calculated. On Table 9 the obtained values of the cumulative distribution which are close to the ones of ROC, are highlighted in green. This shows that these two techniques are not only similar in their forms, but similar in their results too. For the three statistical models all values are close for both techniques for the MLI and the SLI. For SINMAP and all model evaluations using the DSLI

the values differ more. Still, the patterns are similar, and not much additional information can be gained from the cumulative distribution evaluation. As all these first three evaluation techniques showed similar results, the following subchapters all refer only to the ROC.

The last evaluation technique was used for having a totally distinct technique from the other ones. However, the measured distances for the velocity modelling approach do not necessarily depict the susceptibility to shallow landslides of a measured point. Hence, this final tool needs to be considered with care, even more, as no statistical significance can be reached with a dozen of measured points.

The measured distances of all points were corelated with the model results at these points separately for both locations (see Fig. 20). The points of Marcará (triangles in Fig. 20) attest the models generally a good performance. Except for the failure rate ASTER GDEM combination all model runs seem to corelate in the way they should (positively for the statistical models and negatively for SINMAP) with the velocities. Such patterns are not present when the points measured at Safuna are used. In this case rather random correlations occur. Thus, any meaningful conclusions about the model performance cannot been drawn.

6.2. Performance of the Models

The four models have been applied to the Cordillera Blanca, a mountain range of highly variable soil characteristics. It showed that especially the physically based approach SINMAP is problematic for such heterogeneous regions. The fact that it performed better over the area of the MLI (higher AUC for all DEMs, see Table 9) could relate to the lower variability (see following subchapter 6.3) within this region, as the authors of the model propose to use meaningful calibration areas (Pack et al. 1998). The LRM, on the other hand, could handle these variabilities to some degree. AUC values around 0.75 for the SRTM and TDX show that it is possible to establish reasonable models over such regions. A decreasing tendency of the model performance to the larger study area size, the LRM still performed better over the MLI area, is yet visible. There are two reasons which could explain why the statistical models outperformed the empirical one. First, there is a high dependency of the landslides on the slope angle. This was already explained in other chapters (e.g. 3.3.3, 3.4.1) and is now confirmed by the two slope models. Both have a similar performance to the one of the LRM. Hence, the good performance of the LRM compared to SINMAP could be explained by its higher dependency on the slope angle. Additionally, the slope angle is one of the more reliable factors, as it is easy obtainable from the DEM with comparably low uncertainties. SINMAP uses this information too, just like other DEM derived characteristics (see Eq. 9), but the SI is dependent on assumptions of the soil characteristics and more too. These additional parameters seem to be counterproductive, as they increase the uncertainties of the model and remove the focus from the parameters which are spatially distributed available. Other studies showed, that SINMAP can be a useful tool for modelling slope

stabilities (Pack and Goodwin 2001; Meisina and Scarabelli 2007; Terhorst and Kreja 2009; Michel et al. 2014). A thorough calibration seems crucial, though, what was not given in this thesis. Such subdivisions of the study area over such large variable areas would be extremely time consuming. This led to more useful results using empirical statistical approaches for modelling landslide susceptibilities in this study area.

6.3. Impact of Morphologic Variability

As already mentioned, the poor performance of the SINMAP model may to some degree be explained by the morphological characteristics of the study area. Previous works (Klimeš 2008; Thiebes et al. 2016) suggest that the model performs better in regions with contrasting slopes where landslides source areas distribution does not follow slope distribution within the study area. For instance, highest landslide occurrence is related to less frequent slope class within the study area. The high variability of the landslide occurrence conditions considered by the SINMAP model is illustrated in Fig. 23. The studied landslides occurred on a wide range of slopes and flow accumulation. It contrasts with a different study area in the Czech Republic (represented by the blue line in Fig. 23) where the slope angle and the flow accumulation variability are much lower and also the SINMAP model performed better. For the considered study areas this effect is not as pronounced. SINMAP does perform much better using the MLI (the AUC increased by approximately 0.12 for TDX and SRTM), but there are no significant differences of the variability of the slope angle and the flow accumulation for these two DEMs.

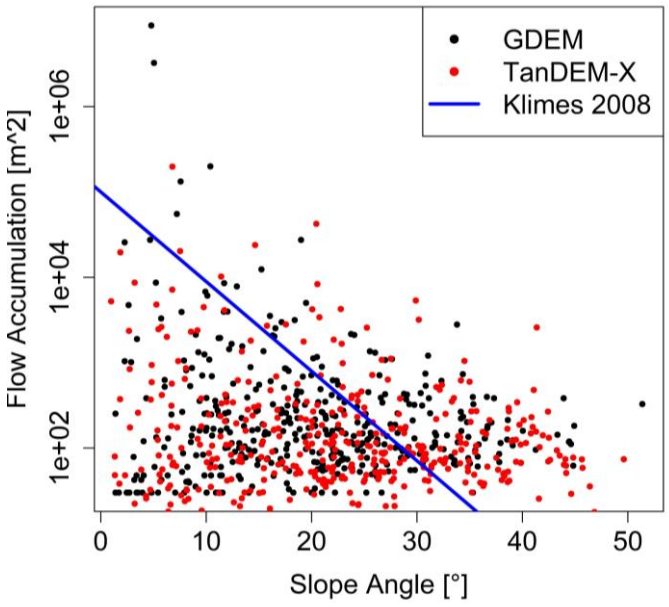

Fig. 23 Comparison of the morphologic characteristics of ASTER GDEM and TDX over the smaller area of the MLI for random points. The blue line indicates the maximal extent of the morphologic variability for a study area in the Czech Republic where SINMAP was applied as well (all points are below this line)

For all models such a dependency of the performance on the variability is hardly visible neither. In favour of such a dependency is the fact that the variability of the DEM derived characteristics (Table 5) show significant differences of the elevation between the MLI and SLI for all DEMs. The better performance of the models within the area of the MLI might be supported by this lower variability. As the ASTER GDEM has higher variabilities within the whole study area for two more characteristics (slope angle and curvature) as well, it performs even worse for all models. Still, it can be doubted that the variability of the DEM derived characteristics is the main explanation for the model performance. There are no significant differences between the DEMs considering the area of the SLI. Still, there are differences in the AUC of around 0.07 for the different DEMs. The study area of the MLI, on the other hand, does have significant differences between the variability of the TDX and the ASTER GDEM, but there, the AUC of these two DEMs is for all models, except the failure rate model, within a range of 0.02. Hence, there need to be other factors influencing the model performance.

6.4. Impact of the DEMs on the Performance of the Model

The impact of the DEMs on the model performance seems low within the area of the MLI. The already mentioned significant morphologic differences between the DEMs within this area are not represented in the model performance. Just the AUC values of the failure rate model show deviations of more than 0.05 of the AUC (TDX vs. SRTM, see Table 9). Considering the large area of the SLI, though, the ASTER GDEM seems to be less suitable to model landslide susceptibilities. For all models, except the failure rate, it has performed worse than the other two DEMs with AUC values which are around 0.05 lower. This can hardly be explained with the quality of the DEMs. The presented validation studies (chapters 4.3.1-4.3.3) showed that the ASTER GDEM has rather higher accuracies in mountainous areas than SRTM (7.4m elevation error vs 10.6m for SRTM). The TDX is, when speaking of vertical errors, certainly the best DEM (3.6m). For modelling landslide susceptibilities TDX and SRTM are for this study area comparable. It needs to be mentioned that none of the DEMs has been validated within the study area. The worse performance cannot be explained by a worse co-registration neither, as the co-registered ASTER GDEM has a lower RMSE than TDX (36.78 m vs. 61.02 m). Thus, it needs to be assumed, that there are other factors of the SRTM and TDX which are beneficial within the study area, for modelling landslide susceptibilities. The spatial resolution of the DEMs does not seem to be one of these factors for the considered models. The performance of the SRTM with its spatial resolution of 30 m is similar or even slightly better than the performance of the TDX which has a spatial resolution of 10 m. This is in accordance with recent studies which compared the effect of the spatial resolution on the performance of landslide susceptibility models (Fuchs et al. 2014; Thiebes et al. 2016; Schlögel et al. 2018). They found similarly, that 10 m DEMs do not perform much better than DEMs with slightly lower spatial resolutions (20 or 30 m).

6.5. Slope Angle Impact on the Performance

This subchapter mainly focusses on the comparison of performances of the three empirical-statistical models. At first the two slope models are compared to see if the influence of the slope angle is visible independently of the model. Table 11 shows that the performance of the two slope models is similar. Using the ASTER GDEM and the SRTM the differences of the two models are maximally 0.015. The results of the TDX differ a bit more between the two slope models. There, the slope regression model is much closer to the results of the LRM. For comparing the failure rate model, it needs to be understood, that it has two significant differences compared to all other models. First, the used values are not continuous. It just consists of 11 independent values which are set for each of the slope classes. This characteristic leads to the second difference. The set values for each slope class can vary a lot for different DEMs. The slope angles at some landslide points of the training set just need to vary slightly (39.8° instead of 40.1°) for changing the values of these two classes significantly. On Fig. 17 it can be seen that this effect is for most classes not that severe, as the values are quite close together. Just the two classes for slope angles between 40° and 50° have quite diverse values. This can be explained as these two classes are the ones with the smallest areal extent. Therefore, their landslide densities, on which the failure rate is based, vary even faster when some landslides fall into another slope class. These two factors could be decisive, why for some DEMs (ASTER GDEM and SRTM) the two slope models performances correspond well and for others, like in this study the TDX, a bit worse. It is interesting to see, that the failure rates of the TDX is for most classes in between the rates of the other two DEMs (see Fig. 17), but for the already mentioned two classes from 40° to 45° and 45° to 50° has the highest, and by far lowest failure rate respectively. Besides the higher deviation from the other slope model, this led to a poor performance over the SLI but the overall highest performance for the MLI.

Table 11 Differences of the performances using the ROC evaluation. The first columns show the differences of the two slope models, the last columns the ones from the regression slope model to the LRM. The sum of the absolute values along the inventories for all DEMs is displayed too, to see if some similarities of the model arise from the DEMs

Slope-failure rate	SLI	MLI	DSLI	Sum	LRM-slope	SLI	MLI	DSLI	Sum
ASTER GDEM	-0.015	0.01	0.01	0.035		0.012	0.032	0.033	0.077
SRTM	0.002	0.013	0.011	0.026		0.017	0.004	0.03	0.051
TDX	0.045	-0.021	0.023	0.089		0.027	-0.003	0.004	0.034

Generally, the performances of the slope models come quite close to the ones of the LRM model. For the combination TDX and MLI they even performed slightly better. For all the other combinations, they just had a slightly lower AUC value. These results show that the slope angle is the most important model parameter of the considered variables for explaining the occurrence of shallow landslides. According to the failure rate model the susceptibility increases for steeper slope angles until it reaches a peak somewhere between 40 and 50°. Afterwards, the susceptibility decreases (Fig. 17). Additional DEM derived parameters used as explanatory variables for the LRM improved the model performance

only slightly. This confirms previous findings by Glade and Crozier (2005) that simply increasing the number of used preparatory and preconditioning factors for susceptibility modelling does not necessarily improve the model performance.

6.6. Landslide Inventory Impact on the Performance

This subchapter compares the performance of the model using different inventories. As the MLI and SLI were already compared from a morphologic point of view in chapter 6.3 special attention is given to the DSLI. Therefore, the usefulness of shallow landslide susceptibility models for other kinds of landslides may be estimated. A dependency of the model performance to the landslide inventory was already described by Steger et al. (2015a). For this thesis, however, it is hardly possible to evaluate to which degree this finding corresponds to the obtained results. None of the landslide inventories was established over the exact same region (see Fig. 1 and 13). Hence, for estimating the impact of the inventory on the model performance, two factors need to be considered, the different areal extent, and the distinct landslides. For the comparison of the SLI and MLI, some of the impact may be attributed to the areal extent, as done in chapter 6.3. Similar effects can be expected when considering the DSLI. This third inventory extents over a larger area than the MLI but a smaller than the SLI. What is of further importance is that it includes exclusively deep-seated landslides. Hence, a third possible factor adds up to the other two impact factors of the inventory on the performance. For analysing how well shallow landslide susceptibility models perform using different kinds of landslides, all three factors need to be considered. These factors are not tried to be quantified, rather is it the aim to generally state, if, under the given conditions, considering these factors, deep-seated landslides were detected too by the models.

The area of the DSLI is considerably larger than the one of the MLI and includes it entirely, but is, on the other hand, entirely included in the area of the SLI and much smaller than it. From this point of view, it would be reasonable, if its performance would lay in between of the SLI and MLI too. The second factor of the impact of the inventory itself cannot be assessed. As it is a rather more complete inventory than the SLI it is not assumed that it would perform much worse than it just by this factor. The final factor of the considered landslides is strongly in favour of the first two inventories, as they both consist of landslides which are meant to be modelled. When looking at the AUC values of the ROC evaluation, the overall best performance of the DSLI was obtained for the LRM using the ASTER GDEM. With an AUC value of 0.69 it is still far lower than best values obtained with the other inventories (0.759 and 0.804). For all other results of the statistical models its performance is worse than the ones of the other inventories and is in the range of 0.632 and 0.683. Such AUC values attest to a bad prediction of landslide susceptibilities. Just for the physically-based model SINMAP, the DSLI comes close to the SLI, but there the AUC values are even below 0.63. Hence, if just the first two factors were

considered, it would have been reasonable, if the DSLI performed better than the SLI but worse than the MLI. The third factor, thus, seems to be that decisive, that it finally performed generally worse, and did in no combination reach a AUC value of a useful model. As expected, shallow landslide susceptibility models do not perform well for deep-seated landslides in the study area. To some degree they seem to have a dependency on the slope angle too but concerning the other preparatory and preconditioning factors they act too different, for being detected by such models.

6.7. Spatial Extent of the Model Classes

The comparison of the spatial extent of the models (Fig. 21 and 22) shows that quartiles classifier generally has a higher agreement for all DEMs. This can be explained by the fact that the original classification method of SINMAP considers much larger areas as unstable or stable than the other two models. This leads to a larger total area considered. This is visible on Fig. 22 too, where especially regions which are considered by one model as most susceptible (pink colour) are much more frequent on the map using natural breaks. The ASTER GDEM again performs worse than the other two models, as it has a lower agreement of the models. SRTM and TDX, on the other hand, have similar agreements, where TDX has a slightly higher accordance using natural breaks and SRTM for quartiles. The agreement rates are generally around 40-50% for all models, and 60 to more than 70% for regions where at least two models coincide. Additionally, the regions of contradictions have an almost negligible extent. Using the SRTM with natural breaks this class is fully absent. This is a bit surprising, as this combination has generally the second highest percentage of areas, where just one model considers certain slopes as most or least susceptible. Generally, it can be stated that there is a high spatial agreement of the models. This is in contrast with findings of other researchers (Sterlacchini et al. 2011) who noted low spatial agreement of susceptibility maps prepared using different combinations of input factors, while maintaining very similar prediction rate. The high ROC and spatial consistency of the results presented here may be attributed to the very similar and limited number of input parameters used for the modelling, and especially their high dependence on the slope angle. This gets obvious when looking at the spatial patterns of the agreement (Fig. 22). It shows that highest agreements of stable areas are along the Santa River around the towns of Yungay, Carhuaz, and Marcará. All three models coincide on unstable regions for the steep slopes in the Llanganuco valley in the southeast of Nevado Huascarán or the slopes in the west of Carhuaz. Hence, the models agree for regions with very steep or flat slope angles (see Fig. 18, the slope regression model shows where steep and flat slope dips occur).

6.8. Physical Interpretation of the Model Results

This final section of the Discussion part shall connect the presented results of the models with the presented scientific background of landslides of chapter 3. The focus is laid on the occurred differences

of the performances between the two study areas of the MLI and the SLI. Most of the preconditioning factors which were presented in the chapters 3.4.1 and 3.4.4 have already been analysed in connection with the morphologic variabilities. What is yet missing are the preparatory and triggering factors. These factors mainly include the porewater pressure, which is related to precipitation and snow melt patterns, the debuttressing effect of the glacier and permafrost degradation, and earthquakes.

As shown in the chapters 3.3 and 3.4 the porewater pressure is a decisive preparatory and triggering factor. Higher water tables reduce the FS without even considering its impact on the cohesion which can reduce the stability of soils even further. Hence, for slopes which have similar surface characteristics the porewater pressure can make the difference between a stable and an unstable slope. This is of importance for the models, as they are all exclusively based on DEMs. There is no explicit information about precipitation patterns. Hence, the models assume the porewater pressure being similar over the considered area. If this is not the case the performance of the model is likely to decrease, as the steep slope modelled as most susceptible may in wet state be more stable than less steep, thus less susceptible slopes which are oversaturated by water. The variability of the precipitation and snowmelt patterns, therefore, could have an influence on the performance of the models.

An analysis of the precipitation patterns in the region of the Cordillera Blanca was performed by Schauwecker et al. (2017). They concluded that there is an increasing tendency of the precipitation with higher elevation and from west to east. Both these factors are much more variable in the area of the SLI than in the one of the MLI. The variability of the elevations has been tested (see Table 5) and is higher in the SLI area. Additionally, the east-west extent is much larger for the SLI area too (see Fig. 1). From this information it can be concluded that the precipitation varies more in the SLI area. Furthermore, this could be a reason why the LRM has generally the best performances over the SLI area. In all model runs of the LRM the elevation is included which gives implicit information about the precipitation patterns.

The impact of the other two preparatory and triggering factors on the two areas is harder to assess. The glacier and rock mask ensured that no parts of the study areas include glaciers nor the surrounding areas which consist of bare rocks. Regions which could have been affected by glaciers or permafrost are likely being within or at least close to the glacier and rock mask. As the SLI entirely includes the glacier and rock mask and the MLI area just has a small area where it borders at it, the SLI area is rather more affected by such factors again. Similar statements can be done for earthquakes. As the SLI area is larger it is more likely that earthquakes exceed certain magnitudes within its area. Looking at the distribution of the earthquakes in Peru of the last century (Bernal et al. 2002) no patterns which could have a significantly higher impact on the SLI area can be revealed.

Even though, for the last two processes, there is no evidence for the higher variability within the area of the SLI, it can be assumed that all these factors have an impact on the outcome of the models. Especially due to the precipitation, it can be assumed that the worse performance using the SLI can to some degree be explained by these variabilities. Still, it is likely that a combination of several factors impacted the differences of the results within the study areas.

7. Conclusion

The aim of this thesis was to apply existing methods of landslide susceptibility modelling in the high mountain area of the Cordillera Blanca. At first a short introduction into the science of landslides was written for getting a reasonable basis of understanding of the involved processes of landslides. In this context two popular classification schemes of Varnes (1978) and Sidle and Ochiai (2006) were introduced. Afterwards, four models were established on three DEMs and evaluated using three landslide inventories and terrain movement rates at several points. The arising uncertainties of the used material and methods was analysed. A combination of these results then led to the following conclusions for the posed research questions.

How do regional-scale landslide susceptibility models perform in areas with highly variable morphology and soil characteristics that are typical for high mountain regions?

Regional-scale landslide susceptibility models can receive reasonable performances in high mountain regions. The ROC evaluation led to an AUC value of 0.759 over the whole study area using a logistic regression model applied on the SRTM DEM. This is a remarkable performance when considering that the study area shows high topographic variability, including elevations between 1400 and up to more than 5000 masl (excluding the glacier and rock mask) and that the information used is restricted to remotely sensed data. It was shown, that these variabilities may relate to the variability of the morphologic characteristics. The ASTER GDEM for example has the highest variabilities of the DEM-derived characteristics between the two study areas and as well the highest difference of the AUCs in the two study areas MLI and SLI. The differences in model performances based on the different DEMs, however, could not be explained with this approach. For this study area empirical statistical models performed much better than the physically based model SINMAP. Therefore, it can be recommended to compare different approaches of modelling slope stabilities in such regions for getting reasonable results. The validation of the models, looking at the most and least susceptible classes, indicates reasonable results as well. Still, the models are surely not precise enough for judging single slopes for their susceptibilities. This gets obvious when looking at the susceptibility classes. Only 63.8% of the mapped landslides happened within the most susceptible classes using the SRTM/LRM model run. The provided models are rather useful tools as a refinement of national scale landslide susceptibility models for scales up to 1:100’000. Besides, the established landslide susceptibility maps of this thesis are only valid for shallow landslides. Hence, for general landslide hazard maps, further modelling would be required to include all kinds of landslides. Furthermore, adjustments of the method for the definition of the susceptibility classes might reduce the number of observed landslides within areas considered as stable by the model. Still, these models can be used for getting a first impression of the situation within an area, and to indicate which slopes could be subject of further research. This is surely

useful, especially, as it is an efficient approach of landslide susceptibility modelling. The only thing required is a DEM and a landslide inventory. Whereof the latter can easily be established in landslide prone areas using high resolution optical data. With the same data, the required glacier and rock mask can be established for getting better and more realistic results.

How much of the performance of a model can be explained by considering only the slope angle?

The best result of the LRM / SRTM combination for the whole study area (AUC = 0.759) was just slightly better than the AUC of similar models considering only slope angle as independent parameter (0.742 slope regression, 0.74 failure rate model). Generally, the results are similar for all statistical models. Hence, it can be stated that the performance of the models is obtained by the high dependency of the landslides occurrence on the slope angle. This assumption is supported by the LRM too, as the slope angle and the elevation were the only independent variables which were used for the LRM of all DEMs.

What is the influence of the used DEMs on the performance of the models?

The presented results showed that, especially when comparing the ASTER GDEM to the other two DEMs, there are considerable differences of the performances. For the study area the SRTM and TDX had similar performances and always led to better results than the ASTER GDEM. The similar performance of TDX and SRTM might to some degree be explained by the SRTM void fills in the TDX. The only exception depicts the failure rate model where the SRTM alone performed better than the TDX and GDEM, which both led to poor results (AUC around 0.67). This is, though, probably more due to the impact of the model than to the one of the DEM. Within the smaller area of the SLI such general tendencies are not visible. The performances of the models using the three DEMs are close and for some (SINMAP, LRM) the ASTER GDEM received the highest AUC values and for others (the two slope models) the TDX was best.

How do these models perform for landslide inventories with different kinds of landslides?

The evaluation using the DSLI showed that shallow landslide susceptibility models cannot, or just very carefully, be used for deep-seated landslides. There still seems to be a dependency of the landslides on the slope angle. It is not as pronounced, however, as for the shallow landslides (see slope model performances on Table 9). Therefore, a model can even reach an AUC value of 0.69 (LRM / ASTER GDEM). This is a remarkable performance, but still not high enough for a reasonable susceptibility map. To enhance the quality of deep-seated landslide susceptibility maps further specific preconditioning and preparatory factors would need to be considered too.

Further studies could use the presented results and combine them with models for different kinds of landslides. Such results could then provide the refinement of the national-scale results of landslide susceptibilities by Villacorta et al. (2012). For the local authorities this could be useful for future land-

use planning. Especially, if the maps do not only concentrate on the origins of landslides, but consider the potential reach of occurring landslides, and thus, provide a general landslide hazard map.

Furthermore, it would be interesting to analyse, if physically based models could achieve better results at this scale using spatially distributed estimators for soil characteristics. As it is time-intensive in such regions to establish useful calibration areas, such estimators might replace them. A physical-based approach needs further information about soils for potentially improving the results.

The local population around the Cordillera Blanca suffered a lot in the past. With the potentially higher landslide hazard in future due to climate change, it is crucial trying to protect the population with the help of such studies. This is the case for other such areas too. The Cordillera Blanca is just one of several data-scarce high mountain regions of the earth. The presented thesis showed that it is still possible to get reasonable results for regional scale landslide susceptibility modelling using only remotely sensed data. Hence, as a next step, it would be interesting to see if this is the case for other study areas with similar characteristics as well. For this it can be recommended to evaluate the performances of different models and DEMs carefully.

Literature

Al-Hurban AE, Allen JRL, Andrews JT, et al (2006) Encyclopedia of Geomorphology, 1st edn. Routledge, London, pp 969-970

Alejandrino IK, Lagmay AM, Eco RN (2016) Shallow Landslide Hazard Mapping for Davao Oriental, Philippines, Using Deterministic GIS Model. In: Drake J, Kontar Y, Eichelberger J, et al. (eds) Communicating Climate-Change and Natural Hazard Risk and Cultivating Resilience, Advances in Natural and Technological Hazards Research. Springer, Cham, pp 131–147

Ambrosi C, Strozzi T, Scapozza C, Wegmüller U (in Press) Landslide Hazard Assessment in the Himalayas (Nepal and Bhutan) Based on Earth-Observation Data. Eng Geol

ANA (2017) Unidad de Glaciología y Recursos Hídricos - UGRH. http://www.ana.gob.pe/gestion-agua/cambio-climatico/page/2. Accessed 21 Dec 2017

ASTER Science Team (2014) ASTGTM: ASTER Global Digital Elevation Model V002. https://lpdaac.usgs.gov/node/1079. Accessed 3 Jan 2018

Athmania D, Achour H (2014) External validation of the ASTER GDEM2, GMTED2010 and CGIAR-CSI-SRTM v4.1 free access digital elevation models (DEMs) in Tunisia and Algeria. Remote Sens 6:4600–4620. doi: 10.3390/rs6054600

Auflic MJ, Komac M (2012) Using remotely sensed data to identify areas at risk: a case of central Slovenia. In: Brebbia CA (ed) Risk Analysis VIII. Wessex Institute of Technology, UK, pp 43–54

Ayalew L, Yamagishi H (2005) The application of GIS-based logistic regression for landslide susceptibility mapping in the Kakuda-Yahiko Mountains, Central Japan. Geomorphology 65:15–31. doi: 10.1016/j.geomorph.2004.06.010

Bai S, Lü G, Wang J, et al (2011) GIS-based rare events logistic regression for landslide-susceptibility mapping of Lianyungang, China. Environ Earth Sci 62:139–149. doi: 10.1007/s12665-010-0509-3

Baraer M, Mark BG, Mckenzie JM, et al (2012) Glacier recession and water resources in Peru's Cordillera Blanca. J Glaciol 58:134–150. doi: 10.3189/2012JoG11J186

Baum RL, Savage WZ, Godt JW (2002) TRIGRS — A Fortran Program for Transient Rainfall Infiltration and Grid-Based Regional Slope-Stability Analysis. pp 2-9

Baum RL, Savage WZ, Godt JW (2008) TRIGRS — A Fortran Program for Transient Rainfall Infiltration and Grid-Based Regional Slope-Stability Analysis, Version 2.0. US Geol Surv Open-File Rep 3-21. doi: Open-File Report 2008–1159

Beguería S (2006) Validation and Evaluation of Predictive Models in Hazard Assessment and Risk Management. Nat Hazards 37:315–329

Bellier O, Dumont JF, Sébrier M, Mercier JL (1991) Geological Constraints on the Kinematics and Fault-plane Solution of the Quiches Fault Zone Reactivated During the 10 November 1946 Ancash Earthquake, Northern Peru. Bull Seismol Soc Am 81:468–490

Benker SC, Langford RP, Pavlis TL (2011) Positional accuracy of the Google Earth terrain model derived from stratigraphic unconformities in the Big Bend region, Texas, USA. Geocarto Int 26:291–303. doi: 10.1080/10106049.2011.568125

Bernal I, Tavera H, Antayhua Y (2002) Zonas Sismogénicas en Perú: Volúmenes de Deformación, Gráficos Polares y Zonificación Preliminar. Boletín la Soc Geológica del Perú 93:31–44

Bertolini G, Pizziolo M (2008) Risk assessment strategies for the reactivation of earth flows in the Northern Apennines (Italy). Eng Geol 102:178–192. doi: 10.1016/j.enggeo.2008.03.017

Bianchini S, Pratesi F (2016) A PSI-based analysis of landslides in the historic town of Volterra (Italy). In: Aversa (ed) Landslides and Engineered Slopes. Experience, Theory and Practice. Associazione Geotecnica Italiana, Rome, pp 411–417

Brenning A (2005) Spatial prediction models for landslide hazards: review, comparison and evaluation. Nat Hazards Earth Syst Sci 5:853–862

Burak A, Zepp H, Zöller L (2006) Reliefenergie – wo die Höhenunterschiede am stärksten sind. In: Nationalatlas Bundesrepublik Deutschland. Springer Spektrum, Leipzig, pp 26–27

Caine N (1980) Duration Control of Shallow Landslides and Debris Flows. Geogr Ann 62:23–27

Capparelli G, Versace P (2014) Analysis of landslide triggering conditions in the Sarno area using a physically based model. Hydrol Earth Syst Sci 18:3225–3237. doi: 10.5194/hess-18-3225-2014

Carey M (2010) In the Shadows of Melting Glaciers - Climate Change and Andean Society, 1st edn. Oxford University Press, New York, p 288

Carlisle BH (2002) Digital Elevation Model Quality and Uncertainty in DEM-Based Spatial Modelling. Diss. University of Greenwich, p 258

Carrara A, Cardinali M, Guzzetti F (1992) Uncertainty in assessing landslide hazard and risk. ITC J 2:172–183

Carson MA, Kirkby MJ (1972) Hillslope Form and Process, 3rd edn. Cambridge University Press, New York, p 476

Cascini L, Fornaro G, Peduto D (2010) Advanced low- and full-resolution DInSAR map generation for slow-moving landslide analysis at different scales. Eng Geol 112:29–42. doi: 10.1016/j.enggeo.2010.01.003

Cascini L, Peduto D, Pisciotta G, et al (2013) The combination of DInSAR and facility damage data for the updating of slow-moving landslide inventory maps Atmospheric at medium scale. Nat Hazards Earth Syst Sci 13:1527–1549. doi: 10.5194/nhess-13-1527-2013

Chatfield C (2006) Model Uncertainty. In: El-Shaarawi AH, Piegorsch WW (eds) Encyclopedia of Environmetrics, 2nd edn. John Wiley & Sons Ltd., Chichester, p 5

Checa CC (2016) Inspección técnica de la obra de seguridad de la laguna safuna alta y baja. Huaraz, p 12

Chen H, Lin GW, Lu MH, et al (2011) Effects of topography, lithology, rainfall and earthquake on landslide and sediment discharge in mountain catchments of southeastern Taiwan. Geomorphology 133:132–142. doi: 10.1016/j.geomorph.2010.12.031

Chen W, Li X, Wang Y, Liu S (2013) Landslide susceptibility mapping using LiDAR and DMC data: A case study in the Three Gorges area, China. Environ Earth Sci 70:673–685. doi: 10.1007/s12665-012-2151-8

Cheng YM, Zhu LJ (2004) Unified Formulation for Two Dimensional Slope Stability Analysis and Limitations in Factor of Safety Determination. Soils Found 44:121–127. doi: 10.1248/cpb.37.3229

Christanto N (2008) Hydrological – Slope Stability Modeling for Landslide Hazard Assessment by means of GIS and Remote Sensing Data. Master's Thesis, Gadjah Mada University, p 89

Ciampalini A, Raspini F, Lagomarsino D, et al (2016) Landslide susceptibility map refinement using PSInSAR data. Remote Sens Environ 184:302–315. doi: 10.1016/j.rse.2016.07.018

Cigna F, Bianchini S, Casagli N (2013) How to assess landslide activity and intensity with Persistent Scatterer Interferometry (PSI): the PSI-based matrix approach. Landslides 10:267–283. doi: 10.1007/s10346-012-0335-7

Cohen D, Lehmann P, Or D (2009) Fiber bundle model for multiscale modeling of hydromechanical triggering of shallow landslides. Water Resour Res 45:1–20. doi: 10.1029/2009WR007889

Constantin M (2016) Landslide Susceptibility, Hazard and Risk Assessment and Control Works. In: World's largest Science, Technology & Medicine Open Access book publisher. p 15

Coppi R (2008) Management of uncertainty in Statistical Reasoning: The case of Regression Analysis. Int J Approx Reason 47:284–305. doi: 10.1016/j.ijar.2007.05.011

Corominas J, van Westen C, Frattini P, et al (2014) Recommendations for the quantitative analysis of landslide risk. Bull Eng Geol Environ 73:209–263. doi: 10.1007/s10064-013-0538-8

Corsini A, Pasuto A, Soldati M, Zannoni A (2005) Field monitoring of the Corvara landslide (Dolomites, Italy) and its relevance for hazard assessment. Geomorphology 66:149–165. doi: 10.1016/j.geomorph.2004.09.012

Crosta GB, Frattini P (2003) Distributed modelling of shallow landslides triggered by intense rainfall. Nat Hazards Earth Syst Sci 3:81–93. doi: 10.5194/nhess-3-81-2003

Crozier MJ, Glade T (2005) Landslide Hazard and Risk: Issues, Concepts and Appproach. In: Glade T, Anderson M, Crozier MJ (eds) Landslide Hazard and Risk, 1st edn. Wiley, Chichester, pp 1–40

Cruden D, Lan H-X (2015) Using the Working Classification of Landslides to Assess the Danger from a Natural Slope. In: Lollino G, Giordan D, Crosta GB, et al. (eds) Engineering Geology for Society and Territory, 1st edn. Springer, Cham, pp 3–12

Cruden D, VanDine DF (2013) Classification, Description, Causes and Indirect Effects – Canadian Technical Guidelines and Best Practices related to Landslides: a national initiative for loss

reduction. Geological Survey of Canada, Natural Resources Canada, p 22

Cruden DM, Couture R (2011) The Working Classification of Landslides: material matters. In: Pan-Am CGS Geotechnical Conference. p 7

Cruden DM, Varnes DJ (1996) Landslide types and processes. In: A. Keith Turner (eds) Landslides: Investigation and Mitigation, National Academy Press, Washington D.C., pp 36–75

D'Amato Avanzi G, Giannecchini R, Puccinelli A (2004) The influence of the geological and geomorphological settings on shallow landslides. An example in a temperate climate environment: The June 19, 1996 event in northwestern Tuscany (Italy). Eng Geol 73:215–228. doi: 10.1016/j.enggeo.2004.01.005

Dai FC, Lee CF (2002) Landslide characteristics and slope instability modeling using GIS, Lantau Island, Hong Kong. Geomorphology 42:213–228. doi: 10.1016/S0169-555X(01)00087-3

Daniels A, Chapin E, Aspilcueta D, Doocy S (2009) Access to Health Services and Care-seeking Behaviours After the 2007 Ica Earthquake in Peru. Disaster Med Public Heal Prep 3:97–103

Davies TRH, Shroder JF (2014) Landslide Hazards, Risks, and Disasters. Elsevier Science, Burlington, p 473

de Blasio FV (2011) Friction , Cohesion , and Slope Stability. In: Introduction to the Physics of Landslides - Lecture notes on the dynamics of mass wastig. Springer Science+Business Media, New York, pp 23–52

De Blasio FV (2011) Introduction to the Physics of Landslides : Lecture Notes on the Dynamics of Mass Wasting. Springer, New York, p 408

Delgado J, Vicente F, García-Tortosa F, et al (2011) A deep seated compound rotational rock slide and rock spread in SE Spain : Structural control and DInSAR monitoring. Geomorphology 129:252–262. doi: 10.1016/j.geomorph.2011.02.019

Deschamps RJ, Lange CB (1999) Landslide Remediation Using Unconventional Methods. Indiana Department of Transportation, Purdue University, West Lafayette, p 121

Devkota KC, Regmi AD, Pourghasemi HR, et al (2013) Landslide susceptibility mapping using certainty factor, index of entropy and logistic regression models in GIS and their comparison at Mugling-Narayanghat road section in Nepal Himalaya. Nat Hazards 65:135–165. doi: 10.1007/s11069-012-0347-6

Dietrich WE, Asua RR de, Orr JCB, Trso M (1998) A validation study of the shallow slope stability model, SHALSTAB, in forested lands of Northern California. Stillwater Ecosyst Watershed Riverine Sciences

Dietrich WE, Montgomery DR (1998) SHALSTAB: a digital terrain model for mapping shallow landslide potential. http://calm.geo.berkeley.edu/geomorph/shalstab/index.htm, accessed 20 Mar 2017

Elkhrachy I (in Press) Vertical accuracy assessment for SRTM and ASTER Digital Elevation Models: A

case study of Najran city, Saudi Arabia. Ain Shams Eng J. doi: 10.1016/j.asej.2017.01.007

England KA (2011) A GIS approach to landslide hazard management for the West Coast region, New Zealand. Master's Thesis, University of Canterbury, p 210

Evans SG, Bishop NF, Fidel Smoll L, et al (2009) A re-examination of the mechanism and human impact of catastrophic mass flows originating on Nevado Huascarán, Cordillera Blanca, Peru in 1962 and 1970. Eng Geol 108:96–118. doi: 10.1016/j.enggeo.2009.06.020

Faraway JJ (2006) Extending the linear model with R: generalized linear, mixed effects and nonparametric regression models, 1st edn., Taylor & Francis Group, Parkway NW, pp 28-57

Farr TG, Rosen PA, Caro E, et al (2007) The Shuttle Radar Topography Mission. Rev Geophys 45:1-43. doi: 10.1029/2005RG000183

Fawcett T (2006) An introduction to ROC analysis. Pattern Recognit Lett 27:861–874. doi: 10.1016/j.patrec.2005.10.010

Felicísimo ÁM, Cuartero A, Remondo J, Quirós E (2012) Mapping landslide susceptibility with logistic regression, multiple adaptive regression splines, classification and regression trees, and maximum entropy methods: a comparative study. Landslides 10:175–189. doi: 10.1007/s10346-012-0320-1

Fisher PF, Tate NJ (2006) Causes and consequences of error in digital elevation models. Prog Phys Geogr 30:467–489. doi: 10.1191/0309133306pp492ra

Foery JR, Sturm PV (2015) Mapping Soil Erosion Risk and Safety Factors of the Massanutten Trail System. Bachelors thesis, James Madison University, p 46

Fredlund DG, Krahn J (1977) Comparison of slope stability methods of analysis. Can. Geotech. J. 14:429–439

Frey H, Strozzi T, Caduff R, et al (2017) An InSAR based landslide inventory for the Cordillera Blanca, Peru: Compilation and validation, Poster, Fringe Conference, Aalto University, Finland

Frich P, Alexander L V., Della-Marta P, et al (2002) Observed coherent changes in climatic extremes during the second half of the twentieth century. Clim Res 19:193–212. doi: 10.3354/cr019193

Fuchs M, Torizin J, Kühn F (2014) The effect of DEM resolution on the computation of the factor of safety using an infinite slope model. Geomorphology 224:16–26. doi: 10.1016/j.geomorph.2014.07.015

Galang JS, Prisley SP, Hammett ALT, Visser JMR (2004) A Comparison of GIS Approaches to Slope Instability Zonation in Virginia. Master's Thesis, Virginia Polytechnic Institute and State University, p 107

Galli M, Ardizzone F, Cardinali M, et al (2008) Comparing landslide inventory maps. Geomorphology 94:268–289. doi: 10.1016/j.geomorph.2006.09.023

GEO-SLOPE International Ltd. (2012) Stability Modeling with SLOPE/W. An Engineering Methodology,

User's Manual, Calgary, p 246

Ghazvinei PT, Zandi J, Ariffin J, et al (2015) Approaches for delineating landslide hazard areas using receiver operating characteristic in an advanced calibrating precision soil erosion model. Nat Hazards Earth Syst Sci Discuss 3:6321–6349. doi: 10.5194/nhessd-3-6321-2015

Glade T, Crozier MJ (2005a) The Nature of Landslide Hazard Impact. In: Glade T, Anderson M, Crozier MJ (eds) Landslide Hazard and Risk, 1st edn. John Wiley & Sons Ltd., Chichester, pp 43–74

Glade T, Crozier MJ (2005b) A review of scale dependency in landslide hazard and risk analysis. In: Crozier MJ (ed) Landslide Hazard and Risk. Wiley, Chichester, pp 75–138

Godt JW, Baum RL, Chleborad AF (2006) Rainfall characteristics for shallow landsliding in Seattle, Washington, USA. Earth Surf Process Landforms 31:97–110. doi: 10.1002/esp.1237

Gokceoglu C, Sonmez H, Nefeslioglu HA, et al (2005) The 17 March 2005 Kuzulu landslide (Sivas, Turkey) and landslide-susceptibility map of its near vicinity. Eng Geol 81:65–83. doi: 10.1016/J.ENGGEO.2005.07.011

Google Earth (2015) Peru, 9°09'05.23'' S, 77°41'36.92'' W. Accessed 15 Nov 2017

Grant RA, Raulin JP, Freund FT (2015) Changes in animal activity prior to a major (M = 7) earthquake in the Peruvian Andes. Phys Chem Earth 85–86:69–77. doi: 10.1016/j.pce.2015.02.012

Greif V, Vlcko J (2013) Application of the PS-InSAR Technique for the Post-Failure Landslide Deformation Monitoring at Lubietova Site in Central Slovakia. In: Margottini C (ed) Landslide Science and Practice, 2nd edn. Springer-Verlag, Berlin, Heidelberg, pp 15–23

Griffiths D (2015) Slope Stability Analysis by Finite Elements: A guide to the use of Program slope64. User's Manual, Geomechanics Research Center, Colorado School of Mines, p 32

Grotzinger J, Jordan T (2017) Verwitterung, Erosion und Massenbewegungen. In: Press/Siever Allgemeine Geologie. Springer Berlin Heidelberg, Berlin, Heidelberg, pp 429–467

Günther A, Reichenbach P, Malet JP, et al (2013) Tier-based approaches for landslide susceptibility assessment in Europe. Landslides 10:529–546. doi: 10.1007/s10346-012-0349-1

Guzzetti F, Manunta M, Ardizzone F, et al (2009) Analysis of Ground Deformation Detected Using the SBAS-DInSAR Technique in Umbria, Central Italy. Pure Appl Geophys 166:1425–1459. doi: 10.1007/s00024-009-0491-4

Guzzetti F, Mondini AC, Cardinali M, et al (2012) Landslide inventory maps: New tools for an old problem. Earth-Science Rev 112:42–66. doi: 10.1016/j.earscirev.2012.02.001

Guzzetti F, Reichenbach P, Ardizzone F, et al (2006) Estimating the quality of landslide susceptibility models. Geomorphology 81:166–184. doi: 10.1016/j.geomorph.2006.04.007

Haneberg WC (2004) A Rational Probabilistic Method for Spatially Distributed Landslide Hazard Assessment. Environ Eng Geosci 10:27–43. doi: 10.2113/10.1.27

Hartge K-H, Horn R, Bachmann J, Peth S (2014) Mechanisch-hydraulische Kräftesysteme in Böden. In:

Einführung in die Bodenphysik, 4th edn. Schweizerbart'sche Verlagsbuchhandlung, Stuttgart, pp 51–89

He S, Pan P, Dai L, et al (2012) Application of kernel-based Fisher discriminant analysis to map landslide susceptibility in the Qinggan River delta, Three Gorges, China. Geomorphology 171–172:30–41. doi: 10.1016/j.geomorph.2012.04.024

Heim A (1932) Bergsturz und Menschenleben. Geol Nachlese 30:14–15

Herrera G, Gutiérrez F, García-Davalillo JC, et al (2013) Multi-sensor advanced DInSAR monitoring of very slow landslides: The Tena Valley case study (Central Spanish Pyrenees). Remote Sens Environ 128:31–43. doi: 10.1016/j.rse.2012.09.020

Highland LM, Bobrowsky P (2008) The Landslide Handbook — A Guide to Understanding Landslides. U.S. Geological Survey Circular 1325, Reston, Virginia, p 147

Hilbe JM (2011) Logistic Regression. In: Kotz, S. (ed) Encyclopedia of Statistical Science. John Wiley & Sons, pp 1-6

Hubbard B, Heald A, Reynolds JM, et al (2005) Impact of a rock avalanche on a moraine-dammed proglacial lake: Laguna Safuna Alta, Cordillera Blanca, Peru. Earth Surf. Process. Landforms 30:1251–1264

Huggel C, Clague JJ, Korup O (2012a) Is climate change responsible for changing landslide activity in high mountains? Earth Surf Process Landforms 37:77–91. doi: 10.1002/esp.2223

Huggel C, Cochachin A, Frey H, et al (2012b) Integrated assessment of high mountain hazards , related risk reduction and climate change adaptation strategies in the Peruvian Cordilleras. Conference Proceedings, IDRC Davos, pp 329–332

Huggel C, Fischer L, Schneider D, Haeberli W (2010) Research advances on climate-induced slope instability in glacier and permafrost high-mountain environments. Geogr Helv 65:146–156. doi: 10.5194/gh-65-146-2010

Huggel C, Gruber S, Korup O (2013) Landslide Hazards and Climate Change in High Mountains. Treatise on Geomorphology 13:288-301

Hungr O, Evans SG, Bovis MJ, Hutchinson JN (2001) A Review of the Classfication of Landslides of the Flow Type. Environ Eng Geosci 7:221–238

Hutchinson JN (1988) Morphological and geotechnical parameters of landslides in relation to geology and hydrogeology. International Journal of Rock Mechanics and Mining Science & Geomechanics Abstracts 26:3-35

IGP (Instituto Geofísico del Perú) (2016) Mapa Sísmico del Perú (1960-2016), Map. http://siar.minam.gob.pe/sialmendoza/mapas/mapa-sismico-peru-periodo-1960-2016. Accessed 18 Jan 2018

INGEMMET (Instituto Geológico M y M (1999) Carta Geológica Nacional Escala 1: 100,000. Map.

http://ingemmet-peru.maps.arcgis.com/apps/Embed/index.html?webmap=e5a7c016da2549f5adeaaf42821bdb5a&extent=-91.0584,-18.9194,-58.6048,0.1509&home=true&zoom=true&scale=true&search=true&searchextent=true&legend=true&basemap_ga. Accessed 18 Dec 2017

Instituto Nacional de Estadística e Informática (2015) Perú: población total al 30 de Junio, por grupos quinquenales de edad, según departemento, provincia y distrito, 2015. In: Población y vivienda. http://www.inei.gob.pe/media/MenuRecursivo/indices_tematicos/cuadro001_1.xls. Accessed 20 Nov 2017

Iverson RM (1997) The Physics of Debris Flows. Rev Geophys 35:245–296

Jäger S, Wieczorek GF (1994) Landslide Susceptibility in the Tully Valley Area, Finger Lakes Region, New York. In: US Geol. Surv. https://pubs.usgs.gov/of/1994/ofr-94-0615/tvstudy.htm. Accessed 7 Dec 2017

Jebur MN, Pradhan B, Tehrany MS (2015) Using ALOS PALSAR derived high-resolution DInSAR to detect slow-moving landslides in tropical forest : Cameron Highlands , Malaysia. Geomatics, Nat Hazards Risk 6:741–759. doi: 10.1080/19475705.2013.860407

Jebur MN, Pradhan B, Tehrany MS (2014) Optimization of landslide conditioning factors using very high-resolution airborne laser scanning (LiDAR) data at catchment scale. Remote Sens Environ 152:150–165. doi: 10.1016/j.rse.2014.05.013

Jeffers JNR (1988) Outline of Modelling Techniques and their Interrelationships. In: Practitioner's Handbook on the Modelling of Dynamic Change in Ecosystems, 1st edn. John Wiley & Sons, Chichester, pp 17–27

Kaser G, Ames A, Zamora M (1990) Glacier fluctuations and climate in the Cordillera Blanca, Peru. Ann Glaciol 14:136–140. doi: 10.1017/S0260305500008430

Kavzoglu T, Sahin EK, Colkesen I (2014) Landslide susceptibility mapping using GIS-based multi-criteria decision analysis, support vector machines, and logistic regression. Landslides 11:425–439. doi: 10.1007/s10346-013-0391-7

Kienholz H, Schneider G, Bichsel M, et al (1984) Mapping of Mountain Hazards and Slope Stability. Mt Res Dev 4:247–266

Kim MS, Onda Y, Kim JK, Kim SW (2015) Effect of topography and soil parameterisation representing soil thicknesses on shallow landslide modelling. Quat Int 384:91–106. doi: 10.1016/j.quaint.2015.03.057

King G, Zeng L (2001) Logistic Regression in Rare Events Data. Polit Anal 9:137–163

Klimeš J (2012) Geomorphology and natural hazards of the selected glacial valleys,Cordillera blanca, Peru. Acta Univ Carolinae, Geogr 47:25–31

Klimeš J (2008) Analysis of preparatory factors of landslides, Vsetínské Vrchy highland, Czech Republic. Acta Res Reports 17:47–53

Klimeš J, Novotný J, Novotná I, et al (2016) Landslides in moraines as triggers of glacial lake outburst floods: example from Palcacocha Lake (Cordillera Blanca, Peru). Landslides 13:1461–1477. doi: 10.1007/s10346-016-0724-4

Klimeš J, Vilímek V (2011) A catastrophic landslide near Rampac Grande in the Cordillera Negra, northern Peru. Landslides 8:309–320. doi: 10.1007/s10346-010-0249-1

Krahn J (2003) The 2001 R.M. Hardy Lecture: The limits of limit equilibrium analyses. Can Geotech J 40:643–660. doi: 10.1139/t03-024

Kritikos T, Davies T (2014) Assessment of rainfall-generated shallow landslide/debris-flow susceptibility and runout using a GIS-based approach: application to western Southern Alps of New Zealand. Landslides 12:1–25. doi: 10.1007/s10346-014-0533-6

Kunkel KE, Palecki M, Ensor L, et al (2009) Trends in twentieth-century U.S. snowfall using a quality-controlled dataset. J Atmos Ocean Technol 26:33–44. doi: 10.1175/2008JTECHA1138.1

Lacroix P, Berthier E, Maquerhua ET (2015) Earthquake-driven acceleration of slow-moving landslides in the Colca valley, Peru, detected from Pléiades images. Remote Sens Environ 165:148–158. doi: http://dx.doi.org/10.1016/j.rse.2015.05.010

Ladd GE (1935) Landslides, subsidence and rock-falls as problems for the railroad engineer. In: American Railway Engineering Association. pp 1091–1161

Lee JH, Park HJ (2016) Assessment of shallow landslide susceptibility using the transient infiltration flow model and GIS-based probabilistic approach. Landslides 13:885–903. doi: 10.1007/s10346-015-0646-6

Lee S (2004) Application of likelihood ratio and logistic regression models to landslide susceptibility mapping using GIS. Environ Manage 34:223–232. doi: 10.1007/s00267-003-0077-3

Lee S, Chwae U, Min K (2002) Landslide susceptibility mapping by correlation between topography and geological structure: The Janghung area, Korea. Geomorphology 46:149–162. doi: 10.1016/S0169-555X(02)00057-0

Lee S, Sambath T (2006) Landslide susceptibility mapping in the Damrei Romel area, Cambodia using frequency ratio and logistic regression models. Environ Geol 50:847–855. doi: 10.1007/s00254-006-0256-7

Legorreta Paulin G, Bursik M, Lugo-Hubp J, Zamorano Orozco JJ (2010) Effect of pixel size on cartographic representation of shallow and deep-seated landslide, and its collateral effects on the forecasting of landslides by SINMAP and Multiple Logistic Regression landslide models. Phys Chem Earth 35:137–148. doi: 10.1016/j.pce.2010.04.008

Lemoine A, Madariaga R, Campos J (2002) Slab-pull and slab-push earthquakes in the Mexican, Chilean

and Peruvian subduction zones. Phys Earth Planet Inter 132:157–175. doi: 10.1016/S0031-9201(02)00050-X

Levermore CD, Beder TS, Brennan PF, et al (2012) Sources of Uncertainty and Error. In: Assessing the Reliability of Complex Models, 1st edn. The National Academies Press, Washington, D.C., pp 19–30

Lin GW, Chen H, Chen YH, Horng MJ (2008) Influence of typhoons and earthquakes on rainfall-induced landslides and suspended sediments discharge. Eng Geol 97:32–41. doi: 10.1016/j.enggeo.2007.12.001

Lineback Gritzner M, Marcus WA, Aspinall R, Custer SG (2001) Assessing landslide potential using GIS, soil wetness modeling and topographic attributes, Payette River, Idaho. Geomorphology 37:149–165. doi: 10.1016/S0169-555X(00)00068-4

Lliboutry LA (1975) La catastrophe de Yungay (Pérou). In: UGGI-IAHS-ICSI Symposium Moscow, 1971, pp 353–363

Lliboutry LA, Arnao BM, Pautre A, Schneider B (1977) Glaciological problems set by the dangerous lakes in Cordillera Blanca, Peru. I. Historical failures of morainic dams, their causes and prevention. J Glaciol 18:239–254

Loucks DP, van Beek E, Stedinger JR, et al (2005) Model Sensitivity and Uncertainty Analysis. In: Water Resources Systems Planning and Management, 2nd edn. Springer, pp 255–290

Malamud BD, Turcotte DL, Guzzetti F, Reichenbach P (2004) Landslide inventories and their statistical properties. Earth Surf Process Landforms 29:687–711. doi: 10.1002/esp.1064

Malkawi AIH, Hassan WF, Abdulla FA (2000) Uncertainty and reliability analysis applied to slope stability. Struct Saf 22:161–187. doi: 10.1016/S0167-4730(00)00006-0

Mark BG, Mckenzie JM (2007) Tracing increasing tropical Andean glacier melt with stable isotopes in water. Environ Sci Technol 41:6955–6960. doi: 10.1021/es071099d

McColl ST (2015) Landslide Causes and Triggers. In: Davies T (ed) Landslide Hazards, Risks, and Disasters, 3rd edn. Elsevier, Amsterdam, pp 17–39

Meisina C, Scarabelli S (2007) A comparative analysis of terrain stability models for predicting shallow landslides in colluvial soils. Geomorphology 87:207–223. doi: 10.1016/j.geomorph.2006.03.039

Michel GP, Kobiyama M, Goerl RF (2014) Comparative analysis of SHALSTAB and SINMAP for landslide susceptibility mapping in the Cunha River basin, southern Brazil. J Soils Sediments 14:1266–1277. doi: 10.1007/s11368-014-0886-4

Mohammed NZ, Ghazi A, Mustafa HE (2013) Positional accuracy testing of Google Earth. Int J Multidiscip Sci Eng 4:6–9

Morgenstern NR, Price VE (1965) The Analysis of the Stability of General Slip Surfaces. Géotechnique 15:79–93. doi: 10.1680/geot.1965.15.1.79

Mouratidis A, Briole P, Katsambalos K (2010) SRTM 3" DEM (versions 1, 2, 3, 4) validation by means of extensive kinematic GPS measurements: A case study from North Greece. Int J Remote Sens 31:6205–6222. doi: 10.1080/01431160903401403

NASA LP DAAC UE (2011) ASTER GDEM version 2

Neukom R, Rohrer M, Calanca P, et al (2015) Facing unprecedented drying of the Central Andes? Precipitation variability over the period AD 1000–2100. Environ Res Lett 10:1–13. doi: 10.1088/1748-9326/10/8/084017

Nuth C, Kääb A (2011) Co-registration and bias corrections of satellite elevation data sets for quantifying glacier thickness change. Cryosph 5:271–290. doi: 10.5194/tc-5-271-2011

ÖAV (Österreichischer Alpenverein) (2006) Alpenvereinskarte Cordillera Blanca Nord (Perú). Map

Pack RT, Goodwin CN (2001) Assessing Terrain Stability in a GIS using SINMAP. In: 15th annual GIS conference. Vancouver, British Colombia, p 9

Pack RT, Tarboton DG, Goodwin CN (1998) The SINMAP Approach to Terrain Stability Mapping. In: 8th Congress of the International Association of Engineering Geology. Vancouver, British Colombia, p 8

Pack RT, Tarboton DG, Goodwin CN (2005) SINMAP 2.0 for ArcGIS - A Stability Index Approach to Terrain Stability Hazard Mapping, User's Manual, Utah State University, p 74

Pack RT, Tarboton DG, Goodwin CN (1999) SINMAP - A stability index approach to terrain stability hazard mapping. User's Man, Utah State University 1–74

Park DW, Nikhil N V., Lee SR (2013a) Landslide and debris flow susceptibility zonation using TRIGRS for the 2011 Seoul landslide event. Nat Hazards Earth Syst Sci 13:2833–2849. doi: 10.5194/nhess-13-2833-2013

Park S, Choi C, Kim B, Kim J (2013b) Landslide susceptibility mapping using frequency ratio, analytic hierarchy process, logistic regression, and artificial neural network methods at the Inje area, Korea. Environ Earth Sci 68:1443–1464. doi: 10.1007/s12665-012-1842-5

Petschko H, Brenning A, Bell R, et al (2014) Assessing the quality of landslide susceptibility maps - Case study Lower Austria. Nat Hazards Earth Syst Sci 14:95–118. doi: 10.5194/nhess-14-95-2014

Petterson KE (1955) The Early History of Circular Sliding Surfaces. Géotechnique 5:275–296. doi: 10.1680/geot.1955.5.4.275

Pieczonka T, Bolch T (2015) Region-wide glacier mass budgets and area changes for the Central Tien Shan between ~1975 and 1999 using Hexagon KH-9 imagery. Glob Planet Change 128:1–13. doi: 10.1016/j.gloplacha.2014.11.014

Popescu ME (2002) Landslide causal factors and landslide remediatial options. 3rd Int Conf Landslides, Slope Stab Saf Infra-Structures, Illinois Institute of Technology, Chicago, pp 1–21

Portes R de C, Spinola DN, Reis JS, et al (2016) Pedogenesis across a climatic gradient in tropical high

mountains, Cordillera Blanca — Peruvian Andes. Catena 147:441–452. doi: 10.1016/j.catena.2016.07.027

Portilla NS, Loyaga MT, Perez SO, et al (2000) Informe de inspección de las lagunas de la Cordillera Blanca Safuna Alta, Safuna Baja, Pucacocha. Ministerio de Agricultura, Huaraz, p 20

Posner AJ, Georgakakos KP (2015) Normalized Landslide Index Method for susceptibility map development in El Salvador. Nat Hazards 79:1825–1845. doi: 10.1007/s11069-015-1930-4

Potere D (2008) Horizontal positional accuracy of google earth's high-resolution imagery archive. Sensors 8:7973–7981. doi: 10.3390/s8127973

Pourghasemi HR, Moradi HR, Fatemi Aghda SM, et al (2014) GIS-based landslide susceptibility mapping with probabilistic likelihood ratio and spatial multi-criteria evaluation models (North of Tehran, Iran). Arab J Geosci 7:1857–1878. doi: 10.1007/s12517-012-0825-x

Pradhan AMS, Kim YT (2015) Application and comparison of shallow landslide susceptibility models in weathered granite soil under extreme rainfall events. Environ Earth Sci 73:5761–5771. doi: 10.1007/s12665-014-3829-x

Pradhan B, Mezaal MR (2017) Optimized Rule Sets for Automatic Landslide Characteristic Detection in a Highly Vegetated Forests. In: Pradhan B (ed) Laser Scanning Applictions in Landslide Assessment, 1st edn. Springer, Cham, pp 51–68

Pugin AJM, Oldenborger GA, Cummings DI, et al (2014) Architecture of buried valleys in glaciated Canadian Prairie regions based on high resolution geophysical data. Quat Sci Rev 86:13–23. doi: 10.1016/j.quascirev.2013.12.007

Raia S, Alvioli M, Rossi M, et al (2014) Improving predictive power of physically based rainfall-induced shallow landslide models: A probabilistic approach. Geosci Model Dev 7:495–514. doi: 10.5194/gmd-7-495-2014

Remesan R, Holman IP (2015) Effect of baseline meteorological data selection on hydrological modelling of climate change scenarios. J Hydrol 528:631–642. doi: 10.1016/j.jhydrol.2015.06.026

Rexer M, Hirt C (2014) Comparison of free high resolution digital elevation data sets (ASTER GDEM2, SRTM v2.1/v4.1) and validation against accurate heights from the Australian National Gravity Database. Aust J Earth Sci 61:213–226. doi: 10.1080/08120099.2014.884983

Riedel B, Walther A (2008) InSAR processing for the recognition of landslides. Adv Geosci 14:189–194

Rosen PA, Hensley S, Joughin IR, et al (2000) Synthetic Aperture Radar Interferometry. Proceedings of the IEEE 88:333–382

Rosi A, Tofani V, Tanteri L, et al (2018) The new landslide inventory of Tuscany (Italy) updated with PS-InSAR : geomorphological features and landslide distribution. Landslides 15:5-19. doi: 10.1007/s10346-017-0861-4

Ross SM (2010) Linear Regression. In: Introductory Statistics, 3rd edn. Elsevier, Burlington, MA, pp 537–

599

Rossi M, Reichenbach P (2016) LAND-SE: A software for statistically based landslide susceptibility zonation, version 1.0. Geosci Model Dev 9:3533–3543. doi: 10.5194/gmd-9-3533-2016

Rowbotham DN, Dudycha D (1998) GIS modelling of slope stability in Phewa Tal watershed, Nepal. Geomorphology 26:151–170. doi: 10.1016/S0169-555X(98)00056-7

Rowe WD (1994) Understanding uncertainty. Risk Anal 14:743–750

Ruiz S, Tavera H, Poli P, et al (2017) The deep Peru 2015 doublet earthquakes. Earth Planet Sci Lett 478:102–109. doi: 10.1016/j.epsl.2017.08.036

Rusli N, Majid MR, Din AHM (2014) Google Earth's derived digital elevation model: A comparative assessment with Aster and SRTM data. IOP Conf Ser Earth Environ Sci 18:7. doi: 10.1088/1755-1315/18/1/012065

Safaei M, Omar H, Huat BK, et al (2011) Deterministic rainfall induced landslide approaches, advantage and limitation. Electron J Geotech Eng 16:1619–1650

Samia J, Temme A, Bregt A, et al (2017) Characterization and quantification of path dependency in landslide susceptibility. Geomorphology 292:16–24. doi: 10.1016/j.geomorph.2017.04.039

Sarkar S, Roy AK, Raha P (2016) Deterministic approach for susceptibility assessment of shallow debris slide in the Darjeeling Himalayas, India. Catena 142:36–46. doi: 10.1016/j.catena.2016.02.009

Satgé F, Bonnet MP, Timouk F, et al (2015) Accuracy assessment of SRTM v4 and ASTER GDEM v2 over the Altiplano watershed using ICESat/GLAS data. Int J Remote Sens 36:465–488. doi: 10.1080/01431161.2014.999166

Sato HP, Harp EL (2009) Interpretation of earthquake-induced landslides triggered by the 12 May 2008, M7.9 Wenchuan earthquake in the Beichuan area, Sichuan Province, China using satellite imagery and Google Earth. Landslides 6:153–159. doi: 10.1007/s10346-009-0147-6

Scaioni M, Longoni L, Melillo V, Papini M (2014) Remote Sensing for Landslide Investigations: An Overview of Recent Achievements and Perspectives. Remote Sens 6:1–53. doi: 10.3390/rs60x000x

Schauwecker S, Lorenzi D, Rohrer M (2017) Línea de Base Climática Cordillera Blanca (Ancash). Proyecto Glaciares, Meteodat, Zurich, p 34

Schellart WP (2000) Shear test results for cohesion and friction coefficients for different granular materials: Scaling implications for their usage in analogue modelling. Tectonophysics 324:1–16. doi: 10.1016/S0040-1951(00)00111-6

Schlögel R, Marchesini I, Alvioli M, et al (2018) Optimizing landslide susceptibility zonation: Effects of DEM spatial resolution and slope unit delineation on logistic regression models. Geomorphology 301:10–20. doi: 10.1016/j.geomorph.2017.10.018

Schmidt KM, Roering JJ, Stock JD, et al (2001) The variability of root cohesion as an influence on shallow

landslide susceptibility in the Oregon Coast Range. Can Geotech J 38:995–1024. doi: 10.1139/cgj-38-5-995

Schneider D, Huggel C, Cochachin A, et al (2014) Mapping hazards from glacier lake outburst floods based on modelling of process cascades at Lake 513, Carhuaz, Peru. Adv Geosci 35:145–155. doi: 10.5194/adgeo-35-145-2014

Sharpe CFS (1938) Landslides and Related Phenomena: A Study of Mass Movements of Soil and Rock. The Journal of Geology 46:137

Sidle RC, Ochiai H (2006) Landslides - Processes, Prediction, and Land Use, 1st edn. American Geophysical Union, Washington DC, p 312

Siebert L, Simkin T, Kimberly P (2010) Volcanoes of the World, 3rd edn. University of California Press, Berkeley, p 551

Slocum T, MacMaster RB, Kesslier FC, Howard HH (2009) Thematic cartography and geovisualization, 3rd edn. Pearson Education, Upper Saddle River, NJ, p 618

Somos-Valenzuela M, Mckinney DC (2011) Modeling a Glacial Lake Outburst Flood (GLOF) from Palcacocha Lake, Peru. Center for Research in Water Resources, University of Texas at Austin, p 16

Stachowiak H (1973) Allgemeine Modelltheorie, 1st edn. Springer, Wien. pp. 1-47 https://archive.org/details/Stachowiak1973AllgemeineModelltheorie

Steger S, Bell R, Petschko H, Glade T (2015a) Evaluating the Effect of Modelling Methods and Landslide Inventories Used for Statistical Susceptibility Modelling. Engineering Geology for Society and Territory 2:201–204

Steger S, Brenning A, Bell R, et al (2015b) Why a high statistical performance cannot be equated with a high plausibility of landslide susceptibility maps. Geophysical Research Abstracts 17:2

Sterlacchini S, Ballabio C, Blahut J, et al (2011) Spatial agreement of predictive patterns in landslide susceptibility maps. Geomorphology 125:51–61

Strozzi T, Klimeš J, Frey H, et al (submitted) Satellite SAR Interferometry for the Improved Assessment of the State of Activity of Landslides: A Case Study from the Cordilleras of Peru. Remote Sensing of Environment

Suárez G, Molnar P, Burchfiel BC (1983) Seismicity, Fault Plane Solutions, Depth of Faulting, and Active Tectonics of the Andes of Peru, Ecuador, and Southern Colombia. J Geophys Res 88:10403–10428

Swanston DN (1973) Judging Landslide Potential in Glaciated Valleys of Southeastern Alaska. Explor J 51:214–217

Tachikawa T, Kaku M, Iwasaki A, et al (2011) ASTER Global Digital Elevation Model Version 2 – Summary of Validation Results. NASA Land Processes Distributed Active Archive Center and the Joint Japan-US ASTER Science Team, p 26

Terhorst B, Kreja R (2009) Slope stability modelling with SINMAP in a settlement area of the Swabian Alb. Landslides 6:309–319. doi: 10.1007/s10346-009-0167-2

Thiebes B, Bell R, Glade T, et al (2016) Application of SINMAP and analysis of model sensitivity - case studies from Germany and. Rev Roum Géogr 60:3–25

Thorne CR, Tovey NK (1981) Stability of Composite River Banks. Earth Surf Process Landforms 6:469–484

Tsai TL, Yang JC (2006) Modeling of rainfall-triggered shallow landslide. Environ Geol 50:525–534. doi: 10.1007/s00254-006-0229-x

Tsai ZX, You GJY, Lee HY, Chiu YJ (2012) Use of a total station to monitor post-failure sediment yields in landslide sites of the Shihmen reservoir watershed, Taiwan. Geomorphology 139–140:438–451. doi: 10.1016/j.geomorph.2011.11.008

Turner TR, Duke SD, Fransen BR, et al (2010) Landslide densities associated with rainfall, stand age, and topography on forested landscapes, southwestern Washington, USA. For Ecol Manage 259:2233–2247. doi: 10.1016/j.foreco.2010.01.051

USGS (2015) Shuttle Radar Topography Mission (SRTM) 1 Arc-Second Global. https://lta.cr.usgs.gov/SRTM1Arc. Accessed 3 Jan 2018

Van Asch TWJ, Buma J, Van Beek LPH (1999) A view on some hydrological triggering systems in landslides. Geomorphology 30:25–32. doi: 10.1016/S0169-555X(99)00042-2

van Beek R, Nieuwenhuis JD, van Asch TWJ (2002) Assessment of the influence of changes in land use and climate on landslide activity in a Mediterranean environment. Diss., Universiteit Utrecht, p 320

van Den Eeckhaut M, Hervás J, Jaedicke C, et al (2012) Statistical modelling of europe-wide landslide susceptibility using limited landslide inventory data. Landslides 9:357–369. doi: 10.1007/s10346-011-0299-z

Van Den Eeckhaut M, Vanwalleghem T, Poesen J, et al (2006) Prediction of landslide susceptibility using rare events logistic regression: A case-study in the Flemish Ardennes (Belgium). Geomorphology 76:392–410. doi: 10.1016/j.geomorph.2005.12.003

van Westen CJ, Jaiswal P, Ghosh S, et al (2012) Landslide Inventory, Hazard and Risk Assessment in India. In: Pradhan B, Buchroithner M (eds) Terrigenous Mass Movements Detection, Modelling, Early Warning and Mitigation Using Geoinformation Technology, 1st edn. Springer, Heidelberg, pp 239–282

van Westen CJ, van Asch TWJ, Soeters R (2006) Landslide hazard and risk zonation — why is it still so difficult ? Bull Eng Geol Environ 65:167–184. doi: 10.1007/s10064-005-0023-0

Varnes DJ (1978) Slope Movement Types and Processes. Spec Rep 176:11–33. doi: In Special report 176: Landslides: Analysis and Control, Transportation Research Board, Washington, D.C.

Varnes DJ (1958) Landslide Types and Processes. Landslides Eng Pract 24:20–47. doi: Fact Sheet 2004-3072

Veliz J, Osorio S, Zamora M, Morales B (1973) Laguna Safuna Estudios Geologicos Complementarios - Base Topografica: Topografia de Mayo de 1971. Electroperu, Glaciologia y Seguridad de Lagunas, Huaraz, p 7

Vilímek V, Zapata ML, Klimeš J, et al (2005) Influence of glacial retreat on natural hazards of the Palcacocha Lake area, Peru. Landslides 2:107–115. doi: 10.1007/s10346-005-0052-6

Vilímek V, Zapata ML, Stemberk J (2000) Slope movements in Callejón de Huaylas, Peru. Acta Univ Carolinae, Geogr 35:39–51

Villacorta S, Fidel L, Carrión BZ (2012) Mapa de susceptibilidad por movimientos en masa del Perú. Rev la Asoc Geológica Argentina2 69:393–399

Visser V, Langdon B, Pauchard A, Richardson DM (2014) Unlocking the potential of Google Earth as a tool in invasion science. Biol Invasions 16:513–534. doi: 10.1007/s10530-013-0604-y

Vuille M, Kaser G, Juen I (2008) Glacier mass balance variability in the Cordillera Blanca, Peru and its relationship with climate and the large-scale circulation. Glob Planet Change 62:14–28. doi: 10.1016/j.gloplacha.2007.11.003

Wang HB, Liu GJ, Xu WY, Wang GH (2005) GIS-based landslide hazard assessment: an overview. Prog Phys Geogr 29:548–567. doi: 10.1191/0309133305pp462ra

Ward WH (1945) The Stability of Natural Slopes. Geogr J 105:170–191. doi: 10.2307/1789732

Wechsler SP, Kroll CN (2006) Quantifying DEM Uncertainty and its Effect on Topographic Parameters. Photogramm Eng Remote Sens 72:1081–1090. doi: 10.14358/PERS.72.9.1081

Wegmüller U, Bonforte A, De Beni E, et al (2014) Morphological changes at Mt. Etna detected by TanDEM-X. In: EGU General Assembly. Wien

Weirich F, Blesius L (2007) Comparison of satellite and air photo based landslide susceptibility maps. Geomorphology 87:352–364. doi: 10.1016/j.geomorph.2006.10.003

Witt AC, Kimberley MM (2005) Using a Gis (Geographic Information System) To Model Slope Instability and Debris Flow Hazards in the French Broad River Watershed, North Carolina. Diss., North Carolina State University, p 178

WP/WLI - Working Party on World Landslide Inventory, UNESCO (1993) Multilingual landslide glossary. p 59

Wu W, Sidle RC (1995) A Distributed Slope Stability Model for Steep Forested Basins. Water Resour Res 31:2097–2110. doi: 10.1029/95WR01136

Xie M, Esaki T, Qiu C, Wang C (2006) Geographical information system-based computational implementation and application of spatial three-dimensional slope stability analysis. Comput Geotech 33:260–274. doi: 10.1016/j.compgeo.2006.07.003

Yilmaz I (2009) Landslide susceptibility mapping using frequency ratio, logistic regression, artificial neural networks and their comparison: A case study from Kat landslides (Tokat-Turkey). Comput Geosci 35:1125–1138. doi: 10.1016/j.cageo.2008.08.007

Yu L, Gong P (2012) Google Earth as a virtual globe tool for Earth science applications at the global scale: progress and perspectives. Int J Remote Sens 33:3966–3986. doi: 10.1080/01431161.2011.636081

Zepp H (2014) Geomorphologie, 6th edn. UTB, Paderborn. pp 104-114

Zimmermann M, Mani P, Gamma P, et al (1997) Murganggefahr und Klimaänderung - ein GIS-basierter Ansatz. vdf Hochschulverlag AG, Zürich. p 161

Zizioli D, Meisina C, Valentino R, Montrasio L (2013) Comparison between different approaches to modeling shallow landslide susceptibility: A case history in Oltrepo Pavese, Northern Italy. Nat Hazards Earth Syst Sci 13:559–573. doi: 10.5194/nhess-13-559-2013

Acknowledgements

This thesis and the related paper (Regional-Scale Landslide Susceptibility Modelling in the Cordillera Blanca, Peru – A Comparison of Different Approaches) would not have been possible without the help of many people. Therefore, I want to express my gratitude for the superb support by all the mentioned people and many more who helped me in any way.

My family for the moral and financial support for making my whole studies possible.

Dr. Holger Frey and PD Dr. Christian Huggel for supervising my thesis, all their valuable inputs, and their patience.

The European Space Agency (ESA) for funding the project Alcantara in which frame the fieldwork of this thesis was financed.

Dr. Jan Klimeš for his huge support on the writing process of the publication.

Alejo Cochachin, César Checa, Eduardo Sánchez, and the whole staff of the "Unidad de Glaciología y Recursos Hídricos" for supporting my fieldwork in Huaraz.

Marco Zapata for supporting my fieldwork with his knowledge and for the shelter.

Dr. Jochen Seidel for his help with the program QGIS and the entertainment in Huaraz.

Dr. Reinhard Furrer for his help with statistical problems.

Dr. Tazio Strozzi for being a co-author of the paper and precious information about several used datasets of this thesis.

Dr. Fangpeng Cuy for giving me a valuable introduction into the wide and interesting topping of slope stability modelling.

Giulia Satiro for her enormous support during and before this thesis, and especially for persuading me to learn Spanish, what was a big help during the stay in Huaraz.

Personal Declaration

I hereby declare that the submitted thesis is the result of my own, independent work. All external sources are explicitly acknowledged in the thesis.

Emanuel Büechi, Zurich, 26th March 2018

Annex

The Unidad de Glaciología y Recursos Hídricos is part of the national water authority of Peru. They have an office in Huaraz and have been doing research in the Cordillera Blanca for several decades (ANA 2017). Over these years many documents like aerial photographies, maps, and documentations have accumulated in their archive. During my stay there, I was looking for documents about the study area. Some of these collected maps and aerial images were used to reconstruct historic DEMs of the region around the Safuna lakes. For this concern two different datasets were used. The first one is a historic map of the Safuna Alta, which was measured in 1971 and established until 1973. This map includes the two lakes Safuna Alta and Baja and the moraine in between. The region where the rockfall occurred which triggered a GLOF in 2002 is not on the map anymore. Hence, just the area of the moraine between the lakes was digitised to detect how it developed with this rockfall and the GLOF.

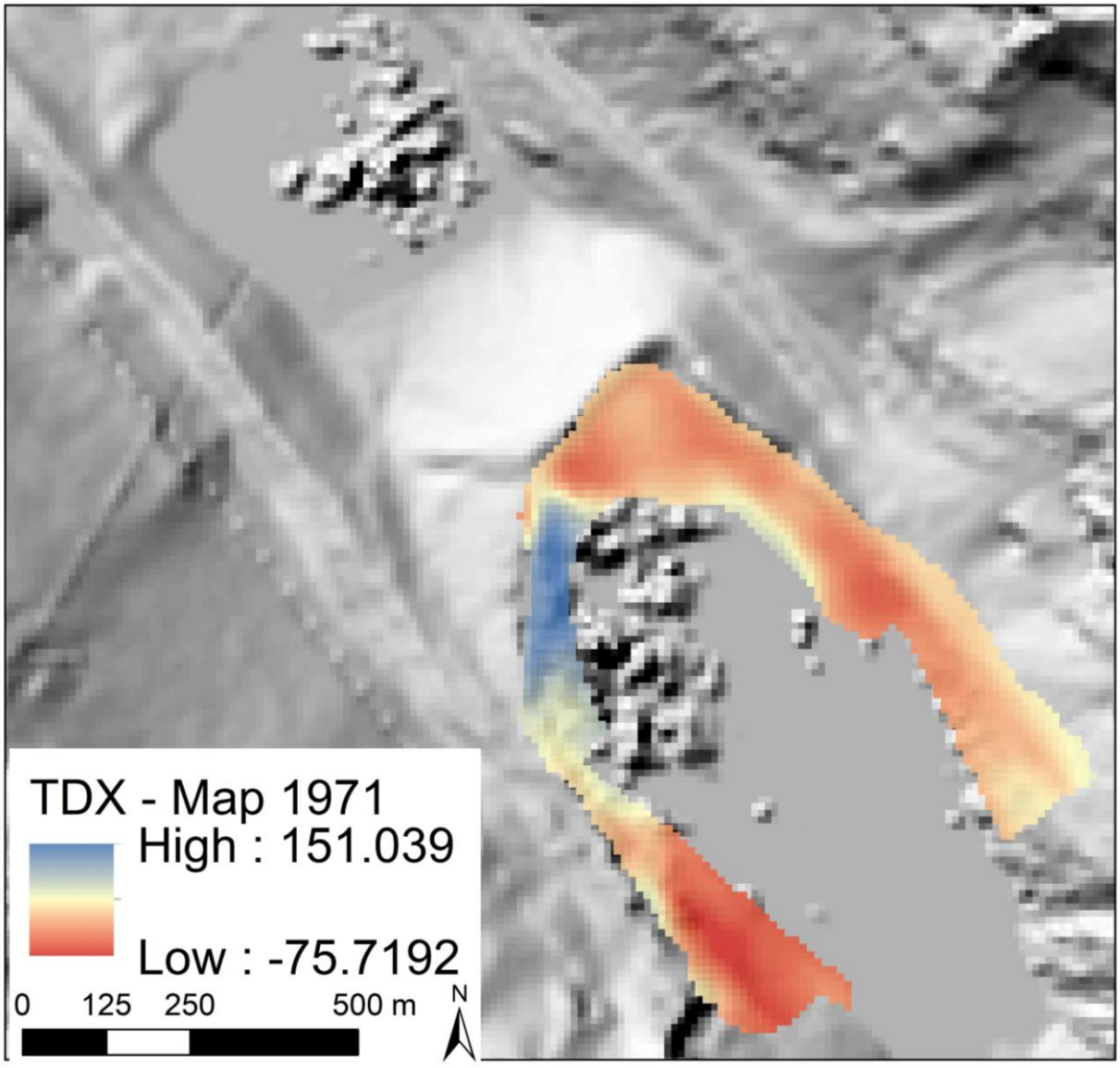

Fig. 24 Development of the moraine between the two Safuna lakes. The DEM which was created from the map of 1971 was subtracted from the TDX

The digitised contour lines were transformed into a DEM and subtracted from the TDX (see Fig. 24). The quality of the map-derived DEM has not been assured, but still some tendencies are visible. The western part in the front seems having increased heights until recent years. Furthermore, are the highest negative changes in the southwestern part, below the region where the rockfall occurred. The rockfall may have caused these parts to fail too.

The second dataset which was used consists of two aerial images from August 1950. They were taken on the same day from slightly different positions. Hence, they could be transformed into a DEM by using structure from motion software. The resulting DEM was a bit distorted and showed an elevation dependent error. At least this seemed the case when comparing it to the TDX. A linear trend was removed to subtract the elevation dependent error. The result still showed some distortions but already revealed some tendencies when comparing it to the TDX (see Fig. 25). The area where the rockfall occurred, for example, is well visible in the south of Safuna Alta.

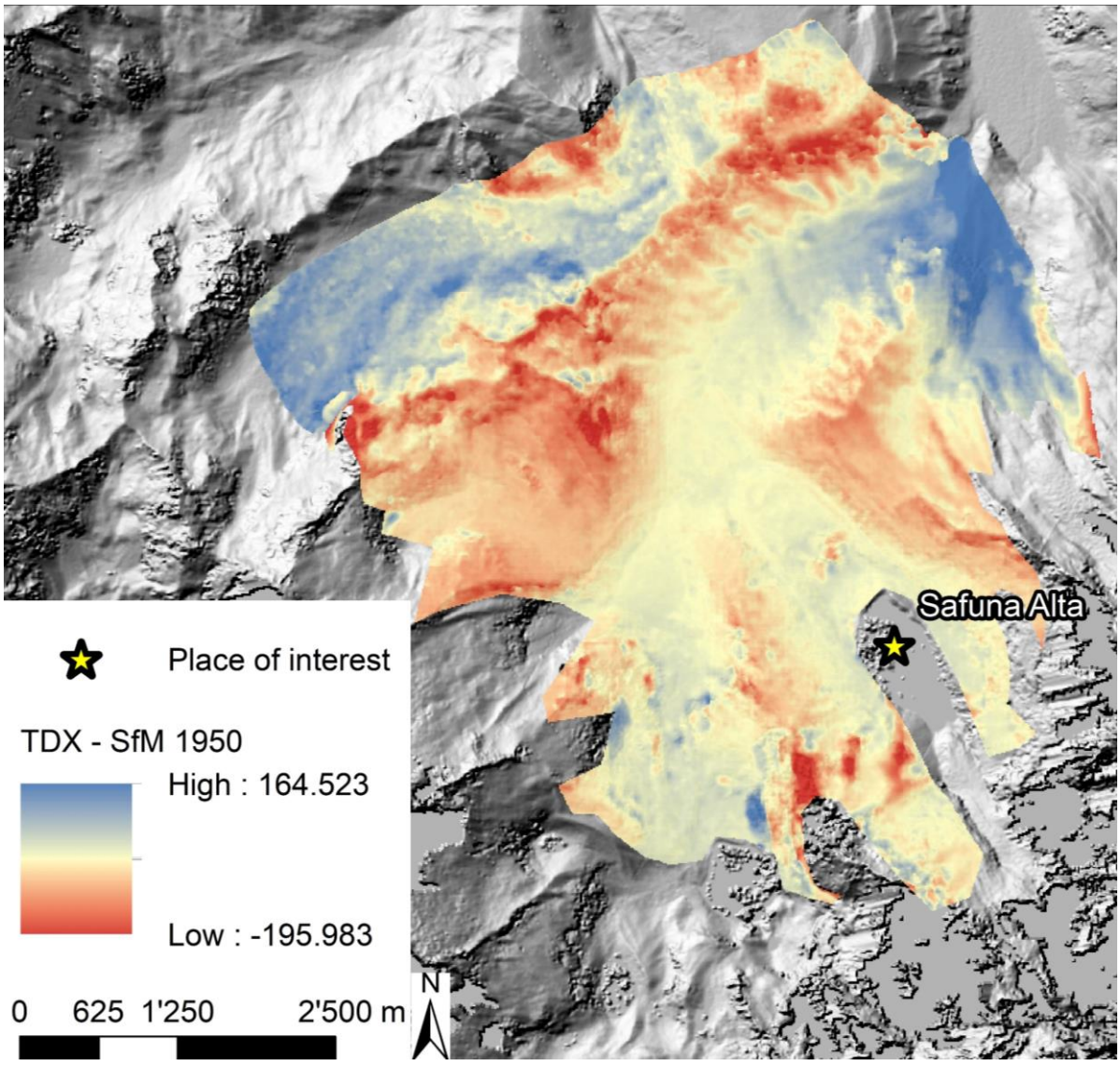

Fig. 25 Comparison of the DEM obtained by the aerial images from 1950 and the TDX